Master Thesis in Geographical Information Science nr 95

Assessing evolution of ice caps in Suðurland, Iceland, in years 1986 - 2014, using multispectral satellite imagery

Alicja Miodońska

2019
Department of
Physical Geography and Ecosystem Science
Centre for Geographical Information Systems
Lund University
Sölvegatan 12
S-223 62 Lund
Sweden

Alicja Miodońska (2019). Assessing evolution of ice caps in Suðurland, Iceland, in years 1986 - 2014, using multispectral satellite imagery

Master degree thesis, 30/ credits in Master in Geographical Information Science
Department of Physical Geography and Ecosystem Science, Lund University

Assessing evolution of ice caps in Suðurland, Iceland, in years 1986 - 2014, using multispectral satellite imagery

---

Alicja Miodońska
Master thesis, 30 credits, in Geographical Information Sciences

Helena Borgqvist
Lund University

Margareta Johansson
Lund University

Abstract

Ongoing climate change is most pronounced in the Arctic and the impacts on the cryosphere have accelerated during the last decades. This study focuses on the application of multispectral satellite imageries in glaciological studies. The study area covers Mýrdalsjökull and Eyjafjallajökull ice caps located in Suðurland, Iceland. The analysis is based on Landsat data. The study includes characterization of the region, mapping glaciers spatial extent and delineating their zones. Several remote sensing techniques are used in order to determine the best semi-automated approach. The changes that the ice caps underwent since the 1980s are evaluated and the probable causes of these variations presented. The ice caps of the Mýrdalsjökull group have dramatically reduced their surface area during the last decades. Eyjafjallajökull has decreased by more than 40%. Once joined, currently, the ice caps form two separate ice bodies. These results are consistent with the Global Land Ice Measurements from Space (GLIMS) program findings and the changes in termini positions observed by World Glacier Monitoring Service (WGMS) and Iceland Glaciological Society.

Sammanfattning

Den pågående klimatförändringen är som mest uttalad i Arktis och påverkan på kryosfären har accelererat under de senaste årtiondena. Den här studien undersöker möjlihgeterna att applicera multispektrala satellitdata inom Kryosfärsstudier. Studieområdet täcker istäcksområdena Mýrdalsjökull och Eyjafjallajökull, belägna i Suðurland på Island. Analysen baseras sig på Landsatdata. Studien inkluderar en beskrivning av området, kartläggning av glaciärernas rumsliga utbredning och avgränsning inom olika zoner (ablations och accumulation). Flera olika metoder inom fjärranalys används för att hitta den semiautomatiska metod som lämpar sig bäst. En utvärdering av resultaten visar hur istäckena har förändrats sedan 1980-talet, och troliga orsaker till dessa presenteras. Istäckena från Mýrdalsjökul har minskat i yta dramatiskt under de senaste decenierna och Eyjafjallajökull har minskat sin yta med mer än 50%. Dessa resultat stämmer väl överens med de globala landismätningar som utförts av rymdprogram och de förändringar av termini-position som observerats av World Glacier Monitoring Service (WGMS) och Islands Glaciologiska Sällskap.

Abstrakt

Arktyka jest obszarem Ziemi, w którym skutki zmian klimatycznych są najbardziej widoczne, a w ciągu ostatnich dziesięcioleci ich wpływ na kriosferę jeszcze przyspieszył. W niniejszej pracy skupiono się na zastosowaniu wielospektralnych obrazów satelitarnych do badaniach glaciologicznych. Obszar badań obejmuje czapy lodowe Mýrdalsjökull i Eyjafjallajökull w rejonie Suðurland, Islandia. Analiza oparta została o dane pochodzące z satelit Landsat. W pracy zawarto charakterystykę regionu oraz wyznaczono zasięg przestrzenny lodowców i ich stref. W celu znalezienia najlepszej semiautomatycznej metody badań, sprawdzono kilka różnych technik teledetekcyjnych. Na podstawie uzyskanych wyników dokonano oceny zmian, jakie nastąpiły od lat 80. XX wieku, a także przedstawiono prawdopodobne przyczyny wahań lodowców. W ciągu ostatnich dziesięcioleci czapy lodowe grupy Mýrdalsjökull skurczyły się dramatycznie. Powierzchnia Eyjafjallajökull zmalała o ponad 40%. Niegdyś połączone, obecnie czapy lodowe tworzą dwa oddzielne lodowe ciała. Wyniki te są zgodne z pomiarami programu Global Land Ice Measurements from Space (GLIMS) oraz ze zmianami pozycji czół lodowcowych obserwowanym przez World Glacier Monitoring Service (WGMS) i Islandzkie Towarzystwo Glacjologiczne.

Keywords:

remote sensing; multispectral satellite imagery; Landsat; Iceland; glaciers; ice caps

Table of contents

List of figures

List of tables

List of abbreviations

CCI	Climate Change Initiative
CLC	Corine Land Cover
DEM	digital elevation model
ELA	equilibrium line altitude
ESA	European Space Agency
ETM	Enhanced Thematic Mapper
ETM+	Enhanced Thematic Mapper Plus
FL	firn line
GCP	ground control point
GHG	greenhouse gas
GLIMS	Global Land Ice Measurements from Space
GRACE	Gravity Recovery and Climate Experiment
L1TP	Level 1 Precision and Terrain Correction
LaSRC	Landsat Surface Reflectance Code
LEDAPS	Landsat Ecosystem Disturbance Adaptive Processing System
LULC	land use - land cover
MAR	Mid-Atlantic Ridge
MSS	Multispectral Scanner
NA	not applicable
NASA	National Aeronautics and Space Administration
NDVI	normalized difference vegetation index
NIR	near infrared
OLI	Operational Land Imager
PR	path/row
QA	quality assessment
RMSE	root mean square error
SL	snow line
SLC	Scan Line Corrector
SWIR	short wavelength infrared
TIR	thermal infrared
TIRS	Thermal Infrared Sensor
TM	Thematic Mapper
TOA	top-of-atmosphere
TSL	transient snow line
USGS	United States Geological Survey
VNIR	visible and NIR waves
WGI	World Glacier Inventory
WGMS	World Glacier Monitoring Service
WRS	Worldwide Reference System

1. Introduction and aim

More than a hundred years ago the Swedish scientist and Nobel laureate Svante Arrhenius published his research on global warming (Arrhenius 1896). Since then numerous studies were conducted to understand and monitor the process.

Earth's cryosphere (the world of frozen water) is an environmental component exceptionally sensitive and threatened by ongoing climate change. Ice and snow are rapidly depleting (AMAP 2017). The cryosphere is an integral part of the global climate system. Its occurrence is not only significantly depending on climatic conditions but also affects the climate (Jania 2008). The importance of the cryosphere in the Earth system and thereby importance of cryosphere studies follows from e.g. its influence on sea level changes, ice-ocean-atmosphere feedbacks, timescales of the variability of cryosphere components including current as well as past fluctuations (AMAP 2017).

Global warming will also have major consequences for the unique ecosystems of polar regions (Vincent et al. 2011; Olsen et al. 2011). The Arctic region comprises a remarkable diversity of habitats and associated ecosystems, from mountain glaciers and ice caps through tundra to icy seas (Vincent et al. 2011). The changing climate has a severe effect on these unique ecosystems. As their habitats undergo rapid contraction, the Arctic endemic species would decline as well (Vincent et al. 2011).

Monitoring the cryosphere can help predict future climate change trends (Jania 2008). Glacier monitoring allows to understand the interaction between glaciers and climate, detect climate and environmental change (due to glaciers climate sensitivity), validate climate models and scenarios as well as assess glacier changes impacts on the environment (e.g. global sea level, water resources, natural hazards etc.) (Pellikka and Rees 2009).

Research and systematic monitoring are essential to better understand this phenomenon and, to forecast its effects and development in the future. Geographic Information Systems (GIS) and remote sensing techniques are great tools for studying these inhospitable areas (Williams and Ferrigno 2012). Satellite remote sensing not only supports and facilitates traditional field studies but also extends the array of variables that can be measured. Satellite observations have also enabled a major step forward towards a uniform global glacier monitoring (Pellikka and Rees 2009).

The aim of this study is to find a remote sensing technique suitable to map the spatial extent and asses the evolution of glaciers over the time, and, based on this methodology, to estimate changes in ice caps located in Suðurland, Iceland during the 1980s to 2014. The analysis is based on NASA Landsat multispectral imageries. The probable causes of observed variations are discusses based on the characterization of environmental variables in the region.

2. Background

2.1. Global warming and the cryosphere

Cryosphere (gr. κρύος kryos – ice, cold) is defined as the ice-coat of the Earth. It is closely related with the atmosphere, the lithosphere and, in particular, the hydrosphere. The solid phase of H_2O counts into the Earth's water resources and plays an important role in the water cycle. The main components of the cryosphere include snow cover (permanent snow in high mountains and polar areas, and periodic in temperate climate zone), sea ice and ice cover of inland freshwater (lake and river ice), glaciers and ice sheets as well as permafrost. The widespread occurrence and overall mass of the cryosphere make it a very important element of the Earth's natural environment (Jania 2008). The cryosphere is a critically important component of the Earth system that has a vital influence on climate. It affects energy balance, air and ocean circulation and sea level (and thus the extent and shape of the Earth's land masses) (Callaghan et al. 2011d; Olsen et al. 2011). Moreover, it poses the greatest storage of Earth's freshwater – a basic resource for Earth's life, and regulates the release of greenhouse gases (GHG; such as methane CH_4 and carbon dioxide CO_2) (Callaghan et al. 2011d; Olsen et al. 2011). At the same time, Earth's cryosphere is an environmental component most sensitive and most threatened by the ongoing climate change (Jania 2008). Currently, due to climate warming, the cryosphere is subjected to dramatic change (Olsen et al. 2011). Although cryosphere response to climate change is relatively quick, some delay occurs, and various cryospheric components react to global warming with varying intensity.

Snow, a frozen precipitation accumulating on a surface, is a dominant feature of the Arctic landscape (Callaghan et al. 2011a; Callaghan et al. 2011b). Snow cover is the most spatially and seasonally variable element of the cryosphere (Callaghan et al. 2011a; Brown et al. 2017). However, generally, a reduction in Arctic snow cover is observed (Brown et al. 2017).

The Arctic sea-ice is generally declining, both in extent and thickness (Barber et al. 2017; Olsen et al. 2011). The ice is getting younger and its speed of movement is increasing (Barber et al. 2017). It is melting earlier, and the ice formation is coming later in the season (Barber et al. 2017). All these changes strongly affect the Arctic ecosystems, from phenology of the ice algae phytoplankton bloom throughout the whole Arctic food web (Barber et al. 2017; Olsen et al. 2011). Due to decline in thick multi-year ice and its stable environment, some ice-associated endemic species might be completely lost (sea-ice dependent seals, polar bears, walrus) (Barber

et al. 2017; Olsen et al. 2011). Moreover, the depleting of ice reduces albedo resulting in more heat absorption and in turn, would enhance the warming (Olsen et al. 2011). Given the projected increase in GHG concentrations, there is a high probability that the summer sea-ice will be essentially gone within the coming decades (Overland et al. 2017a, 2017b).

Freshwater ice, covering rivers and lakes, is a cryospheric component interwoven into the Arctic landscape through water flow and storage networks (Olsen et al. 2011; Prowse et al. 2011b2.)**.** Its occurrence strongly depends on other cryospheric components which govern its genesis (Prowse et al. 2011b). In general, the Arctic hydrological cycle is accelerating (Prowse et al. 2017) - observed long-term trends exhibit increasingly later freeze-ups and earlier break-ups (Olsen et al. 2011; Prowse et al. 2011a).

Permafrost shows the slowest reactions among cryosphere elements (Romanovsky et al., 2017). The changes in permafrost results in multiple consequences for landforms (e.g. ground slumping, slope instability), ecosystems (e.g. drying of wetland habitats and, simultaneously, new ponds formation) and biogeochemical cycles (e.g. methane emissions from new wetlands, release of stored carbon from permafrost) (Olsen et al. 2011). Permafrost thaw also leads to the release of toxic mercury (Mård et al. 2017).

Glaciers and ice sheets react with varying intensity to global warming; small glaciers and ice caps are most sensitive to global warming whereas ice sheets, such as Greenland and Antarctica, react more slowly to ongoing changes (the Greenland Ice Sheet was in balance until 1990; Olsen et al. 2011). Local climate also affects the response time of a glacier. The glaciers located in marine temperate and polar climates responds faster and more intensively than glaciers in cold continental climates (Jania 2008). However, changes in glaciers and ice caps around the world are visible regardless of their scale.

Glacier extent and volume are gradually decreasing (WGMS 2017; Olsen et al. 2011). A widespread acceleration of ice loss across the Arctic is observed (Overland et al. 2017b). The majority of the loss is attributable to anthropogenic causes (Box and Sharp 2017). As a consequence, the water runoff gets altered (initial increase followed by the eventual decline, as glaciers melt) and water outbursts occur more often (e.g. glacier lakes dams fail) (Olsen et al. 2011). From a local perspective, it poses a great threat for indigenous communities for which glaciers often serve as a source of potable water and power supply (hydropower plants set on glacial rivers) (Jania 2008).

Arctic glaciers are also a significant contributor to global sea-level rise (Olsen et al. 2011; Box and Colgan 2017). Taking into account all influences (land ice loss, ocean thermal expansion, land water storage charges), the global sea level rise is projected to reach 0.52 – 0.74 m in this century (Box and Colgan 2017). Another impact originating from melting glaciers is the export of nutrient and contaminant released from glaciated systems into Arctic seas (Box and Sharp 2017).

Although the shift in climate state is generally forced by increases in atmospheric GHG concentrations (especially carbon dioxide (CO_2) and methane (CH_4)) (Overland et al. 2017a), this primary driving process is a subject to complex interactions between the atmosphere, hydrosphere, biosphere, and cryosphere (Olsen et al. 2011).

Cryosphere reduction triggers mostly positive feedback loops with the climate change, accelerating further warming (Callaghan et al. 2011c; Olsen et al. 2011). One example is the albedo reduction of both land and sea surfaces changing from high values of surfaces covered with snow and ice to lower values of bare ground or ocean water (Callaghan et al. 2011c). Melting snow cover and retreating sea ice contributes to the absorption of solar radiation.

Another example of a positive feedback from changing cryosphere is the thawing of permafrost, and the release of greenhouse gases from organic sediments, which enhance the greenhouse effect (Schuur et al. 2015). Due to microbial breakdown inducted by climate warming, the large quantiles of organic carbon stored in perennial frozen soils might be released in the form of GHG, mainly CO_2 and CH_4 (Schuur et al. 2015).

Furthermore, there is a positive feedback between accelerating the flow of glaciers masses that terminate in the ocean and rising the global ocean level. Raising sea level reduces the friction of calving glaciers, and the contact with warmer ocean water facilitate their movement (Olsen et al. 2011).

However, some negative feedback loops were also observed. The increase in evaporation from the oceans conduce the formation of clouds, which reduce the amount of solar radiation (Jania 2008). Increased intensity of the hydrologic cycle accompanying the global warming, might lead to increase in water vapor and precipitation levels (Prowse 2009; Mård et al. 2017). In areas remaining below freezing temperatures, it might also lead to increase in snow precipitation and thus ice bodies accumulation (Jania 2008; Prowse 2009).mainly

2.2. Glaciers

Glaciers and ice sheets constitute over 98% of the total ice volume on Earth. Glaciers cover about 11% of land areas. They contain approximately 2.2% of all water on Earth, which makes 75% of the total global freshwater resources (Jania 1997).

A glacier is a dynamic and open system – the circulation of mass (ice, snow, water and moraine material) and energy exchange are realized through accumulation, ice flow, and ablation. These processes are influenced by external factors but at the same time actively affect them (Jania 1997).

Glacier formation depends on environmental conditions including geographical placement, altitude above sea level and landform, solar radiation and temperature as well as the amount of rainfall (Jania, 1997). A glacier is built up by the accumulation of snow over a long time period. In the transformation process from snow to glacial ice, the air is eliminated from the pores between the ice grains. The intermediate stage of metamorphosis is firn. Glacial ice differs from snow and firn in that the air tubules between the grains are sealed up and therefore the ice is impermeable to meltwater. In glacial ice, air only occurs in the form of bubbles (Jania 1997).

2.3. Mass balance and Equilibrium Line Altitude (ELA)

To assess current state and ongoing changes in a glacier, the glacier's mass balance is studied, i.e. the difference between accumulation and ablation for a specific year.

The accumulation includes all processes in which the material is added to the glacier. Typically, the material accumulates as snowfall. Other possible types of accumulation are avalanches, rime ice (factor especially important in Iceland – occurs in the specific cold and humid climate conditions, deposits when the wind runs cool fog), freezing of raindrops and meltwater. The amount of precipitation increases with altitude up to the level of the precipitation inversion. Precipitation decreases with increasing distance from the seas and oceans (moisture sources). In a maritime climate (e.g. Iceland), accumulation occurs mainly in winter (Jania 1997).

The term ablation is used to describe any processes that result in a mass loss. It is usually the melting and runoff of meltwaters, evaporation and sublimation, blowing snow away by the wind, calving of glaciers disemboguing into the sea as well as melting the bottom layers in contact with the ground (susceptible to geothermal activity), ejection of ice blocks in a wake of the eruption of sub-glacial volcanoes (Jania 1997). In addition, volcanic ash and tephra layers reduce albedo and enhance ablation (Kargel et al. 2014).

Glaciers can be divided into some characteristic zones (facies), which differ from each other in the properties of snow or ice (grain size, water saturation) and processes occurring in them (soaking, melting). Stratification is vertical – it depends primarily on the altitude and associated temperature gradient. The smallest grains of snow are highest on the glacier (at the lowest temperatures and with relatively low melting). They gradually increase in size with decreasing height. The largest grains of snow are just above the snow line (Williams et al. 1991; Górzyńska 2008).

The division of glaciers into faces was first published by Benson in 1960. Since then, various authors have proposed various modifications of this classification. For Icelandic glaciers, Brown (Brown et al. 1999) proposed a somewhat simplified schema (Fig. 1).

At the base, there are ablation facies (bare ice facies). Snow and firn cover does not occur, possibly could remain in crevasses or ice falls. Upper parts of this zone can be covered with aprons of long-lasting snow.

Above the ablation zone runs an equilibrium line altitude (ELA). Equilibrium line altitude (ELA) is the glacier feed limit, where the accumulation is equal to the ablation. It separates the area in which the accumulation takes place (positive mass balance), from the zone in which ablation predominates (negative balance). During the summer season, as the snow melts, the zones move up the glacier. Thus, it is possible to determine the temporal positions of individual zones. With the progression of ablation in the summer season, transient snowline (TSL) is gradually moving up the glacier. Usually, glaciers reach their maximum annual extent by late spring, while the minimum extent occurs at the end of the summer or in early autumn. At the end of summer, ELA is in its uppermost position – at that time the only area covered with snow is the accumulation zone, and in the ablation zone there is only ice. In temperate climates, the position of ELA during the minimum surface extent of the glacier snow cover (SL, the highest TSL position) usually concur with firn line (FL).

ELA is often covered by a superimposed ice. This ice is formed when an avalanche of soaked snow flows from the slush zone and freezes up in the ablation zone on contact with cold ice. In Icelandic glaciers, superimposed ice forms irregular patches. Observations on Eyjafjallajökull show that on Icelandic ice caps a superimposed ice zone is not a continuous permanent feature. The presence of superimposed ice complicates the delineation of ELA (Jania 1997). In such case, ELA is displaced down-glacier from the SL/FL (Williams et al. 1991). Superimposed ice**,** often distributed in small accumulations around the firn line, is considered as an extension of the slush zone (Brown et al. 1999).

Lower accumulation zone begins with slush zone. Slush is typically a thin layer with a thickness of about 50 cm. Firn is saturated with water and has large crystals (> 2 mm). Water, saturating from the percolation zone, accumulates in the lowest parts of the layer, because underneath is an impermeable glacial ice.

Above is the upper accumulation zone. In Iceland, due to the heavily marine climate, snow usually has a significant water content and does not appear in a completely dry form (Williams et al. 1991), but still, it is the driest in this layer.

Usually, the boundaries between the individual facies are patchy and irregular, rarely present a linear form (Williams et al. 1991). Additionally, not always and not on all glaciers all facies are present (Brown et al. 1999).

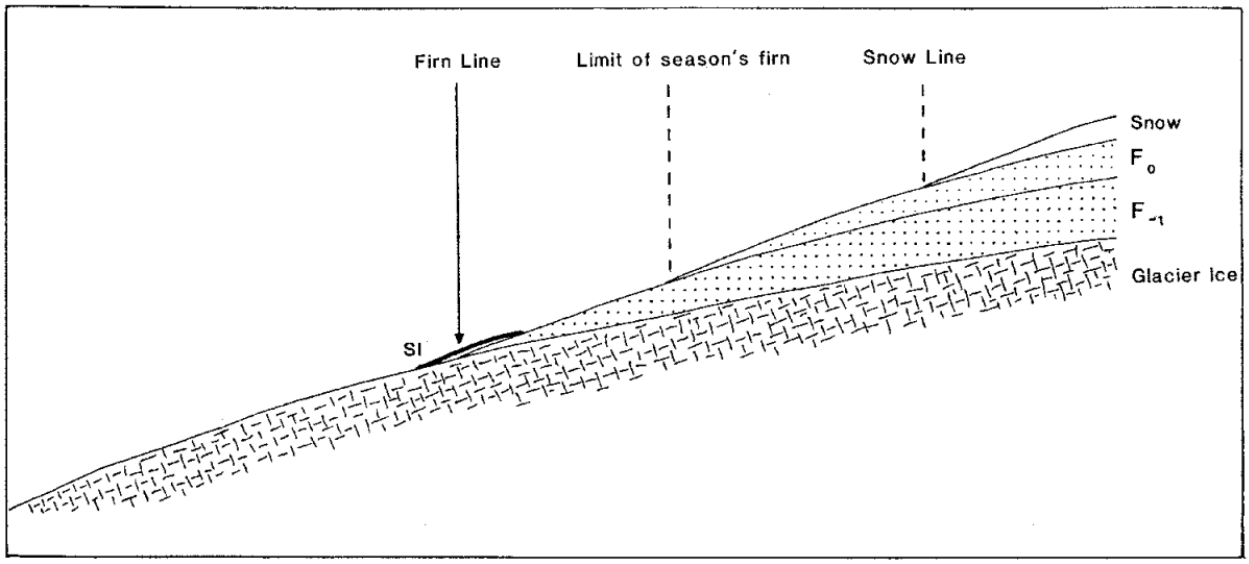

Fig. 1. Glacier faces – scheme for Icelandic glaciers, where F0 is firn one year old or less, and F_{-1} is firn older than one year. The superimposed ice (SI) is located around the firn line indicating the patchy nature of the firn line and superimposed ice (Brown et al. 1999)

In late summer Mýrdalsjökull studies, two facies were distinguished: the ablation facies (bare glacier ice) and the wet-snow facies (consisting of melting snow and/or firn) separated by TSL (FL) which at the end of balance year equals ELA (Jaenicke et al. 2006).

Williams et al. presented different even more simplified, glacier-faces concept adjusted to remote sensed satellite data (Williams et al. 1991). He noted that even though at the end of balance year ELA of glaciers in temperate climates usually overlie the FL or SL, this border may not be unambiguous due to superimposed ice. In such cases, the EL is displaced down-glacier from the snow or firn line (Williams et al. 1991).

2.4. Glacier flow and surging glaciers

Glacier flow is generally triggered by the gravity. The movement has an important influence on glacier mass exchange. As a result, the ice flows far below the snowline into areas where the melting significantly outweighs snowfall.

Movement is the result of both ice deformation and slide on the surface. The thermal structure of the glacier determines the rheological properties of ice (plastic deformations and material flow), hence the rate of its melting. For temperate (warm-based). and polythermal glaciers speed, crucial is slipping on the surface, associated with the amount of meltwater that reached the subglacial surface. Increased ablation due to global warming may lead to an acceleration of the movement (Jania 1997).

There are also glaciers that, from time to time, experience a sudden acceleration of movement speed and advance. These are so-called surging glaciers. The movement may be faster by about one or two orders of magnitude than in non-surging glaciers. One of the most famous surges was an advance of approximately 8 km, 45 km wide Brúarjökull glacier in Iceland in 1963 – 1964 when it reached the velocity of 5 m h^{-1}. The relatively short active phase of a surge is separated by a long phase, in which such glacier behaves similarly to normal glaciers (Jania 1997). Duration of surge intervals varies between glaciers, lasting from several years up to a century (Björnsson and Pálsson 2008). Surges leads to significant changes in the glacier profile and usually a great advance of glacier front (Jania 1997). Due to increased melting, also the runoff of glacial rivers rises (Björnsson and Pálsson 2008). Surge can be determined by many conditions. The main ones are changes in the thermal structure of the glacier, dynamics of shear stress, the nature of the subglacial surface, etc. (Molewski 2005).

2.5. Fluctuation of glacier fronts

Fluctuations of glaciers are related to glacier fronts (termini) variations but are not a direct indicator of mass balance changes (which is regulated also by processes like thinning, surges etc.). Reasons for glacier fluctuations include changing mass balance exchange between the glacier and the environment as well as the glacier flow.

With a constant ice flow to ablation zone, intensified ablation will have an effect in front recession. Acceleration at the turn of spring and summer coincides with a more intensive ablation, which usually prevents termini advancement, and most often dominates, so recession takes over. The wane of ablation in autumn and winter allows seasonal advance, despite the fact that the ice flow is smaller than in the summer. The role of accumulation is less visible (Jania 1997).

Termini reaction to climatic change is delayed. The time period between the input impulse and reaching the new equilibrium state by the glacier is called a response time (Jania 1997; Jóhannesson and Sigurdsson 1998).

2.6. Glacial hydrology and jökulhlaup phenomena

Most glaciers acquire water through surface melting, rainfall, and runoff on an impermeable ice surface, as well as through melting of ice in contact with the ground surface. The latter is influenced by, among other things, geothermal activity. In volcanic areas, a stream of geothermal energy from the Earth's interior is so intense that vast subglacial lakes can be formed. Geothermal energy melts the glacier from below and traps the water inside the ice cauldron (Kargel et al. 2014). Ice of temperate glaciers, characteristic for the temperate marine climate, is soaked with water and both phases are in equilibrium. Surface streams are rare due to easy ice penetration (Jania 1997).

There might also occur episodic great glacial outburst floods (is. jökulhlaup) (Jania 1997). Jökulhlaup might have different genesis – might happen either as a result of subglacial volcanic and/or geothermal activity as well as an effect of subglacial or proglacial (ice-marginal) lake dam failure (Kargel et al. 2014). Jökulhlaup significantly shape the landscape (Björnsson and Pálsson 2008) – this is an important geomorphological factor. Glacial outburst floods transport large amounts of material from eruption spot to the foreground to glacial outwash plain. These processes are enhanced by an explosive eruption, which creates significant amounts of fine-grained tephra. The rapid outflow of water creates sandur plains and deltas in the foreland. The effect of the erosive activity of the water is subglacial canyons cut into the landscape (Kargel et al. 2014; Molewski 2005). Some major Icelandic river canyons have been formed through such catastrophic floods during the Pleistocene (Björnsson and Pálsson 2008). The sudden glacial outburst floods pose a great threat to inhabited areas, roads and bridges built near the glacier (Björnsson and Pálsson 2008; Jania 1997).

3. Study area

3.1. Basic information

The study area is located in Iceland, an island situated in the Atlantic Ocean, slightly south of the Arctic Circle. Despite being just outside the threshold latitude, Iceland is still counted as an Arctic region (AMAP 2017). In the west, the Denmark Strait separates it from Greenland. Its area is about 103 000 km² (Guðjónsdóttir 2015). The island is tectonically distinct from Europe, but the Republic of Iceland culturally belongs to Europe's Nordic countries. It is the most westerly European country.

Invariably, as in historical times, life is concentrated along the coast. The towns and villages are connected by a road running around the island. The 2016 Icelandic census counted 333,000 inhabitants (Statistics Island).

The capital and the largest city of the state is Reykjavík – the northernmost capital of the world. In 2016, according to the census list, there were 123 000 residents (as of 01.01.2016; Statistics Island).

Iceland is currently divided into 8 regions, 74 municipalities, and 6 constituencies. The analyzed glaciers are situated in Suðurland – the southern region.

3.2. Geology and volcanism

The Icelandic basalt plateau covers an area of approximately 350 000 km². Only 30% of this area rises above the ocean level in the form of a 103 000 km² island (Molewski 2005).

Iceland emerged from the Atlantic about 25 million years ago. Given the geological time, it is one of the younger islands on Earth (the age of the Earth is estimated to be about 4.5 thousand million years) (Kohut and Kwaśniak 2012). Iceland continues to evolve - in a small area of the island, there are concentrated continually active phenomena and processes that in the past formed the contemporary surface of the Earth. This is because Iceland is founded on an active crust rifting zone - the Mid-Atlantic Ridge (MAR), which forms the border between the North American Plate and the Eurasian Plate. Part of the MAR that includes the island of Iceland is called Reykjanes Ridge (Fig. 2). Location on the divergent type of boundary, where lithosphere plates drift away from each other results in the occurrence of numerous endogenous processes (Molewski 2005). As the Earth's mantle is melting (due to decompression) and solidified on the surface (mainly in the form of basalts – alkaline igneous (magmatic) effusive rocks), the island is constantly being built. The SW-NE orientation of the MAR causes the symmetrical age distribution of rocks – the youngest rocks occur in the central part of the island along the running rift, while the oldest form the eastern and western fringes of the island and are dated to the Miocene (Kohut and Kwaśniak 2012).

Iceland is the area most seismically active in Europe – volcanic eruptions occur relatively frequently, on average every 3-4 years, with half of the events being subglacial eruptions (Kargel et al. 2014). A series of parallel fissure volcanoes runs through the middle of the plateau (Fig. 2). There are about 130 volcanic cones. Out of these, more than 20 are active volcanoes (Sudnik-Wójcikowska 2011). The scientific interesting fact is an island on the southern coast of Iceland – Surtsey. It emerged on the surface November 14, 1963, as a result of the submarine eruption (Kokelaar and Durant 1983).

The glaciers that are the subject of this study are in close relations with volcanoes. Beneath the ice of Mýrdalsjökull is the Katla volcano, and Eyjafjallajökull incase the volcano of the same name (Fig. 2). The largest Icelandic volcanic eruption in the 20th Century was that of Katla volcano in 1918 (Molewski 2005). Another ‘well known’ eruption in Iceland took place in March and April 2010 of the Eyjafjallajökull volcano (Kohut and Kwaśniak 2012).

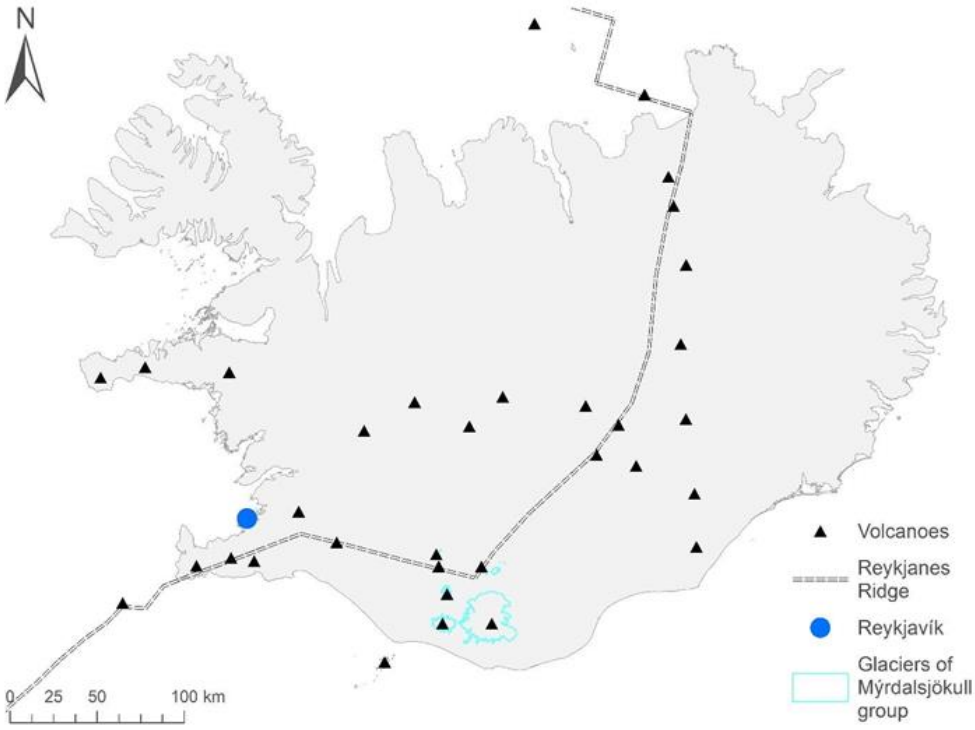

Fig. 2. Reykjanes Ridge (MAR) dividing Northamerican and Eurasian Plates and locations of Icelandic volcanoes (based on data from National Land Survey of Iceland; GLIMS and NSIDC (2005, updated 2017): Global Land Ice Measurements from Space glacier database. Compiled and made available by the international GLIMS community and the National Snow and Ice Data Center, Boulder CO, U.S.A.; USGS ScienceBase; USGS Earthquake Hazards program)

3.3. Topography, hydrology and land use – land cover

The landscape in Iceland is mainly shaped by volcanic activity. It is dominated by heights and a plateau (Fig. 3, 8) with extensive tuff and lava cover, 700-1000 m high, sloping steeply towards the seashores (Sudnik-Wójcikowska 2011). Lowlands are situated in the coastal zone belt. The highest located point of the island is the Hvannadalshnúkur summit (2110 m a.s.l.) – a mountain peak of volcanic origin – the remains of the highly eroded Öræfajökull volcano. Together with the adjacent peaks, it protrudes in form of a nunatak (peak rising above the ice surface) from the Vatnajökull glacier. The mountain lies in the area of the Skaftafell National Park (Kargel et al. 2014).

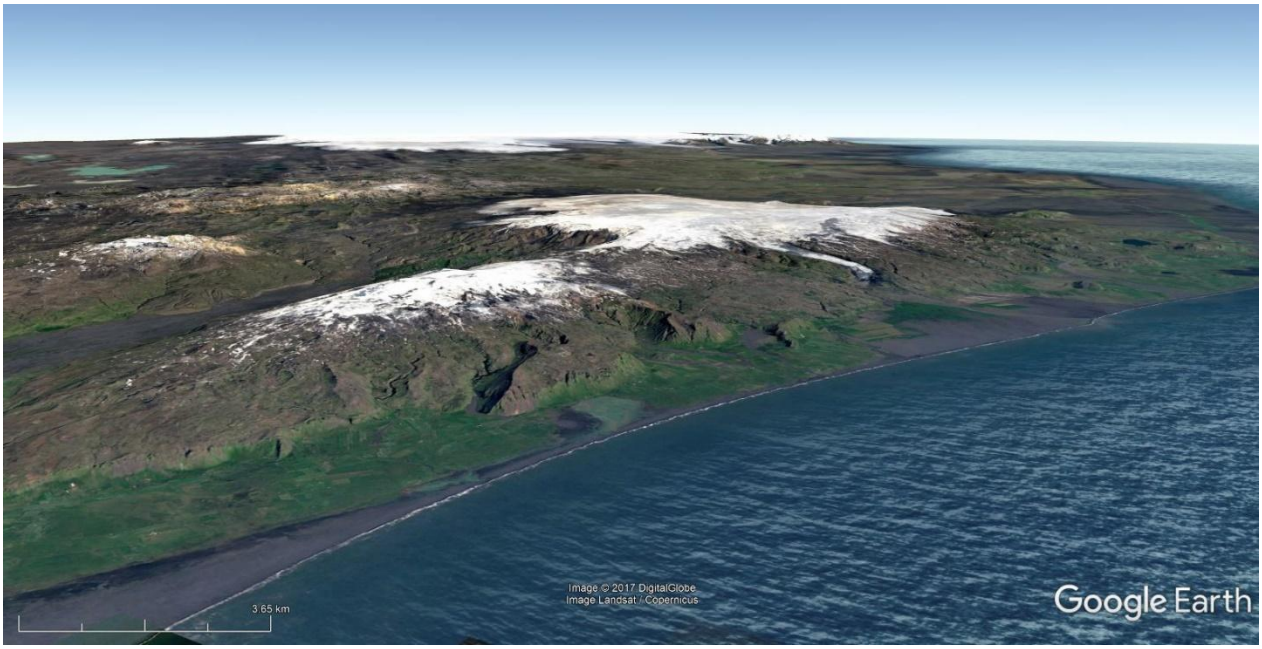

Fig. 3. An overview of the Mýrdalsjökull region (Google Earth: Landsat / Copernicus)

Major rivers in Iceland are fed by glaciers - the glacial contribution is estimated at around one-third of the total runoff (Björnsson and Pálsson 2008). Many of them have been developed to generate hydropower. Glacial outburst floods (jökulhlaup) occurs episodically.

According to the Corine Land Cover (CLC) project data (release v.18.5. dated 02/2016), most of the Iceland area is covered with open spaces with little or no vegetation (49%) and scrub and/or herbaceous vegetation associations (38%). From these major groups, moors and heathlands covers slightly more than 1/3 (34%) of total area of the island, next there are bare rocks (23%), sparsely vegetated areas (13%) and glaciers and perpetual snow (10%) (Fig. 4) (EEA – CLC).

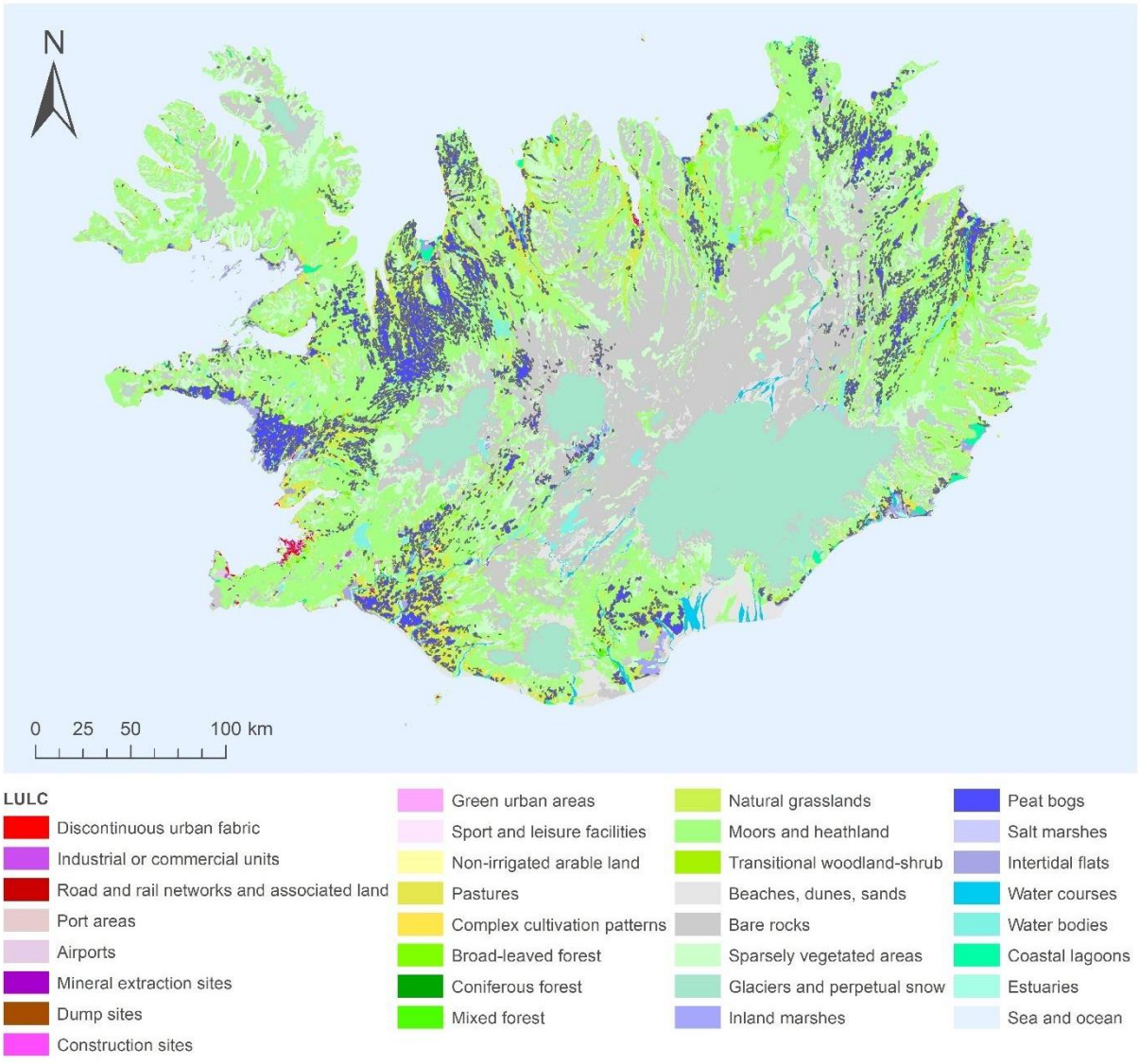

Fig. 4. Land use – land cover (LULC) map of Iceland (based on Corine Land Cover (CLC) European Environment Agency (EEA) program data, release v.18.5. dated 02/2016)

3.4. Climate

Located in the Atlantic Ocean, slightly south of the Arctic Circle, the island has a maritime climate with high precipitation (Molewski 2005). The climate is relatively warm, especially on the southern and western coasts. The climate is strongly affected by sea currents.

The extension of the Gulf Stream – the North Atlantic warm sea current, flows to Iceland from the south. Its branch – warm Irminger Current – flows from east to west along the southern coast of Iceland, flows the island around clockwise, bringing a mass of warm air (Bonecki 1974). Concurrently, from the North comes the East Greenland Current – a cold sea current, compassing the east coast of Greenland, flowing south through the Danish Strait to Farvel Cape in the south of Iceland. In the south, it links with the warm Irminger Current. It is indictable for the harsh climate of northern Iceland. The current carries ice packs and icebergs from the Arctic.

Monthly average temperatures vary from -11°C to 6°C during winter, and from -2°C to 12°C in summer. The climate is milder along the coastline and cools down as the elevation rise (Fig. 9).

Precipitation is higher in the south-east and in the peninsula of Vestfirðir (Westfjords). It also increases with elevation. It ranges from 400 mm to more than 2000 mm (Fig. 9). The major Icelandic ice caps receive an annual precipitation greater than 2000 mm (Kargel et al. 2014).

Five meteorological stations located in the nearest neighborhood of the Mýrdalsjökull glaciers group were selected to investigate the climatic conditions in the study region (Tab. 1; Fig. 5). For the stations mean monthly temperature and precipitation values were calculated for the period 1950 to 2016 (Fig. 6).

Tab. 1. Meteorological stations located close to the study area Mýrdalsjökull group (Icelandic Meteorological Office)

ID	Name	Location	Height above sea-level [m a.s.l]
1	Vatnsskarðshólar	63°25.416'N, 9°10.982'W	20
2	Sámsstaðir	63°44.122'N, 0°06.544'W	90
3	Hella	63°49.541'N, 0°21.923'W	20
4	Básar á Goðalandi	63°40.745'N, 9°28.883'W	239
5	Kirkjubæjarklaustur – Stjórnarsandur	63°47.583'N, 8°00.717'W	22

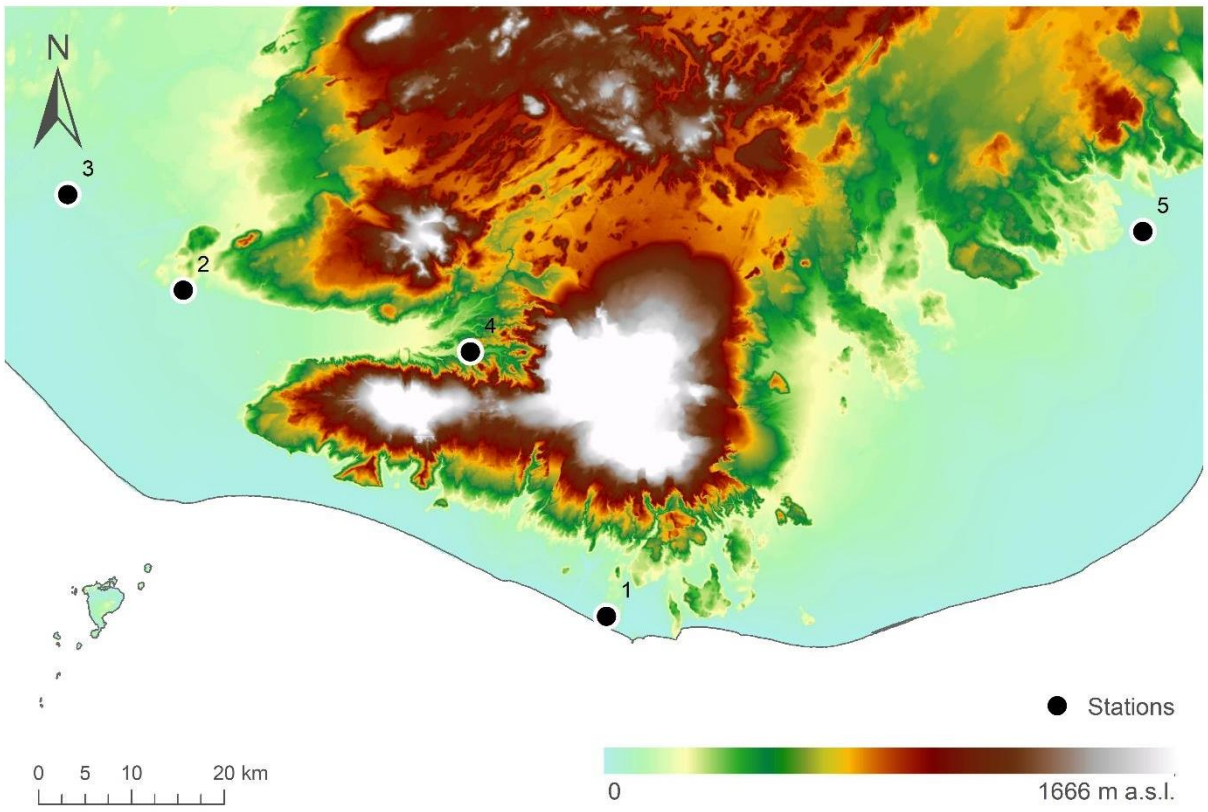

Fig. 5. Meteorological stations located close to the Mýrdalsjökull group (labels as per ID in Tab. 1.) (Icelandic Meteorological Office; based on data from National Land Survey of Iceland, www.lmi.is)

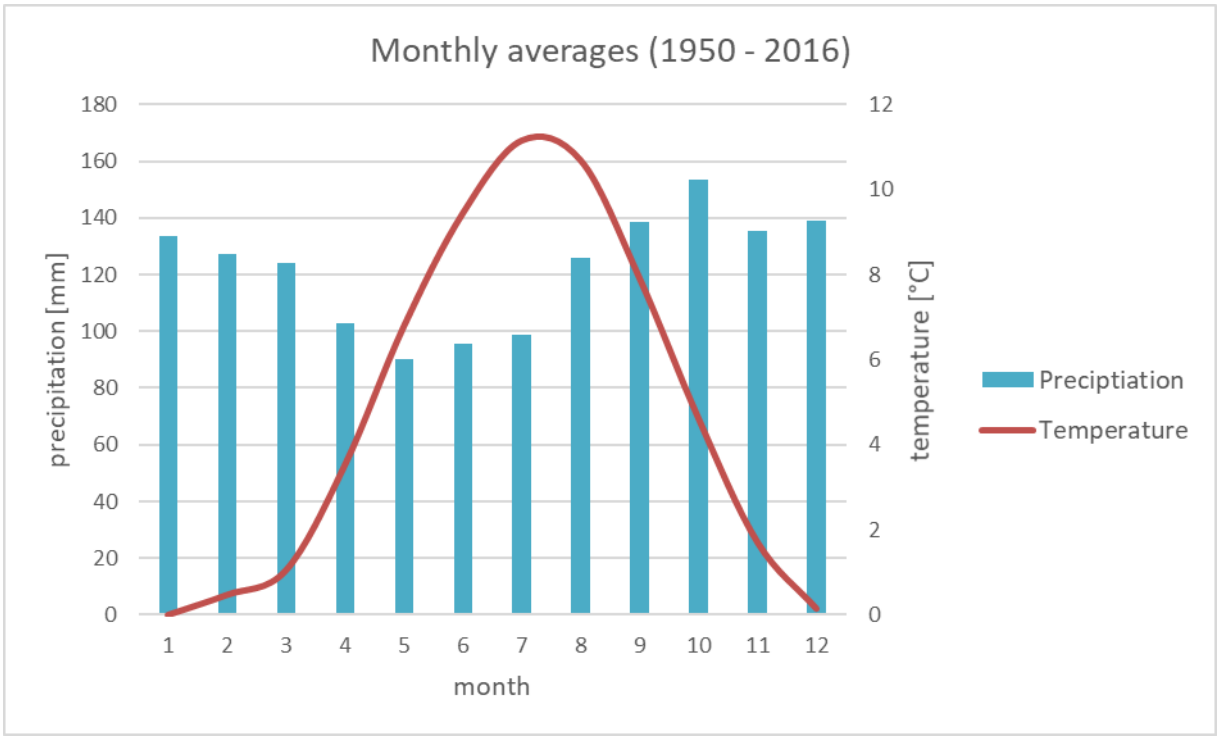

Fig. 6. Monthly average temperature and precipitation in Mýrdalsjökull group region (Icelandic Meteorological Office)

The temperature rises steadily from March, reaches its maximum (about 11°C) at the turn of July and August and drops at the turn of August and September. Precipitation is higher during Autumn and Winter.

Mean annual air temperatures and precipitation were also calculated for the period 1950 – 2016 (Fig. 7). In addition to the average temperature, daily mean maximums and daily mean minimum were also computed. Increasing trends were found for all the three temperature parameters. During the last 65 years, annual air temperature has raised by approximately 1-1.5°C. It is especially noticeable for average daily minimum temperatures. The increase was especially pronounced from the 1980s. Simultaneously also the precipitation records raised steadily. Both whole-year precipitation as well as winter season precipitation (snow) were calculated. For both similar trends were observed.

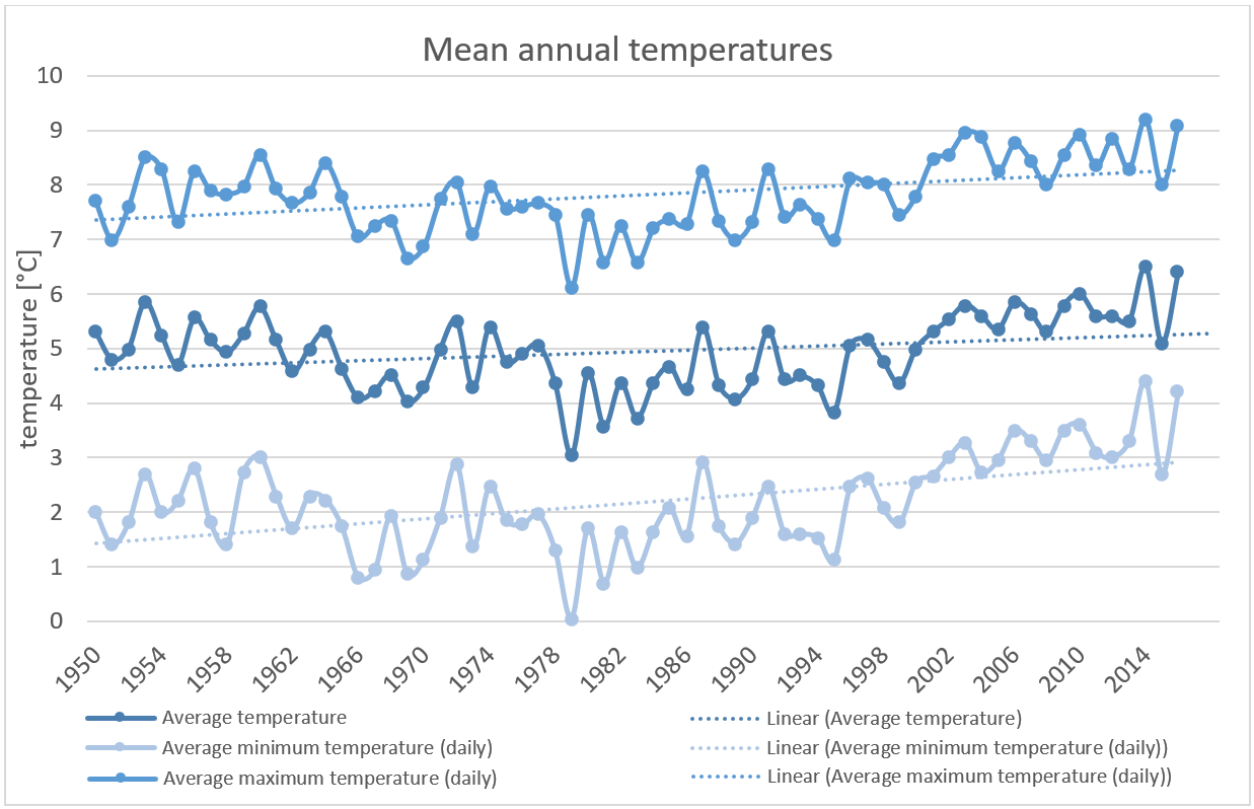

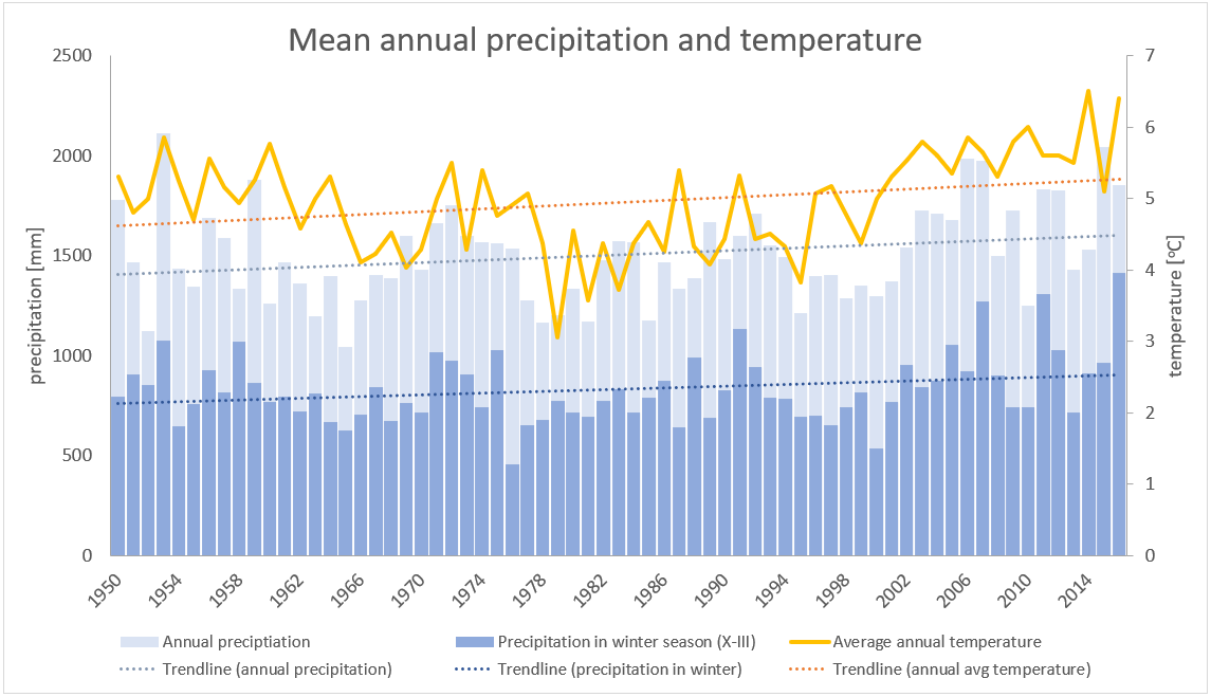

Fig. 7. Mean annual air temperatures (top) and mean annual air temperature and precipitation in Mýrdalsjökull group region (bottom) (Icelandic Meteorological Office)

3.5. Glaciers

Currently, glaciers (is. Jökull) occupy more than 11 000 km^2, which is about 11% of the area of Iceland (Tab. 2) (Kargel et al. 2014; Orheim 2013). The ice volume accumulated in the Icelandic glaciers is estimated to be about 3600 km^3 (Björnsson et al. 2013; Jóhannesson et al. 2013). The largest ice caps are located in the southern and central highlands. The largest is Vatnajökull ice cap with an area of over 8000 km^2 (Kargel et al. 2014).

Tab. 2. Biggest Icelandic glaciers and their area (Kargel et al. 2014)

Name	Type	Area [km^2]	Year of analysis
Vatnajökull	ice cap	8086	2000
Langjökull	ice cap	920	2000
Hofsjökull	ice cap	889	1999
Mýrdalsjökull	ice cap	597	1999
Drangajökull	ice cap	146	2004
Eyjafjallajökull	ice cap	80	2003
Tungnafellsjökull	ice cap	38	2000
Þórisjökull	ice cap	30	2000
Eiríksjökull	ice cap	22	2000
Tindfjallajökull	mountain glacier	15	2000
Torfajökull	mountain glacier	11	1999
Þrándarjökull	ice cap	17	2000
Snæfellsjökull	ice cap	12	2002
Hrútfellsjökull	ice cap	7	2000
Hofsjökull (eystri)	ice cap	5	2000
Okjökull	mountain glacier	4	2000
North	-	179	2004–2006
East	-	13	2003
Other	-	8	-
Total	Iceland glaciers	11 079	-

Glacier distribution in Iceland reflects topographical and climatic conditions (Molewski 2005; Ingólfsson website). Icelandic glaciers are generally located in highlands and mountains (Fig. 8) (Ingólfsson website). Snow line runs relatively low. On the southern slopes of Vatnajökull and Mýrdalsjökull glaciation limit lies at 1100 m a.s.l. and rises to around 1700 m a.s.l. in rain shadow north of Vatna. In the northernmost parts of the island (Vestfirðir West Fjords), it drops to about 550 m a.s.l. The development of local ice covers is also favored by the terrain relief, especially the extensive basalt plateaux, craters and volcanic ridges (Fig. 8) (Kargel et al. 2014; Molewski 2005).

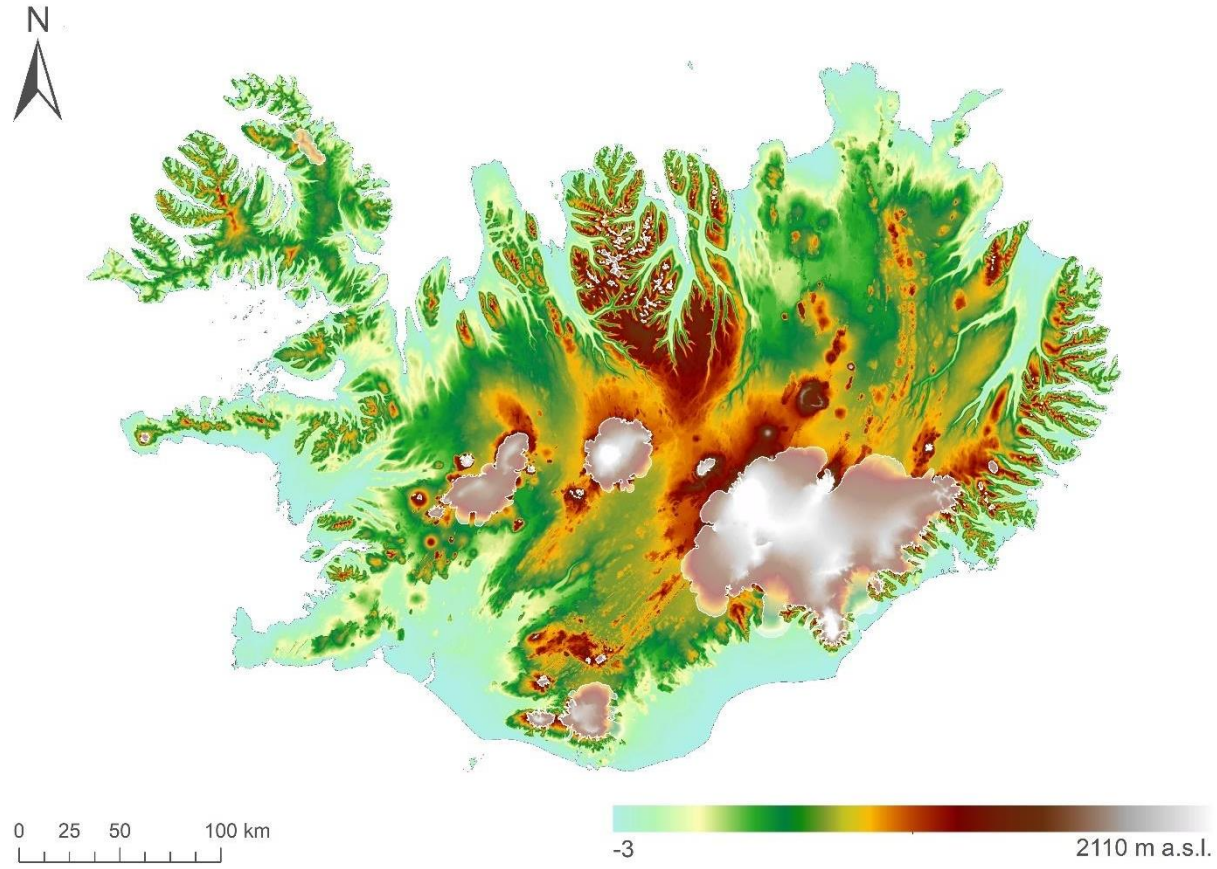

Fig. 8. Glaciers distribution in Iceland on the background of DEM. It shows clear influence of topographical relief and elevation on the presence of glaciers (denoted in semi-transparent white). (based on data from National Land Survey of Iceland www.lmi.is; GLIMS and NSIDC (2005, updated 2017): Global Land Ice Measurements from Space glacier database. Compiled and made available by the international GLIMS community and the National Snow and Ice Data Center, Boulder CO, U.S.A.)

The principal climate factors comprise mean annual temperature (especially summer temperature) and mean annual precipitation (especially winter precipitation) (Fig. 9) (Kargel et al. 2014). Glaciers receive around 20% of the total precipitation that falls on Iceland. When the glaciers are in a steady state, they contribute to about 20% of river runoff and infiltration to groundwater aquifers. It is particularly important for Iceland since many glacier-fed Icelandic rivers have been harnessed for generating hydropower (Jóhannesson and Sigurdsson 1998). On top of the larger ice caps, mean temperatures are below or close to 0°C throughout the year, with most of the precipitation falling as snow (Fig. 9). In addition, accumulation might be locally increased through snow drift. At the same time melting might be reduced by the shadowing effect in narrow valleys (Björnsson and Pálsson 2008).

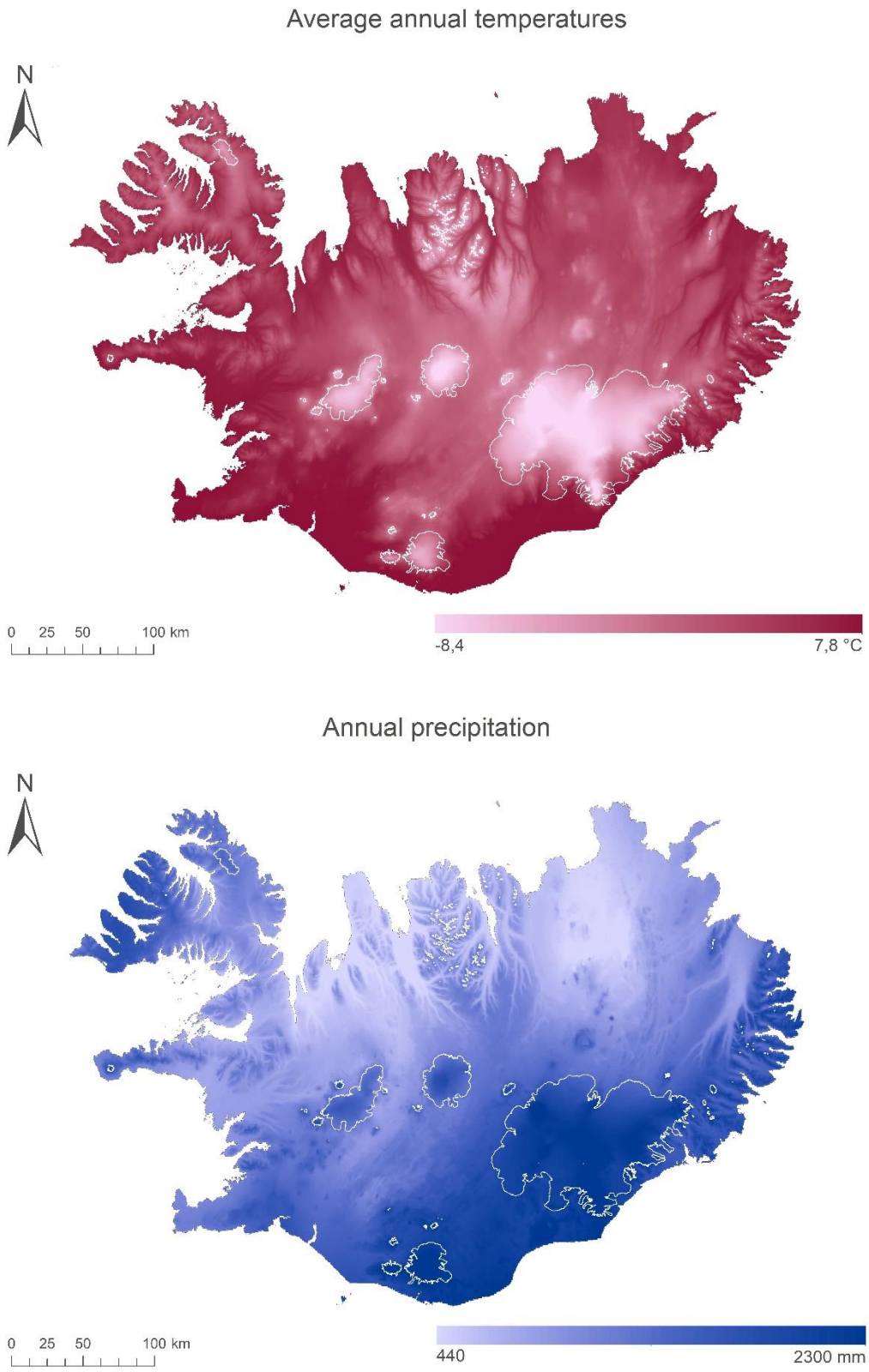

Fig. 9. Annual average temperatures (top) and precipitation (bottom), and the spatial distribution of the Icelandic glaciers (derived from WorldClim version 2 average monthly climate data for 1970-2000 Fick, S.E. and R.J. Hijmans, 2017. Worldclim 2: New 1-km spatial resolution climate surfaces for global land areas. International Journal of Climatology.; GLIMS and NSIDC (2005, updated 2017): Global Land Ice Measurements from Space glacier database. Compiled and made available by the international GLIMS community and the National Snow and Ice Data Center, Boulder CO, U.S.A.)

Iceland's glaciers represent various types, e.g. ice caps with associated glaciers, ice flow basins, cirque glaciers, mountain glaciers, and valley glaciers (Tab. 2; Kargel et al. 2014). In the mountainous highlands of central northern Iceland, numerous small cirque glaciers and rock glaciers can be found (Ingólfsson website). The largest glaciers form ice caps (is. jökulhetta). An ice cap has the shape of a convex dome (Jania 1997) and an area of less than 50 000 km^2 (Górzyńska 2008). It covers the surface relief (Jania 1997), several internal or marginal nunataks might occur (Górzyńska 2008). In Iceland, many volcanoes are covered with ice caps including Mýrdalsjökull and Eyjafjallajökull. Usually, an ice cap has at least one or more glacial outlets, they can take the form of mountain or valley glaciers, depending on the topography of the terrain (Górzyńska 2008). A number of outlet glaciers can be classified as ice falls (is. falljökull) e.g. Gígjökull – an outlet glacier from the Eyjafjallajökull (Ingólfsson website). Ice caps, especially in temperate zones of the Northern Hemisphere, are very vulnerable and sensitive to climate change (Jania 1997; Williams et al. 1997)

Icelandic ice domes are classified as so-called temperate (warm-based) glaciers. The source of thermal properties of temperate glaciers is the sufficient amount of snowmelt waters, which percolate through the accumulation zone and freezes inside the ice. Temperate glaciers are typical for mild climatic conditions with high winter accumulation and strong summer ablation, giving the necessary amount of meltwater in the accumulation zone. The constant temperature close to the melting point keeps ice and water in equilibrium (Jania, 1997)

In Iceland catastrophic glacial outburst floods (is. jökulhlaup) are frequent – there are about five to ten jökulhlaups per year (Björnsson and Pálsson 2008; Kargel et al. 2014). They are associated with fifteen glacial lakes (Molewski 2005). Glaciological hazards in Iceland includes both types of jökulhlaup – volcanic and lacustrine (Kargel et al. 2014). The largest ice eruptions occur in the neo-volcanic zone under the Vatna and Mýrdals ice caps.

3.6. Iceland's glacial history and current trends

Over the course of the Pleistocene, there were several glacial-interglacial cycles in Iceland (Molewski 2005). During the last glaciation (Vistulian glaciation – the youngest of the Pleistocene glaciations), Iceland was almost completely covered with glacial ice (Kargel et al. 2014). Whereas during the Holocene Climatic Optimum the glaciers disappeared almost completely – only high mountain ice caps retained (Björnsson and Pálsson 2008; Flowers et al. 2008; Geirsdóttir et al. 2009).

Both during the glacial and warming periods, the island was strongly shaped by glacial and fluvioglacial processes – both erosion and sedimentation. The glaciers changed the mountain landscape, carved U-shaped valleys, and fjords. Fluvioglacial sediments were deposited in the southern and western parts of the island, which enabled later agricultural use of these areas. Glacial rivers eroded the canyons. From the sediments transported by the river current, sandurs were formed in the river deltas (Björnsson and Pálsson 2008).

Since the settlement of the island around the 9th century, the climate has remained relatively warm (Björnsson and Pálsson 2008). The major glaciers were preserved during this period, however, they were significantly smaller than in the 20th century (Kargel et al. 2014).

With the end of the Medieval Warm Period, a cooling period called the Little Ice Age followed. Woods, pastures and inhabited areas were overrun by glaciers (Sigurðsson 2005). At that time some glacier outlets extended around 10 – 15 km. In southern Iceland, the firn line crept down from 1100 to 700 m (Björnsson and Pálsson 2008). Glaciers reached their maximum extent around 1890 (Kargel et al. 2014; Sigurðsson 2005; Orheim 2013). It was the greatest post-glacial advance of Icelandic glaciers (Sigurðsson 2005).

Since the 20th century, there has been a loss of glacial mass. This retreat became quite rapid especially since the 1930s. The climate, however, began to cool down again, and so, many glaciers started to advance in the 1970s (Björnsson and Pálsson 2008; Orheim 2013).

In the last decade of the 20th century, the recession began to dominate again, and in 1995 virtually all non-surging glaciers had started retreating again (Fig. 10) (Björnsson and Pálsson 2008; Jóhannesson and Sigurdsson 1998; Orheim 2013; Sigurðsson 1998, 2005; Sigurðsson et al. 2007) and thinned very rapidly in response to the warmer climate (Sigurðsson 2005). Since the mid-1990s, a majority of the Icelandic glaciers have been undergoing mass loss at an

average rate of 0.3% a year (Kargel et al. 2014; Sigurðsson 2005). Glaciers decreased proportionally to their size, several smaller glaciers have completely disappeared leaving only remnants such as ice-cored moraines (Jóhannesson et al. 2007): 3 mountain glaciers and 3 outlet glaciers that receded into their respective ice caps (Kargel et al. 2014)

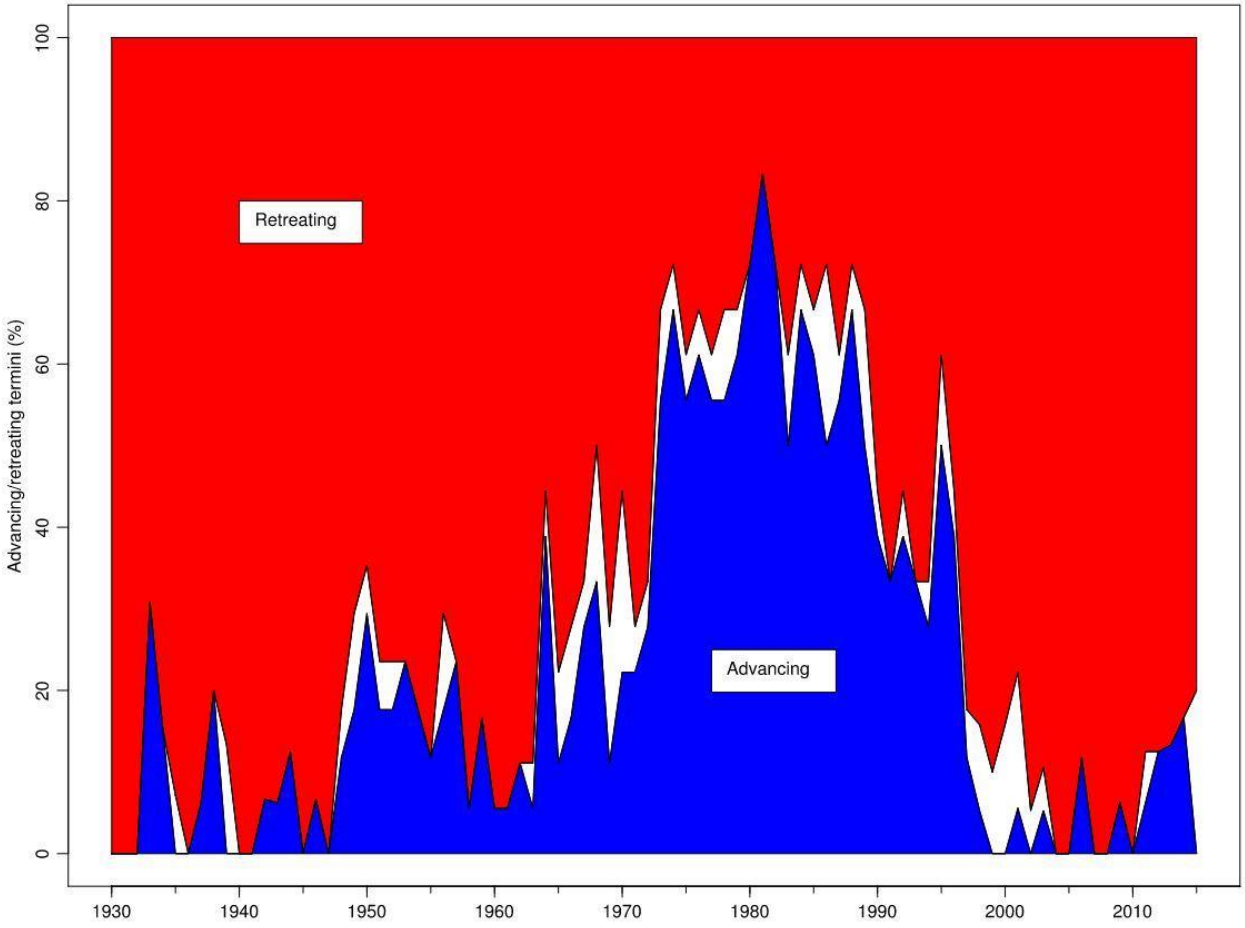

Fig. 10. The relative proportion of advancing and retiring Icelandic glaciers termini during the last Century (Iceland Glaciological Society)

During the first decade of the 21st century, Icelandic glaciers have shrunk faster than ever since 1930 (Jóhannesson and Sigurdsson 1998; Sigurðsson 1998).

The recent warming trend continues to the present day. Plausible future scenarios projected Icelandic glaciers to be reduced by more than half within the next 100 years. At such a melting rate, Iceland is likely to become nearly totally deglacierized (except for ice at the highest elevations) by 2200 (Björnsson and Pálsson 2008; Jóhannesson et al. 2007).

Glacier variations in Iceland since 1930 (when Iceland Glaciological Society began glacier monitoring) show a clear response to changes in climate (Jóhannesson and Sigurdsson 1998; Kargel et al. 2014). The driving factor for glacier fluctuations is rising temperature, rather than precipitation (Björnsson and Pálsson 2008; Jaenicke et al. 2006; Jóhannesson and Sigurdsson 1998; Sigurðsson et al. 2007).

Non-surge-type glaciers usually almost immediately react to mass balance changes (Sigurðsson et al. 2007). Long-term comparison of changes in the position of non-surging glacier fronts with the average summer temperature shows that the reactions of glacier fronts (advancement or retreating) to climate changes were delayed by just a few years (Górzyńska 2008; Jóhannesson and Sigurdsson 1998). Variations of surge-type glaciers are primarily dependent on the surge events. Nonetheless, the impact of climate change is also noticeable in long-term observations (Jóhannesson and Sigurdsson 1998). For surging glaciers, these relationships are less obvious and more difficult to determine (Górzyńska 2008; Jóhannesson and Sigurdsson 1998).

3.7. The Mýrdalsjökull group

Icelandic glaciers can be subdivided into eight regional groups (Fig. 11). This study is focused on the Mýrdalsjökull group in Suðurland (Southern Region).

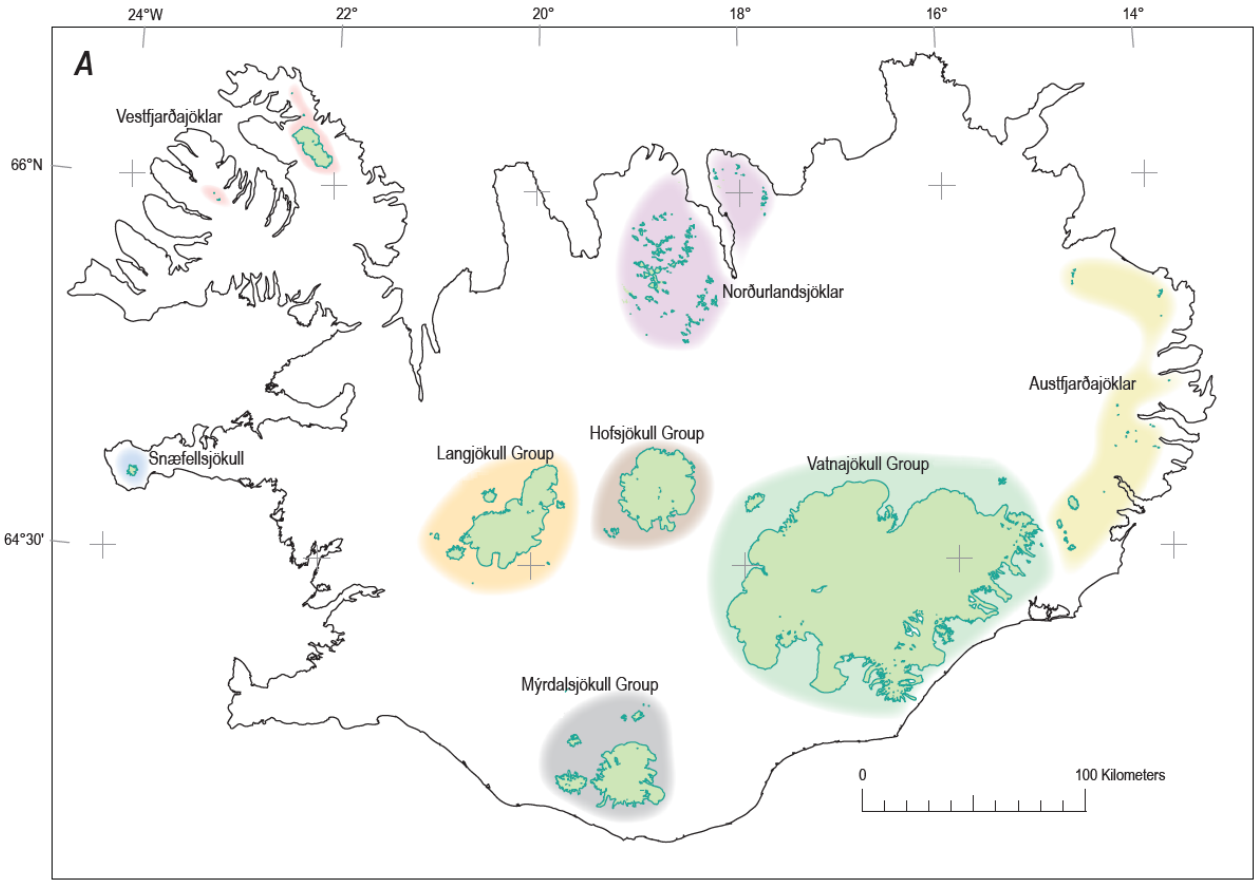

Fig. 11. Regional groups of Icelandic glaciers (adapted from Geographic Names of Iceland's Glaciers: Historic and Modern, Sigurðsson and Williams 2008)

Mýrdalsjökull group includes two main ice caps – the major Mýrdalsjökull (Fig. 12.a) and the smaller Eyjafjallajökull (Fig. 12.b) with associated outlet glaciers and several minor glaciers in the northern part: Torfajökull ice cap, Kaldaklofsjökull, Tindfjallajökull (Tindafjallajökull), Blesárjökull (Sigurðsson and Williams 2008) (App. 1). Detailed analyses were performed on Mýrdalsjökull and Eyjafjallajökull ice caps.

Mýrdalsjökull is a temperate (warm-based) ice cap. It is the 4th largest Icelandic glacier of an area of 597 km^2 (as of 1999) (Tab. 2.), (Kargel et al. 2014). The glacier rises to about 1300-1500 m above the surrounding lowland (Björnsson et al. 2000). It is associated with numerous outlet glaciers (App. 1; Fig. 12.a), including two surge-type glaciers – Sléttjökull on the North and Öldufellsjökull North-East (Sigurðsson and Williams 2008). Recently recorded surge-events associated with Öldufellsjökull took place in 1974, 1984, 1989 (WGMS 2017) while Sléttjökull experienced a surge in 1992 (WGMS 2017). These events are easily readable from termini variation charts (Fig 13; App. 2)

In the south-eastern part, the glacier sits astride the active Katla volcano (Fig. 2) (Sigurðsson 1998; Sigurðsson and Williams 2008). The volcano caldera encircles an area of more than 100 km^2 (Björnsson et al. 2000; Sigurðsson 1998) and is 600 to 750 m deep. It is surrounded by numerous ridges that radiate out from the caldera (yet, none towards south), so that the mountain rises to rims reaching up to 1380 m a.s.l. Katla is considered to be one of the most seismically active and hazardous volcanoes in Iceland. Twenty eruptions have been documented over the last 1100 years. Most of them caused catastrophic jökulhlaups that flowed southeast down to the Mýrdalssandur outwash plain. Presently, geothermal activity is manifested by several small ice cauldrons of the diameter of 0.5-1 km. Meltwater is frequently drained in small jökulhlaups. (Björnsson et al. 2000). Recent jökulhlaup occurred from Sólheimajökull Vesturtunga (W) on the 18th of July 1999 (WGMS 2017).

The glacier has high rates of summer melting and receives heavy winter precipitation (both main ice caps – Mýrdalsjökull and Eyjafjallajökull exceed annual precipitation of 4000–5000 mm, peaking even at 7000 mm (Kargel et al. 2014) and is thus drained by many rivers. The meltwater reaches the glacier bed via numerous veins, crevasses, and moulins, where it fuses with basal meltwater produced by frictional and geothermal heat. Subglacial drainage takes place through a number of conduits and tunnels. In the foreland, water joins glacial rivers. (Björnsson et al. 2000).

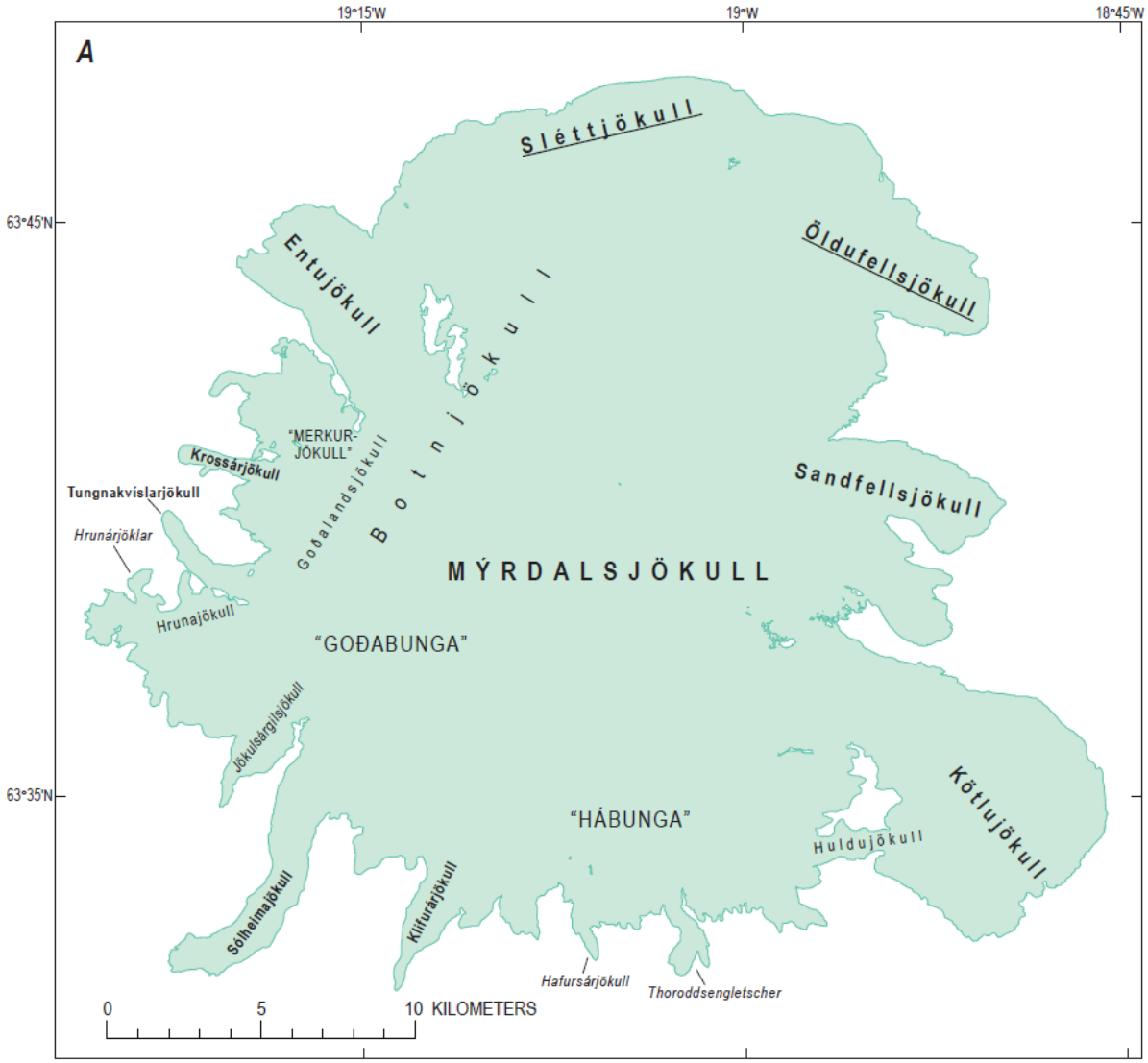

Fig. 12.a. Mýrdalsjökull ice cap, outlet glaciers, and other glacier-associated places (from Geographic Names of Iceland's Glaciers: Historic and Modern, Sigurðsson and Williams 2008)

Eyjafjallajökull is a temperate (warm-based) ice cap. It is the 6th largest Icelandic glacier covering an area of 80 km^2 (as of 2003) (Tab. 2.), (Kargel et al. 2014). It is one of the oldest named Icelandic glaciers – its name comes from the mountain massif it covers (Sigurðsson and Williams 2008).

In recent years Eyjafjallajökull became 'well known' for the eruption of the volcano of the same name which lies directly beneath the glacier (Fig. 2). It took place in March and April 2010. After 187 years of silence, the sub-glacial volcano Eyjafjallajökull awoke. The first eruption began on the 20th of March 2010. Volcanic activity gradually faded, but on the 14th of April, it arose again. Through the central caldera lava and a huge amount of pyroclastic material have been ejected. A cloud of hot volcanic ash and tephra partially fell in the nearby area, but the smallest particles floated and were spreading in the atmosphere for many days. Due to suspended eruption plume, air traffic in Europe was severely disrupted. Another consequence were floods on the rivers flowing from the Eyjafjallajökull slopes (Kohut and Kwaśniak 2012; WGMS 2017).

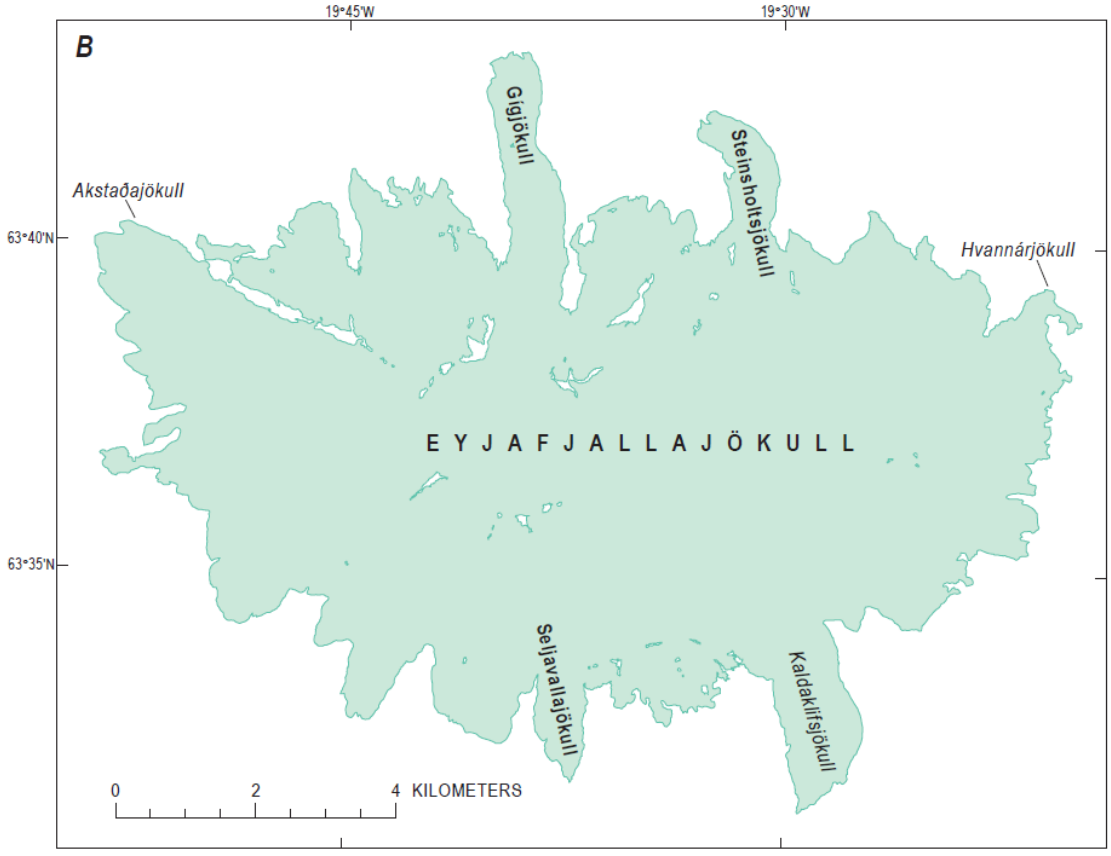

Fig. 12.b. Eyjafjallajökull ice cap, outlet glaciers and other glacier-associated places (from Geographic Names of Iceland's Glaciers: Historic and Modern, Sigurðsson and Williams 2008)

The ice caps of Mýrdalsjökull group follow the fluctuation trend observed in other Icelandic glaciers (Fig. 11, 13; App. 2). Several associated outlet glaciers' front positions were systematically monitored. Both World Glacier Monitoring Service (WGMS) and Iceland Glaciological Society measurements virtually coincide (App. 2, 3). From the 1930s to 1970s there was a general downturn in glaciers extent recorded. Then up to mid-1970s some advancement was noted but before the 21st century a sharp drop was observed, and glaciers continue retreating until today (Fig. 13; App 3). It is most clearly presented on Sólheimajökull termini measurements – it is the best documented and the longest continuously observed outlet glacier. In comparison with 1930, the glacier retreated by almost 1.8 km until 2015 (App. 2) **(**WGMS 2017; Iceland Glaciological Society)**.** Measurements of Mýrdalsjökull thickness shows that between 2010 and 2015, the glacier thinned for about 1.9 m (App. 3) (WGMS 2017).

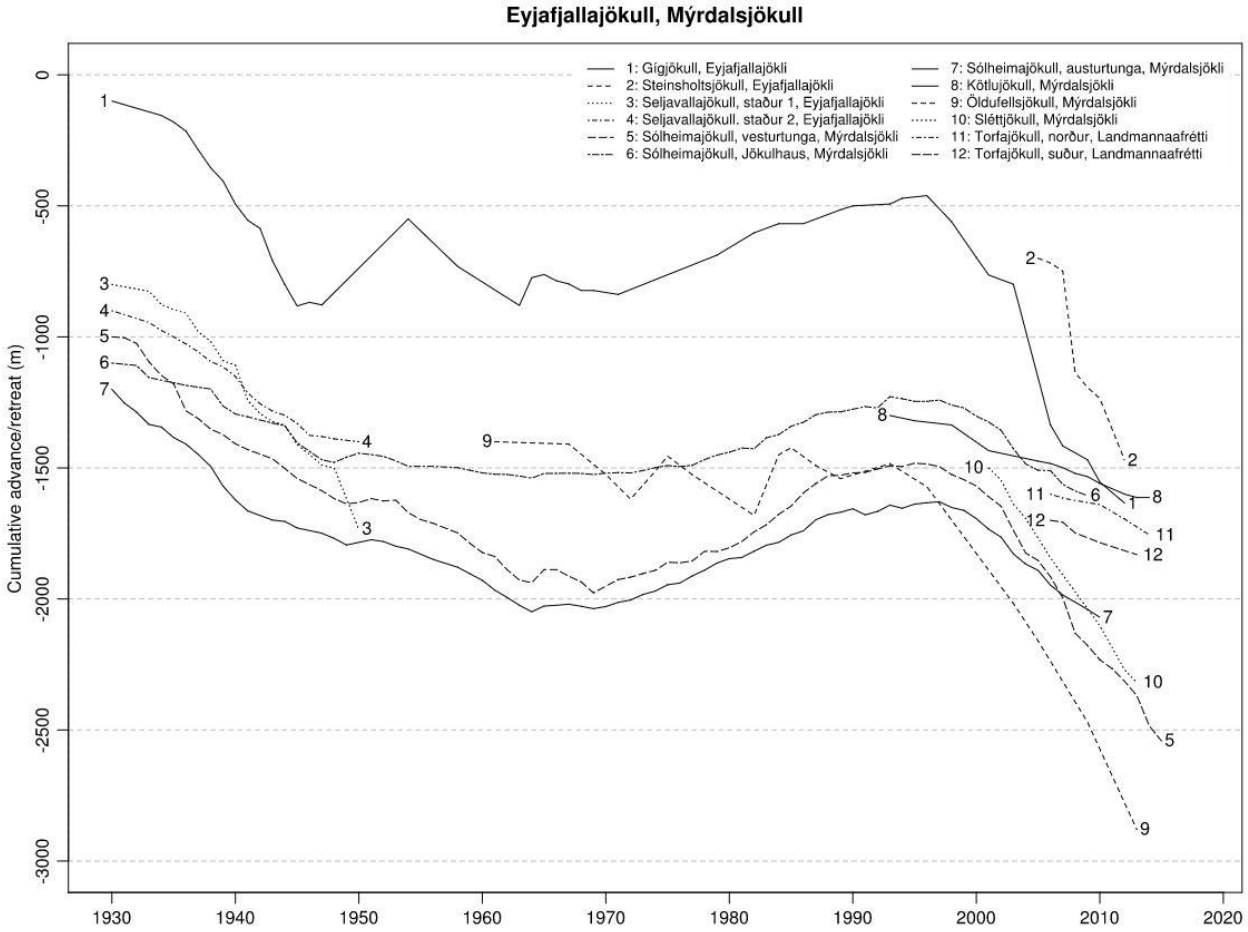

Fig. 13. Glaciers termini variation – Mýrdalsjökull group (Iceland Glaciological Society)

4. Data and methods

4.1. Remote sensing – theory

Each and every object emits, reflects and absorbs the energy all the time (unless its absolute 0 temperate −273.15°C) (NASA – Earth Observatory). Radiation (energy emitted by the body) can take a form of, for instance, acoustic waves, gravitational radiation (used in e.g. GRACE mission – Gravity Recovery and Climate Experiment) or, commonly used in the satellite remote sensing, electromagnetic radiation.

Photons (elementary particle of electromagnetic radiation) travel at the speed of light (approximately 300 000 km sec^{-1}) in form of waves. An electromagnetic wave is composed of electric and magnetic fields. The amount of radiation depends preliminary on the temperature of the emitter (the energy). The frequency rises with the temperature and the wavelength shorten. Consequently, in lower temperatures, longer waves are emitted with lower frequency (NASA – Earth Observatory).

The entire wide array of electromagnetic waves constitutes the electromagnetic spectrum. Gamma and X-rays are found on the highly energetic end of the spectrum. As the energy decreases the ultraviolet regions spans. Only a narrow range of visible light can be perceived by the human eye (400 – 700 nm). Further part of the spectrum is occupied by infrared waves. This portion of radiation comprises: Near Infrared (NIR), Short Wavelength Infrared (SWIR), and longer wavelengths referred as Thermal Infrared (TIR). Visible and NIR waves are abbreviated jointly as VNIR. Longer wavelengths are transmitted in form of microwaves and radio waves.

All ranges of radiation are influenced by the atmosphere. Solar radiation, like Earth's reflected radiation, is scattered (diffusion by particles of e.g. dust, fumes, molecules of atmospheric gases), reflected or absorbed.

Atmospheric influences depend on the wavelength. In the area of visible light, in which the Sun emits the highest intensity radiation, the atmospheric transmissivity is highest (atmospheric window). In the range of larger wavelengths, the transmissivity is reduced to narrow bands. Part of the radiation spectrum is absorbed (absorption bands), mainly by water vapor (H_2O) e.g. in form of clouds, carbon dioxide (CO_2) and ozone (O_3).

Elements of the Earth's landscape reflect the various ranges of radiation with different intensity. Variation of spectral responses of a given object in respective electromagnetic spectrum intervals is known as its spectral signature. Knowledge of the spectral signatures can be used for discrimination and identification of an object and assessing its properties.

Remote sensing of Earth can be made by sensors mounted onrd airborne (aircrafts, balloons, drones – aerial photography) or spaceborne platforms (satellites, space shuttles). Earth observation satellites travel across the sky in specific orbits distinguished based on their altitude and position in relation to Earth (polar e.g. Sun-synchronous; or geosynchronous e.g. geostationary – a satellite hovers over a single location on the equator).

Considering the source of the radiation, the remote sensing techniques can be distinguished into two groups. Passive systems use energy from outside sources e.g. reflected solar radiation or thermal radiation emitted by the object. To the contrary, active remote sensing system has its own source of radiation. The signal is sent from the instrument and, after being reflected by the observed object, it is registered by the receiver of this instrument. The signal can be in form of e.g. microwaves (radar – Radio Detection and Ranging), optical light (lidar – Light Detection and Ranging) or acoustic waves (sonar – Sound Navigation and Ranging).

There are four different types of resolutions that characterize remote sensing image. They depend on the sensor and platform abilities.

- Spatial resolution determines the area of the terrain, which is represented by one pixel of the remote sensing image.
- Temporal resolution determines the revisiting time (repeat cycle).
- Radiometric resolution determines the number of levels into which the range of signal received in each channel is divided (Adamczyk and Będkowski 2005).
- Spectral resolution determines the number of channels collecting measurements from particular wavelengths (number of atmospheric windows the sensor operates in). The narrower the range of radiation in a channel that the sensor is tuned to collect (spectral bandwidth), the more precise the detector (Adamczyk and Będkowski 2005).

4.2. Remote sensing in cryosphere research

Remote sensing plays an important role in the glacier monitoring. It not only supports and facilitates traditional field studies, but also extends the array of variables that can be measured. Satellite observations have also enabled a major step forward towards a uniform global glacier monitoring (Pellikka and Rees 2009). A number of worldwide projects have been launched to support this idea (e.g. World Glacier Inventory – WGI by World Glacier Monitoring Service – WGMS, later GLIMS – Global Land Ice Measurements from Space; European Space Agency's Climate Change Initiative – ESA's CCI).

The glacier monitoring is not only an end in itself. It is important also for the following objectives (Pellikka and Rees 2009):

- understanding interactions between glaciers and climate
- detection of climate and environmental change due to glaciers climate sensitivity
- validation of climate models and scenarios
- assessment of glacier changes impacts to the environment (e.g. global sea level, water resources, natural hazards etc.)

In the cryospheric research, data from both passive and active sensors are applied. VNIR imaging makes use of different spectral responses of various environmental components including snow and ice of different characteristics in the visible and infrared range of the electromagnetic spectrum. The technique is useful in studying 2D features of glaciers.

There are various remote sensing methods used in glacier mapping (Paul 2000) based on multispectral VNIR imagery. These includes:

- manual outline delineation
- ratio images thresholding (segmentation)
- supervised and unsupervised classification methods

In relation to other elements of the environment, such as water, soil or vegetation; snow cover is characterized by a high reflection of radiation in visible wavelengths and low degree of reflection in the SWIR. Generally, the reflectance of snow and ice drops with the crystal size and wavelength (Fig. 14). The highest reflectance is characteristic for fine snow and frost, while

coarse granular snow and glacier ice have relatively low reflectance values. It is mainly an effect of air-ice interfaces reduction and consequently scattering decrease. Impurities (such as dust and soot) also lower the snow reflectance (depending on a load of debris) (Tedesco 2014). In general, the reflectance values drop dramatically between NIR and SWIR windows. The low reflection in the SWIR is related to water content (ESA – EduSpace).

Typically, during the winter, glaciers are entirely covered with snow. As the seasonal snow melts in the summer, the ice is getting exposed. The reflectance decreases as snow ages and thus undergoes melting/refreezing cycles (Jonsell et al. 2003) (Fig. 14). Therefore, generally, the glacier reflectance increases from terminus to upper elevations (Tedesco 2014).

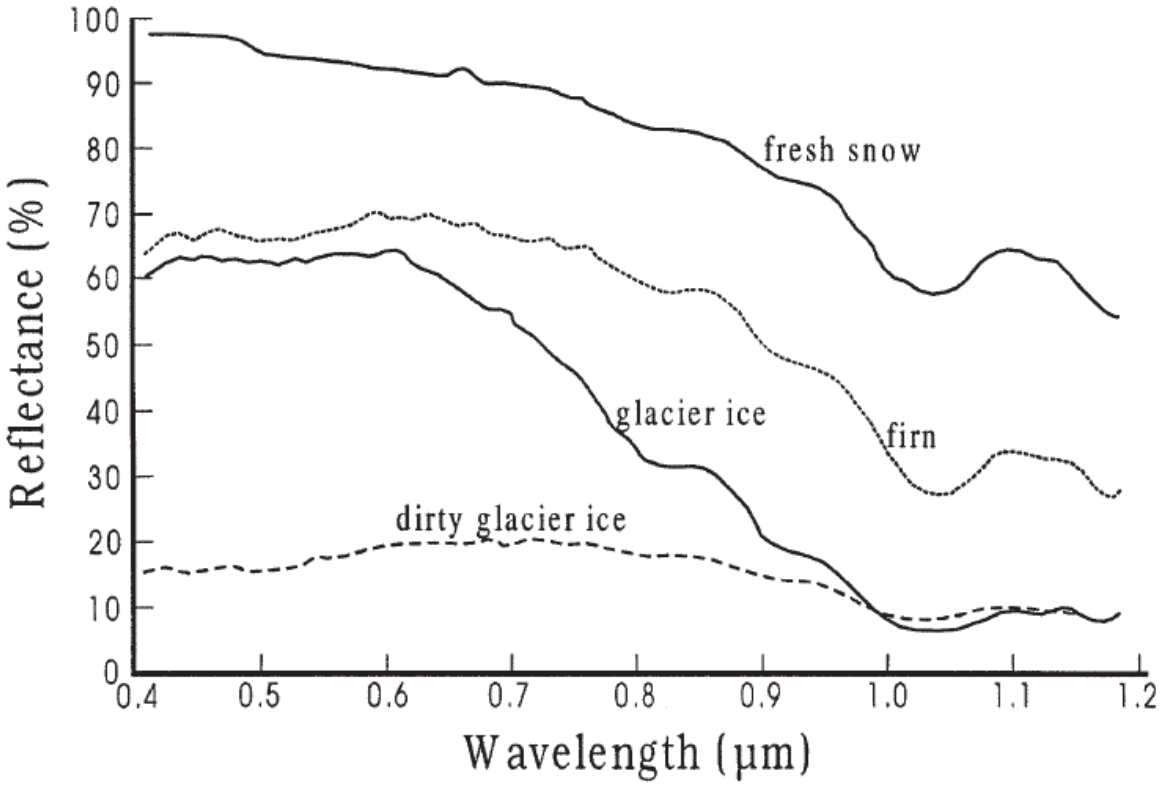

Fig. 14. Spectral reflectance curves of different snow and ice cover types in VNIR spectrum (Gao and Liu 2001)

4.3. Landsat mission

The Landsat program is implemented by NASA (National Aeronautics and Space Administration) and USGS (United States Geological Survey).

As the name suggests the satellites are designed to collect information about the lands (in contrary to the Seasat series which aim is to acquire data about the seas and oceans). Data are widely used in many sectors – in science, change detection, biodiversity conservation, natural hazards and crisis management (Young et al. 2017).

In the program framework, eight satellites have been launched so far. The first one – Landsat 1 was launched on the 23rd of July 1972, and since then the Landsat Earth images archive is constantly expanding. It is the longest continuous satellite Earth observation program.

According to a classification suggested by Young et al. (2017), based on their characteristic, the Landsat satellites can be organized into three groups (Fig. 15.):

- The first group includes Landsat 1 – 3. These platforms carried the Multispectral Scanner (MSS). Data were recorded in four spectral bands; two visible and two near-infrared (NIR). Landsat 1-3 had a revisit interval of 18 days.
- The next group includes Landsat 4 – 7. Landsat 4 and 5 were in addition to the MMS scanner onboard also equipped with Thematic Mapper (TM). Landsat 6 carried Enhanced Thematic Mapper (ETM) but failed to achieve orbit. Landsat 7 has an Enhanced Thematic Mapper Plus (ETM+) instrument and is still active. Satellites from this generation deliver images of finer spatial resolution, increased radiometric resolution and augment the spectral resolution of the MSS group with the addition of a middle-infrared/shortwave infrared (SWIR) and thermal-infrared wavelengths bands.
- The last group currently consists of Landsat 8, equipped with Operational Land Imager (OLI) and Thermal Infrared Sensor (TIRS). The OLI expanded spectral coverage of its predecessor adding deep blue and cirrus bands and the TIRS added an extra thermal band. Landsats 4 – 8 have the revisit interval shortened to 16 days.

In December 2020 the new member will join the group – to maintain the continuity of Landsat data collection, a new Landsat 9 launch has been scheduled (NASA – Landsat Science).

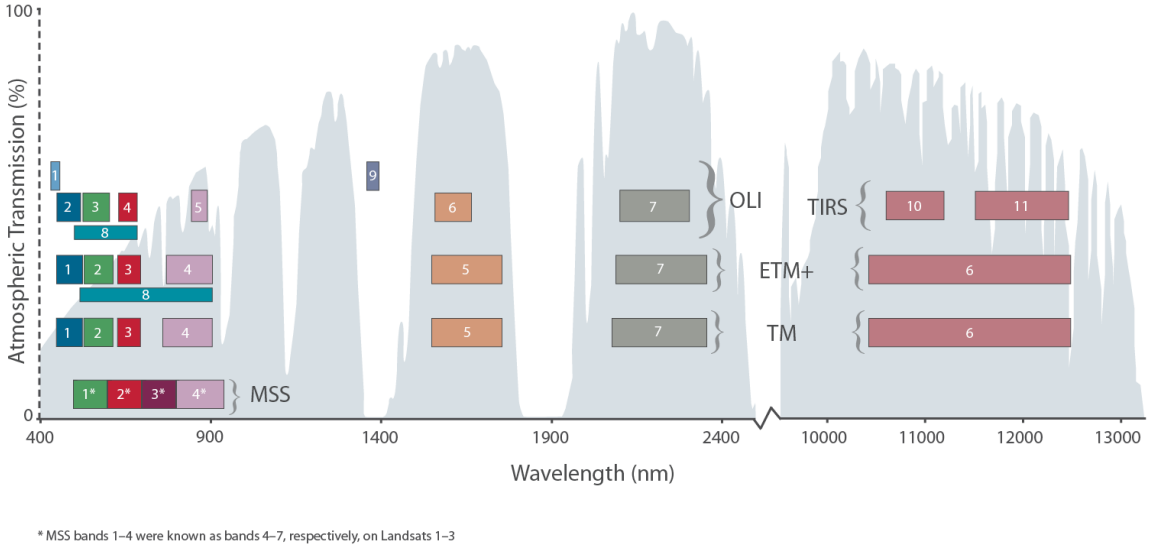

Fig. 15. Visual comparison of Landsat spectral bands (NASA – Landsat Science)

4.4. Data search and selection

The suitable Landsat scenes were identified for the study area and Landsat path/row shapefiles were downloaded from Landsat missions section on USGS website.

Landsat data are cataloged according to the Worldwide Reference System (WRS). Due to different satellites orbit altitudes Landsats 1-3 follow WRS-1 while Landsats 4-8 – WRS-2 (Young et al. 2017). Since the desired scenes should have been acquired in the period between 80's and today, the WRS-2 footprints were used.

For this study, only the daytime images were needed and therefor footprints of descending node were used (indicating the satellite traveling direction from north to south).

There are three path/row (PR) combinations that covered the study area and meet above conditions (Fig. 16). These are PR: 218015, 218016 and 219015. However, the first pair would need to be mosaiced in order to create a continuous surface across the Mýrdalsjökull group (Fig. 16). Knowing the path/row identifier enables to search for these specific scenes that cover the whole area of interest and skip these that only overlap the small fragment of it.

The data used was from 1982 (when the new generation of Landsat satellites – Landsat 4 was launched) to present. Only imageries from August and September were taken into consideration. This was decided due to the fact that the late summer (the end of a mass balance year), is, as mentioned before, the most suitable season to outline glaciers and delineate equilibrium line altitude (ELA) which is then equal to transient snow line (TSL). These parameters further enable to define the accumulation and ablation zones of the glacier.

For Landsat 7, only images when the sensor was fully operated (SLC-on mode) were used. On the 31st of May 2003, there was a failure of Scan Line Corrector (SLC) and since then there are no-data gaps in the Enhanced Thematic Mapper Plus (ETM+) images.

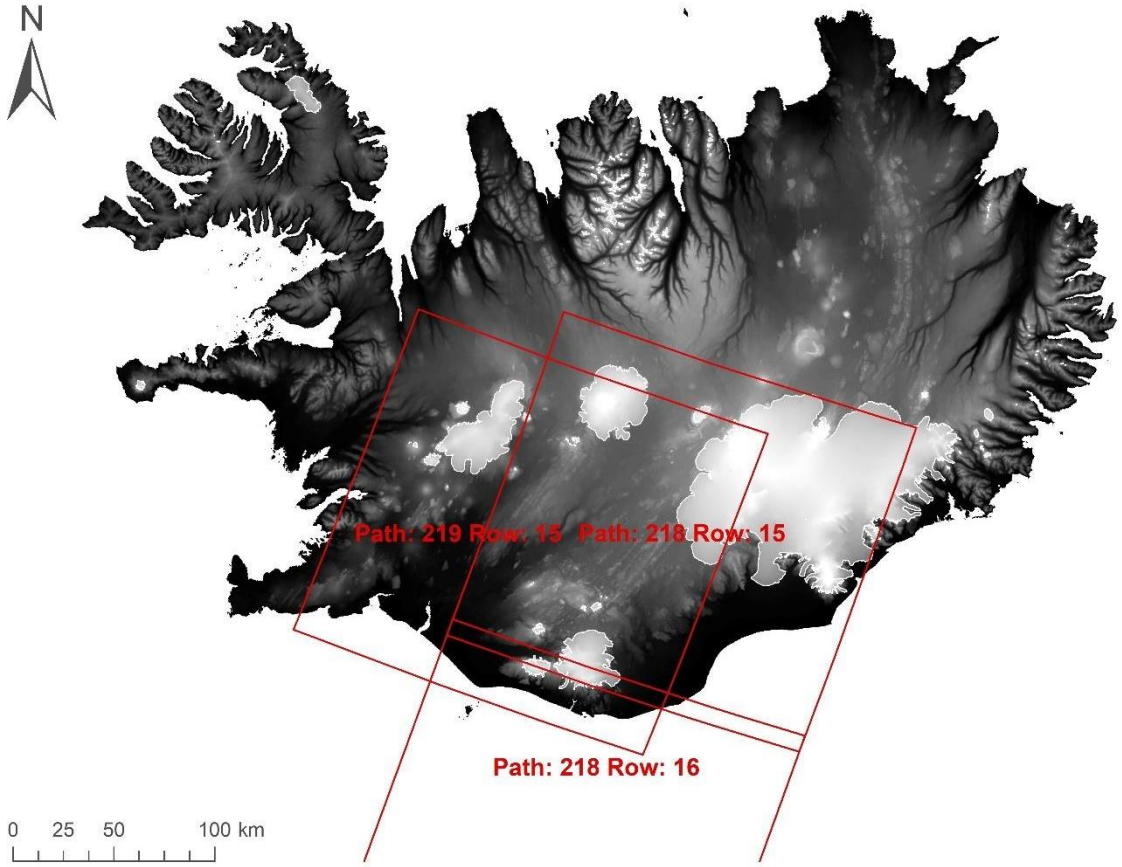

Fig. 16. Landsat footprints (path/row combinations) covering the study area – Mýrdalsjökull group (based on data from National Land Survey of Iceland, www.lmi.is; United States Geological Survey – Landsat Missions)

It was decided that the land cloud cover has to be less than 40%. In addition, each scene was inspected manually and only the ones with no or a negligible amount of clouds above the Mýrdalsjökull group were selected.

Landsat 4, 5, 7 and 8 are structured into Collections. The images acquired most recently are inventoried as Real-Time images and after processing are directed into one of the Tiers depending on their quality. Only the images that were placed into Landsat Collection Tier 1 were taken into account. This assured that only the scenes with the highest available quality have been selected.

In order to obtain images suitable for time series analysis, imageries have to be co-registrated. Datasets processed to Level 1 Precision and Terrain Correction (L1TP) assure the highest quality of the product. Data are calibrated and geometrically corrected using ground control

points (GCPs) and digital elevation model (DEM). The process requires sufficient reference data. Root Mean Square Error (RMSE) for the images cannot be higher than 12 m. Only datasets which meet L1TP criteria were considered.

After selecting all the above-mentioned conditions, the scenes that met the criteria were selected (Tab.3).

Tab. 3. Preselected Landsat Imageries

Acquisition date	Satellite and Sensor	Path	Row
15.08.1986	Landsat 5 (TM)	218	15
15.08.1986	Landsat 5 (TM)	218	16
07.09.1986	Landsat 5 (TM)	219	15
16.09.1986	Landsat 5 (TM)	218	15
16.09.1986	Landsat 5 (TM)	218	16
20.08.1988	Landsat 5 (TM)	218	15
20.08.1988	Landsat 5 (TM)	218	16
12.09.1988	Landsat 5 (TM)	219	15
12.08.1994	Landsat 5 (TM)	219	15
12.08.2014	Landsat 8 (OLI/TIRS)	218	15
12.08.2014	Landsat 8 (OLI/TIRS)	218	16
20.09.2014	Landsat 8 (OLI/TIRS)	219	15

Thus, the desired images were either acquired by Thematic Mapper (TM) sensor carried by Landsat 5 or taken by Operational Land Imager (OLI) on Landsat 8. It is worth to note that these two sensors differ in spectral resolution (Tab. 4.a, 4.b). The scene size for both is approximately 170 km NS by 183 km EW.

Tab. 4.a. Landsat Thematic Mapper (TM) sensor carried on Landsat 5

Bands		Wavelength [μm]	Resolution [m]
1	Blue	0.45-0.52	30
2	Green	0.52-0.60	30
3	Red	0.63-0.69	30
4	Near Infrared (NIR)	0.76-0.90	30
5	Shortwave Infrared (SWIR) 1	1.55-1.75	30
6	Thermal	10.40-12.50	120 (resampled to 30)
7	Shortwave Infrared (SWIR) 2	2.08-2.35	30

Tab. 4.b. Landsat Operational Land Imager (OLI) and Thermal Infrared Sensor (TIRS) carried on Landsat 8

Bands		Wavelength [μm]	Resolution [m]
1	Ultra Blue (coastal/aerosol)	0.435 – 0.451	30
2	Blue	0.452 – 0.512	30
3	Green	0.533 – 0.590	30
4	Red	0.636 – 0.673	30
5	Near Infrared (NIR)	0.851 – 0.879	30
6	Shortwave Infrared (SWIR) 1	1.566 – 1.651	30
7	Shortwave Infrared (SWIR) 2	2.107 – 2.294	30
8	Panchromatic	0.503 – 0.676	15
9	Cirrus	1.363 – 1.384	30
10	Thermal Infrared (TIRS) 1	10.60 – 11.19	100 (resampled to 30)
11	Thermal Infrared (TIRS) 2	11.50 – 12.51	100 (resampled to 30)

Firstly, the LandsatLook images for these scenes were downloaded (Fig. 17). The products served as the next line of sifting through the Landsat data. The images are compressed and optimized stretched, which make them perfect for image selection and visual interpretation. Nonetheless, they are not suitable for performing the analysis.

LandsatLook image with geographic references bundle contains:

- Natural Color Image (false color SWIR – NIR – Red composite; Fig. 17)
- Thermal Image
- Quality Image

The Quality Image is derived from Landsat Level-1 Quality Band. It enables the user to quickly preview the quality of pixels composing the scene and assess the usefulness of the image for the planned application. It can point out phenomena such as cloud and cloud shadow, indicate snow and ice and, in case of the OLI/TIRS sensor, also cirrus occurrence (Fig. 17).

Scenes from patch 218 were mosaiced into a new raster using ArcGIS ArcMap ESRI software.

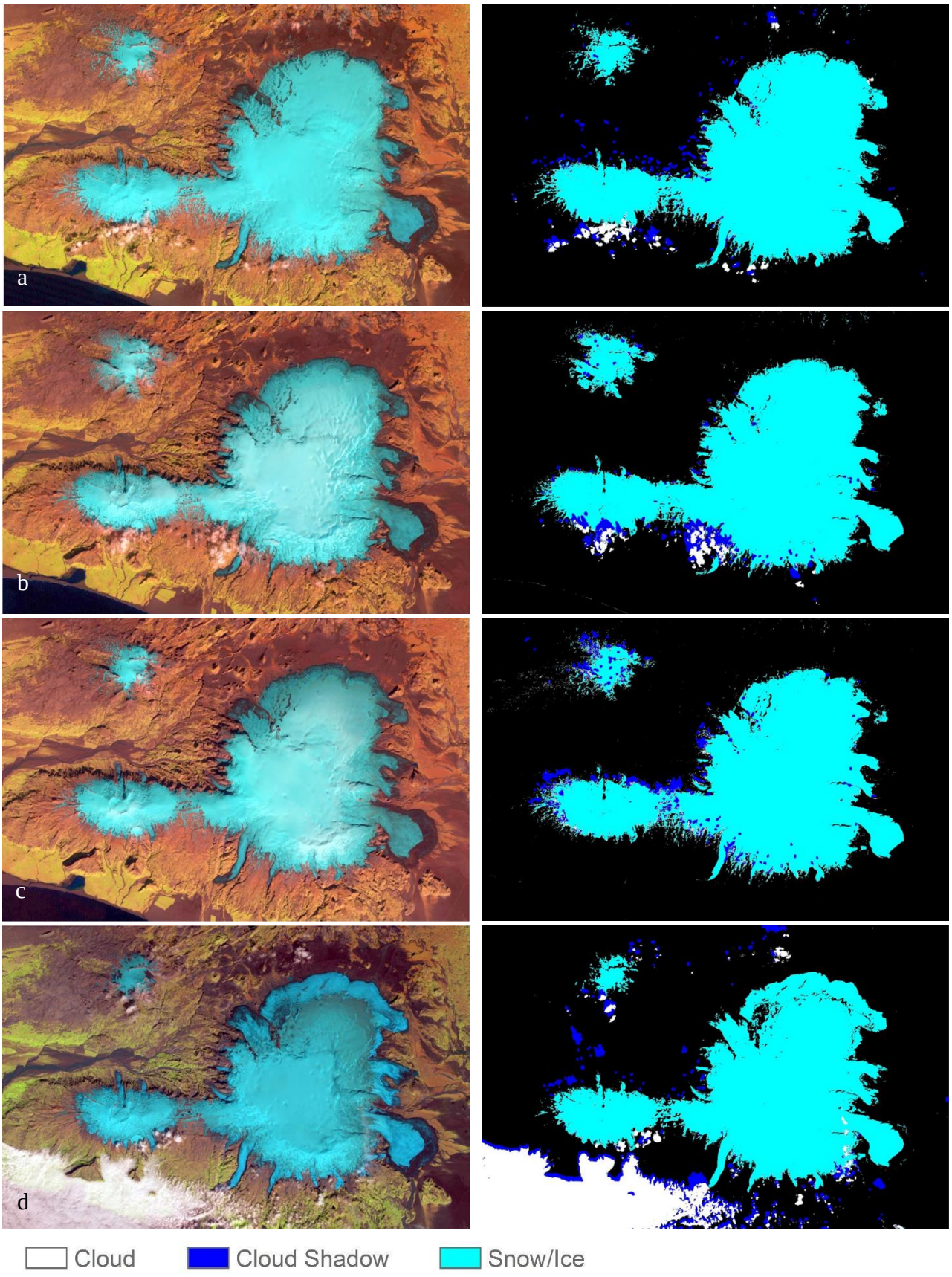

Fig. 17.a. LandsatLook natural color images (left) and LandsatLook quality images (right) 1986 - 1988; a – 15th Aug. 1986, b – 7th Sept. 1986, c – 16th Sept. 1986, d – 20th Aug. 1988 (LandsatLook products courtesy of the U.S. Geological Survey Earth Resources Observation and Science Center)

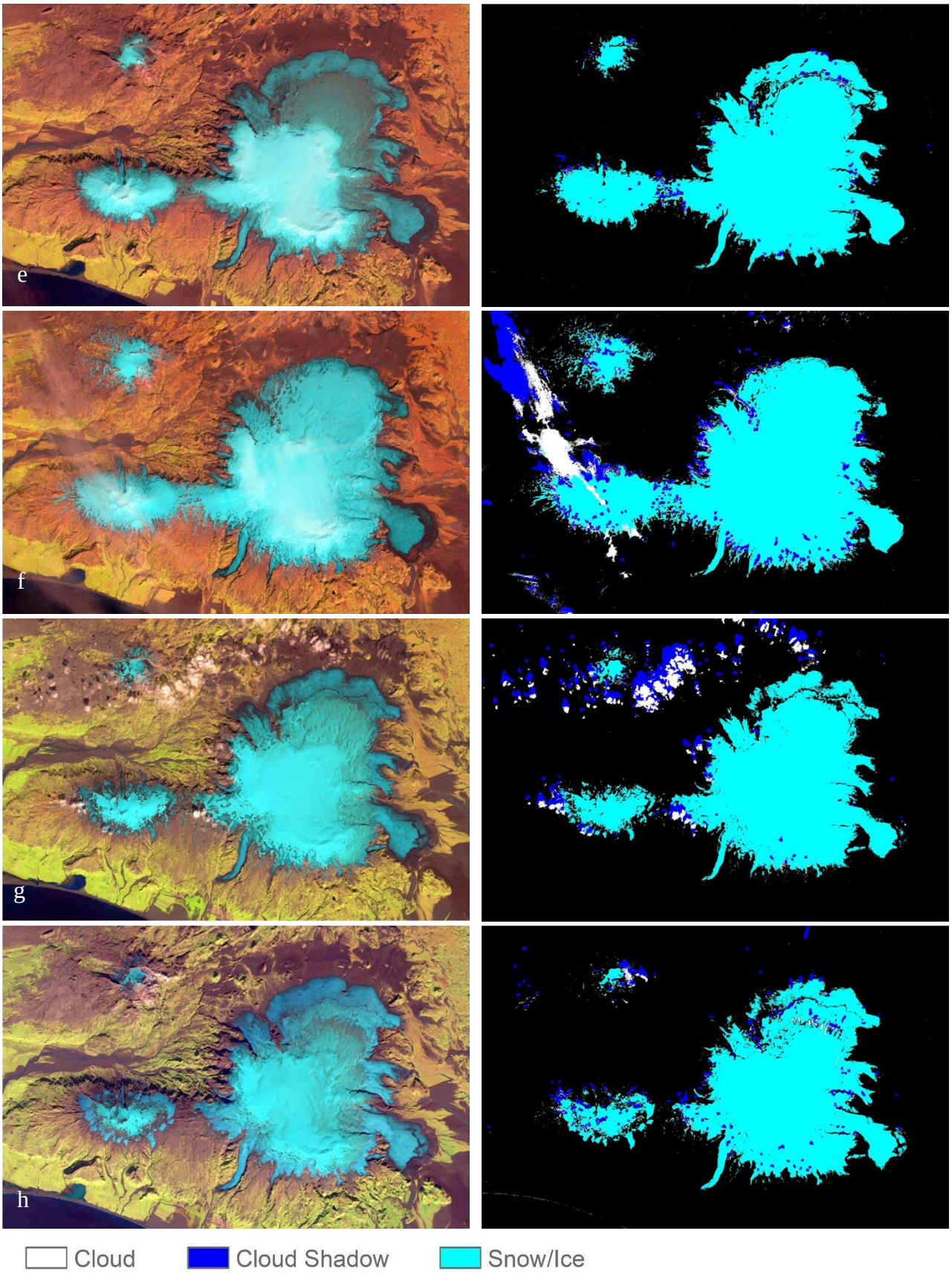

Fig. 17.b. LandsatLook natural color images (left) and LandsatLook quality images (right) 1988 - 2014; e – 12th Sept. 1988, f – 12th Aug. 1994, g – 12th Aug. 2014, h – 20th Sept. 2014 (LandsatLook products courtesy of the U.S. Geological Survey Earth Resources Observation and Science Center)

The scene from 1994 was excluded due to cloud cover in the north-west part of the subset including Eyjafjallajökull slopes. They were not visible from Earth Explorer level on the preview window, but now, when identified, it was decided that they could affect the proper ice and snow identification, and therefore should be excluded from further analysis.
Based on the LandsatLook images it was decided that the study on Mýrdalsjökull group glaciers should be conducted rather on the September images since the equilibrium line altitude (ELA) in August is still rising and the glaciers are still melting. Even in early September, the ice is still melting (as it can be seen when comparing images from the 7th and 16th of September 1986). Therefore, only images from late September were chosen for further analysis.

After applying these new conditions there were three images left which fulfilled the set criteria for further analyses. They were taken on: 16th September 1986 (two scenes mosaiced), 12th September 1988 and 20th September 2014.

4.5. Landsat data processing levels

Original remote sensing images are affected by a number of radiometric and geometric distortions related to the nature of the observed object, sun exposition, and the method of record (properties of sensors and platforms). All these 'errors' make it necessary to 'improve' both the pixel values and their position in the image matrix (Adamczyk and Będkowski 2005).

Level-1 Landsat images are delivered as digital numbers. Precision and Terrain Correction (L1TP) products are initially preprocessed and assure high quality of geometric correction. The geometric correction process consists of georeferencing (alignment to correct geographic location) and orthorectification (correction of distortion related to elevation, relief, and view-inclination (Adamczyk and Będkowski 2005). Landsat Level-1 data are georegistered using ground control points (GCPs) and digital elevation model (DEM). Root Mean Square Error (RMSE) for the terrain-corrected images should not exceed 12 m. The accuracy should, however, be double-checked when the mosaicking of adjacent images is involved (as the images taken on 16th September 1986 required) (Young et al. 2017).

Geometric correction is the first and crucial step in preprocessing satellite images and might provide a sufficient accuracy for a single-scene analysis. However, for the land surface change studies that utilize multi-temporal data, where values need to be in a comparable scale, the images also need to be radiometrically corrected. Radiometric correction is also a particularly important issue in studies performed on the large spatial extent and is necessary to ensure the comparability of images recorded by various sensors (e.g. inter-calibration across Landsat missions) (Adamczyk and Będkowski 2005).

There are several stages of radiometric correction processing. Using a band-specific rescaling factor the data is converted to radiance. Then, with the solar correction, exoatmospheric solar influences are removed, and the information is converted to Top-Of-Atmosphere (TOA) reflectance. Additionally, a correction for the solar elevation angle is applied.

Finally, there is an atmospheric correction. It corrects TOA reflectance to surface reflectance. This is a crucial step for multi-temporal and/or multi-scene analysis. Atmospheric particles such as gases, water vapor, and aerosols bring on scattering and absorption of electromagnetic waves (Young et al. 2017). The detector located on the upper limit of the atmosphere registers direct radiation reflected from the object, diffuse radiation reflected from the object and diffuse sky radiation coming directly from the atmosphere (Adamczyk and Będkowski 2005). The

correction removes atmosphere influences on electromagnetic radiation (Young et al. 2017). Surface reflectance data products are free of artifacts from the atmosphere, illumination, and viewing geometry. The reflectance values should closely correspond with in-situ measurements (Gao and Liu 2001; Hall et al. 1989). This increases the consistency and comparability between satellite images taken at different times (USGS 2015). It is also particularly important for deriving ratio-based spectral indices (used to highlight a specific environmental phenomenon e.g. NDVI – Normalized Difference Vegetation Index) – due to possible additive artifacts and atmospheric effect (Young et al. 2017). To perform a precise atmospheric correction, the state of the atmosphere at the moment of acquisition must be known (Adamczyk and Będkowski 2005).

USGS recommends using the corrected Higher-Level Landsat Products that they currently provide. Selkowitz and Forster (2015), as well as Young et al. (2007), also opted to use standardized Landsat surface reflectance products. These images are considered suitable for time-series analysis and are inter-calibrated across different Landsat sensors.

Level-2 Landsat Science Products inherit the L1TP geometry and provide radiometrically corrected surface reflectance data. The preprocessing includes all above-described stages including atmospheric correction (USGS 2012). Level-2 from Thematic Mapper (Landsat 4-5 TM) and Enhanced Thematic Mapper Plus (Landsat 7 ETM+) data is generated with software called Landsat Ecosystem Disturbance Adaptive Processing System (LEDAPS) (USGS 2017a). Operational Land Imager (Landsat 8 OLI) Level-2 data are generated from algorithm known as Landsat Surface Reflectance Code (LaSRC) (USGS 2017b). The surface reflectance products are used by USGS to derive further Science Products such as various spectral indices.

Surface reflectance uncertainty is greatest at high latitudes. However, since the Eyjafjallajökull summit is located at 63.6ºN, and USGS (USGS 2017a, 2017b) gives a threshold of 65º, it was decided to proceed with this data. Also, according to the approach presented by Selkowitz and Forster (2015), if the manual checking does not rise a flag on significant errors that could violate the ability to discriminate snow and ice, the standardized Landsat surface reflectance products might be successfully used even on higher latitudes.

Surface reflectance Level-2 data products were ordered via an on-demand ESPA interface (U.S. Geological Survey (USGS) Earth Resources Observation and Science (EROS) Center Science Processing Architecture).

The text file (*.txt) listing the desired Landsat surface reflectance products was uploaded to ESPA service. It contained following Landsat scenes:

- LT05_L1TP_218015_19860916_20170216_01_T1*
- LT05_L1TP_218016_19860916_20170216_01_T1*
- LT05_L1TP_219015_19880912_20170206_01_T1
- LC08_L1TP_219015_20140920_20170419_01_T1

*two scenes from 1986 were needed to cover the whole area (Fig. 16).

Since the Landsat data was quite heavy and performing analysis on them might have been time-consuming, the subset representing the study area was cropped from the full scene extent. To automatize this step a tool that iterated through raster datasets was created in ESRI model builder.

4.6. Quality assessment

The scenes from 16th September 1986 were mosaiced to new rasters in ArcGIS ArcMap ESRI software. As recommended by Young et al. (2017), the accuracy of the geocoded mosaic was visually double-checked, and no errors were detected.

More meticulous and exhaustive level-2 quality assessment (QA) bands were previewed. The QA bands in level-2 Landsat products include:

− Level-2 Pixel Quality Assurance band (pixel_qa) – populated using information from the Level-1 quality assurance band, derived from the C-Function of Mask (CFMask) algorithm. CFMask estimates cloud confidence, creates cloud shadows (by iteratively approximating heights of clouds and projecting them onto the ground) and flags snow/ice pixels. Known issues include difficulties with thinner clouds, that are potentially at higher risk to be omitted. Also, bright targets such as snow and ice might be challenging for the algorithm.

− Radiometric Saturation Quality Assurance band (radsat_qa) – flags which sensor channels were saturated during data capture

− Surface Reflectance quality files (sr_cloud_qa, sr_atmos_opacity) – produced only by LEDAPS algorithm

− Surface Reflectance Aerosol Quality (sr_aerosol) – produced only by the LaSRC algorithm – provides information about the factors that influenced surface reflectance generation and brought upon potential artifacts

Each bit-packed combination of QA band pixel carries the information on various surface and atmospheric features or sensor conditions. To interpret pixel values the Decode QA tool from Landsat Quality Assessment (QA) ArcGIS Toolbox was used. 'Remove low confidence labels' options was checked as it donates the last probable outcome and therefore it might be superfluous for visualization purposes (USGS 2017c) (Fig. 18).

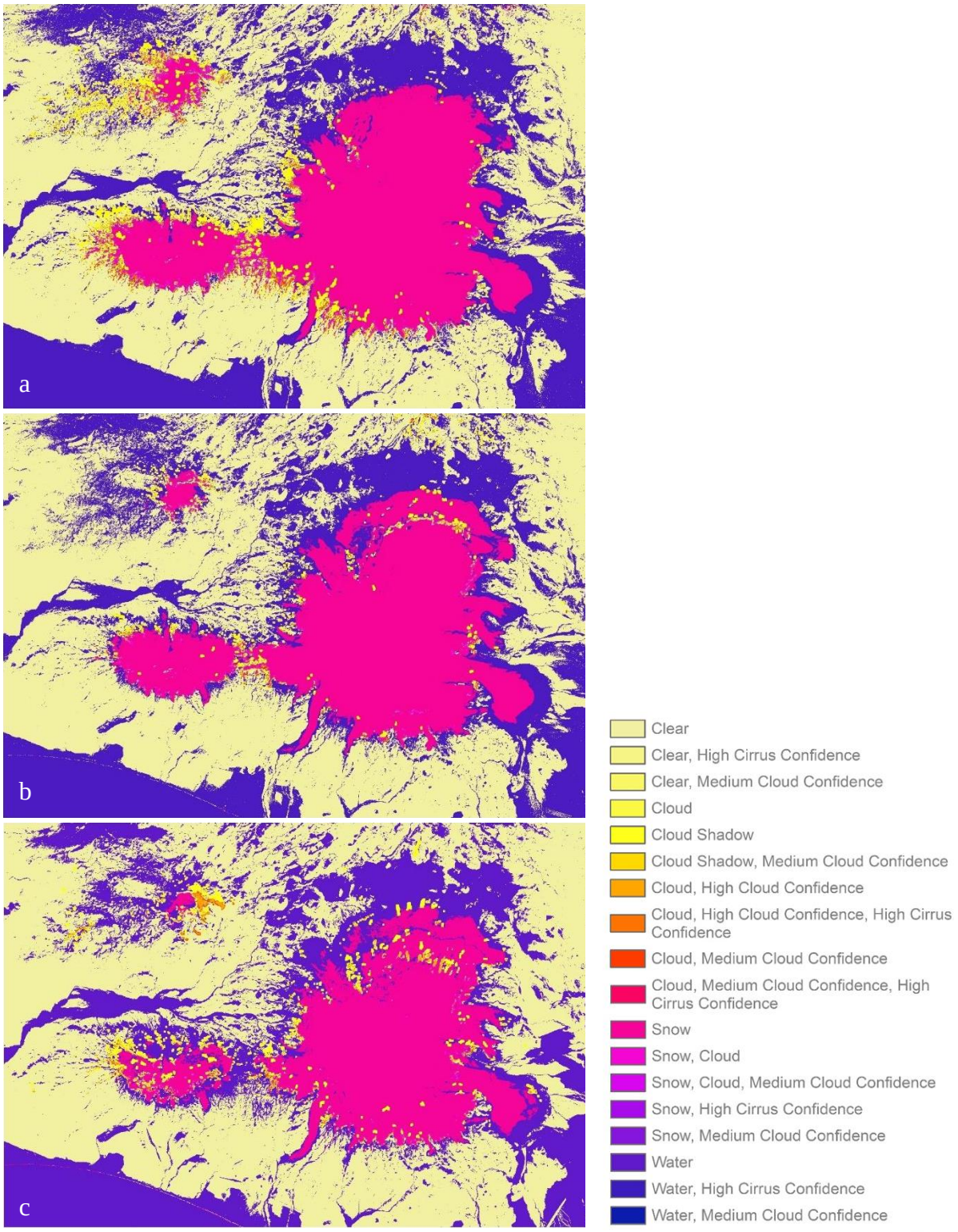

Fig. 18. Decoded quality assurance bands; imageries from a – 16th Sept. 1986, b – 12th Sept. 1988 and c – 20th Sept. 2014 (Landsat Level-2 Science products courtesy of the U.S. Geological Survey Earth Resources Observation and Science Center)

Pixel quality assurance bands are generally in accordance with LandsatLook quality images (Fig. 17). According to the Landsat documentation, pixel quality assurance band is likely to present more accurate results than surface reflectance quality files (USGS 2017a). This is indeed in line with the assessment of the study area – pixel_qa seems to flag problematic features more reliably. In-depth manual checking of surface reflectance bands confirmed this finding. The most striking is snow and ice that are labeled much more correctly on level-2 pixel quality assurance band than on surface reflectance quality files.

Images acquired by Landsat 5 TM show some saturation especially in the red band, however, affected pixels are located on the top of the glaciers and not on more 'sensitive' boundary zone, so it should not influence the delineation of the glacier body.

Surface reflectance values derived with both LEDAPS and LaSRC algorithms varies between -2000 and 16 000. The valid reflectance ranges from 0 to 10 000 (USGS 2017a, 2017b). This information is important since some of the bands exceed this range over the study areas. Such pixels have to be excluded in further analysis.

All in all, the quality of the three scenes were estimated as sufficient for further analysis.

4.7. Composites

The operation of creating color composites is based on the transparent combination of images recorded in individual channels. Any three images may be used to create color composites (Adamczyk and Będkowski 2005).

True color Red-Green-Blue composite (where the three bands populate RGB channels respectively) is useful for a general overview and preliminary analysis (Fig. 19.f). Nevertheless, making use of other bands can significantly improve the visibility of particular glacial features. During this study, several band composites were utilized in order to correctly identify ice caps and their characteristics. No scheme has been found to be universal for all applications; in visual interpretation, several composites were used. They serve as a base and benchmark for testing various methods and defining thresholds in further stages of the study.

The created band composites can be divided into two groups – those, which were helpful with differentiation of glacier from surrounding rocks and inside nunataks, and those, which were useful in identifying glacial facies – the icier ablation zone and the rather snow-covered – accumulation zone.

Band stacks, which were used to separate glacial body from rocks included combinations of NIR-SWIR1-SWIR2 (proposed e.g. by Aniya et al. 1996; Hall et al. 1987; Williams 1987) where snow and ice appear in red, while surroundings in shades of blue (Fig. 19.b); and the combination of SWIR1-Green-Blue bands (utilized by Aniya et al. 1996); where the color representation was pretty much reverse (Fig. 19.a).

Using combinations of SWIR, NIR, Blue and Green bands is often mentioned by a number of authors as useful in glaciological research. Several composites built of these bands were tested (SWIR1-NIR-Green – used by Hall et al. (1988, 1995); SWIR1-NIR-Red – presented on LandsatLook Natural Images and also used in Burns and Nolin (2014) research; SWIR2-NIR-Green – used by Selkowitz and Forster (2015), SWIR2-NIR-R). Even though there is a strong similarity between them (they show the study area in light green with red-brown stains and blue ice caps), there are some differences in shades and picturing some important details. It was found that incorporating green band instead of red, gives better ‘contrast’ between snow (green-blue) and ice (more saturated blue). It was also noticed that SWIR2 gives better distinction between glacier and surroundings (more reddish) than SWIR1, where the ambient rocks seemed

to be ‘enshadowed’. Out of these combinations, the particularly useful for differentiation of glacier facies was the composite of SWIR2-NIR-Green (Fig. 19.c).

Another composite that proved to be useful for dividing glacial zones was a Blue-NIR-SWIR1 combination (suggested e.g. by Aniya et al. 1996). It shows ice in orange-yellow and snow in green-yellow (Fig. 19.d). The last band stack used, consists of bands Red-NIR-Green (utilized by Dozier and Marks 1987). The deglaciated surface is depictured in vibrant green, ice in purple and snow in white (Fig. 19.e).

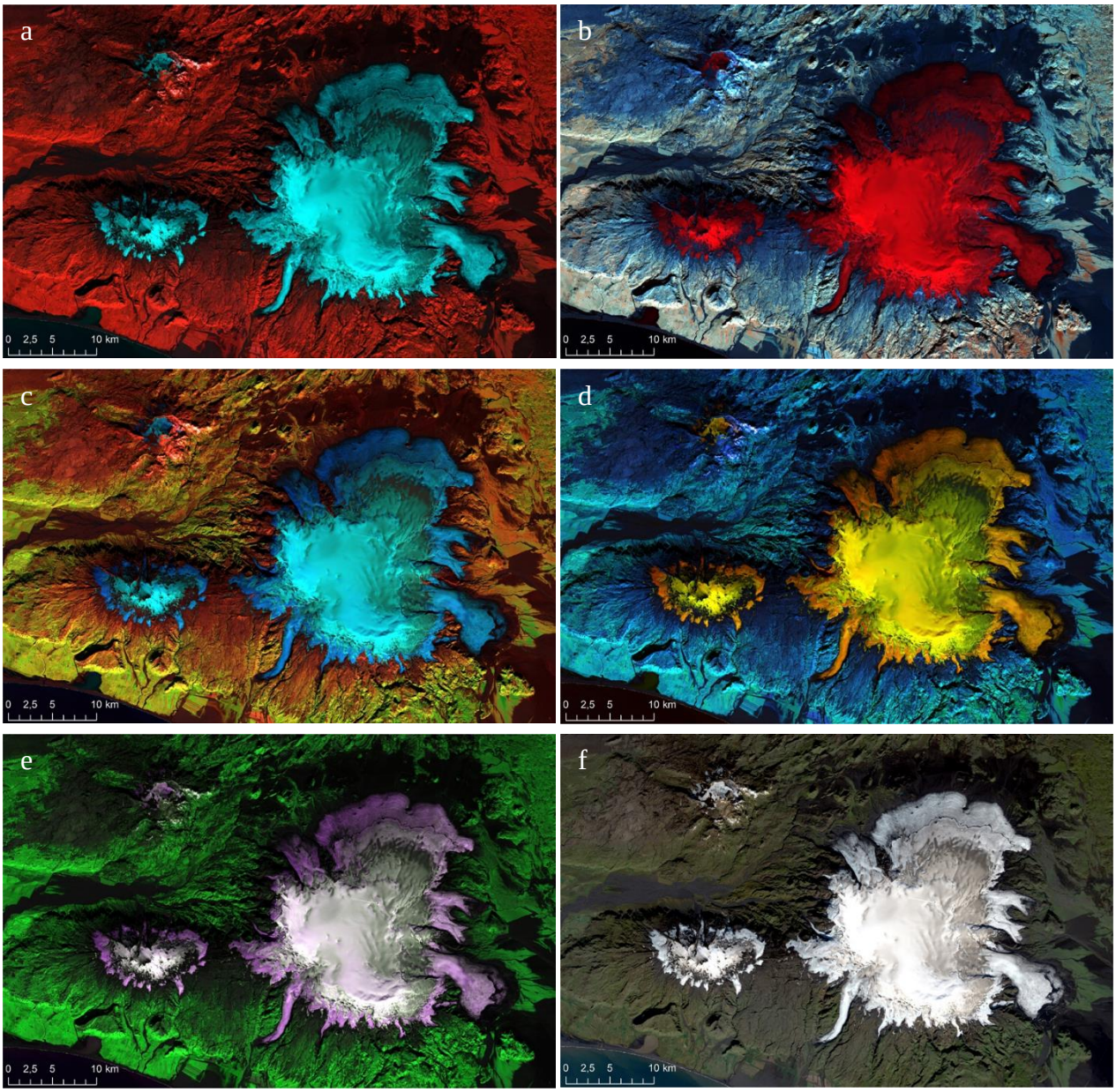

Fig. 19. Composites used in the analysis (on the example of scene from 20th September 2014); a – SWIR1-G-B, b – NIR-SWIR1-SWIR2, c – SWIR2-NIR-G, d – B-NIR-SWIR1, e – R-NIR-G, f – R-G-B (true color), (derived from Landsat Level-2 Science products courtesy of the U.S. Geological Survey Earth Resources Observation and Science Center)

4.8. Delineation of glaciers boundaries

Normalized Difference Snow Index (NDSI), proposed by Hall et al. (1995) was used to highlight snow and ice in satellite images.

NDSI is based on the fact that snow reflects radiation more intensively in the visible part of the spectrum than in mid-infrared/shortwave infrared (SWIR), where it dramatically drops (Fig. 14). On the contrary, clouds reflectance remains high in the SWIR region, which allows a separation between snow and most of the clouds (Hall et al. 1988, 1995). The NDSI equation looks as follows:

$$\mathrm{NDSI} = \frac{\mathrm{Green} - \mathrm{SWIR1}}{\mathrm{Green} + \mathrm{SWIR1}}$$

Green – the value of the pixel representing the green part of the spectrum (approx. 0.52 – 0.60 μm; TM – Band 2; OLI – Band 3)

SWIR1 – the value of the pixel representing the Shortwave Infrared part of the spectrum (approx. 1.55 – 1.70 μm; TM – Band 5; OLI – Band 6)

Hall et al. (1995) highlight that the use of reflectance (instead of digital number cf. '4.5. Landsat data processing levels') improves identification of snow. The applied pre-processing atmospheric correction is particularly crucial for the NDSI due to the fact that it incorporates Landsat Green band where atmospheric scattering is especially high (Selkowitz and Forster 2015). Using surface reflectance images can improve the accuracy of the results (Burns and Nolin 2014; Selkowitz and Forster 2015).

Some studies suggest that the range of the spectrum involving red visible light is useful for identifying snow and ice (Bronge and Bronge 1999). Another indicator for distinguishing areas covered with snow and ice, Normalized Difference Snow/Ice Index (NDSII), proposed by Xiao et al. (2001), utilities this part of the spectrum. The formula is as below:

$$\mathrm{NDSII} = \frac{\mathrm{Red} - \mathrm{SWIR1}}{\mathrm{Red} + \mathrm{SWIR1}}$$

Red – the value of the pixel representing the red part of the spectrum (approx. 0.63 – 0.68 μm; TM – Band 3; OLI – Band 4)

SWIR1 – the value of the pixel representing the Shortwave Infrared part of the spectrum (approx. 1.55 – 1.70 μm; TM – Band 5; OLI – Band 6)

Values of indices range from -1 to +1. The greater the value, the higher the possibility of snow occurrence within the pixel.

NDSI and NDSII were calculated in ESRI ArcGIS with Raster Calculator – a tool supporting map algebra operations. Keeping in mind the valid range of surface reflectance, some conditions have been established. Pixels of bands incorporated into the indices calculation, of value below 0 or above 10 000, were filtered out (USGS 2017a, 2017b) and set as Null (Fig. 20).

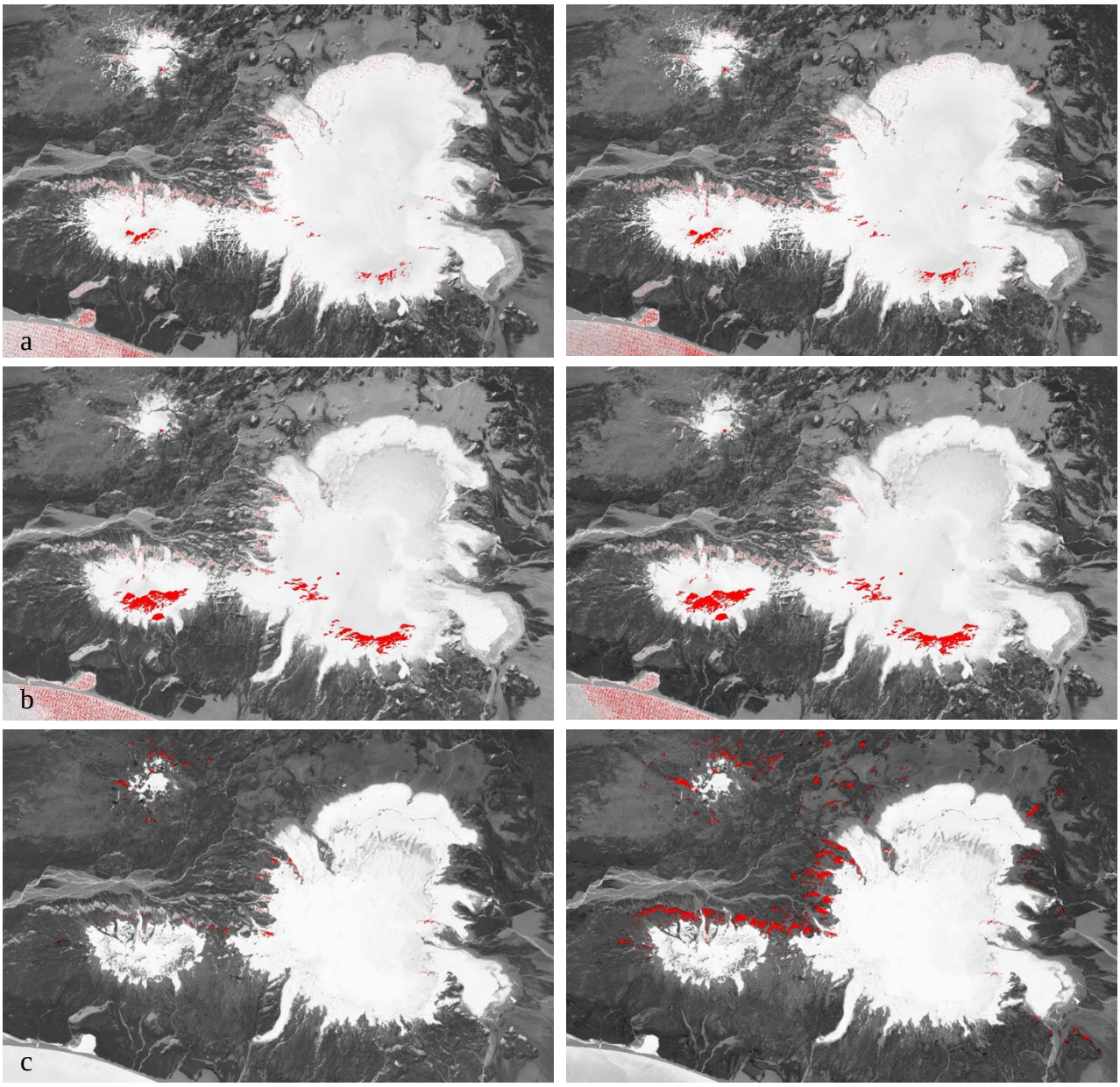

Fig. 20. Normalized Difference Snow Index (NDSI; left) and Normalized Difference Snow/Ice Index (NDSII; right); imageries from a – 16th Sept. 1986, b – 12th Sept. 1988 and c – 20th Sept. 2014. The gray scale was stretch from the minimum possible value (-1, dark) to maximum (+1, light) in all images in order to make them comparable and symbology consistent. Invalid excluded pixels highlighted. (derived from Landsat Level-2 Science products courtesy of the U.S. Geological Survey Earth Resources Observation and Science Center)

The next step was to find NDSI and NDSII thresholds which would distinguish ice and snow from other surfaces. Various values in the range 0.0 – 0.5 were tested.

In order to estimate the accuracy and chose the most suitable threshold, 1000 of random sample points were generated. Due to lack of in situ observation, the points were verified individually and classified as a glacier or as other surface by visual examination of the Landsat true color images and various false color band composites (Fig. 19).

Then the accuracy of the "ground truth" was checked against the three NDSI and three NDSII segmented images that show the best results according to visual estimation (0.3, 0.4 and 0.5 threshold values). This comparison was performed through the use of a confusion matrix (error matrix) (App. 4). Several accuracy measurements were calculated.

- Overall (total) accuracy – the probability that a randomly chosen point is correctly mapped $\frac{\sum A}{N}$
- User (object) accuracy – for each class, the probability that a randomly chosen to point on the map represents the same class in the field $\frac{A}{C}$
- Producer (classification) accuracy – for each class, the probability that a randomly chosen point in the field represents the same class on the map $\frac{A}{B}$
- Mean accuracy – for each class, a combination of user and producer accuracy, calculated for each class $\frac{2A}{B+C}$
- Areal difference – for each class, the areal over- or underestimation of a class related to the number of ground truth data points $\frac{C-B}{B}$
- Coefficient of agreement – Kappa – total and for each class, incorporates the influence of chance, informs about the map quality vs random agreement (chance) $\kappa = \frac{N * d - q}{N^2 - q}$

where:

- A – number of correctly mapped points
- B – number of "ground truth points"
- C – number of "map data points"
- N – total number of points
- d – sum of correctly mapped points: 495
- q – sum of the products between B and C for each class

Both NDSI and NDSII show best results for 0.4 threshold value - for all three images from 1986, 1988 and 2014 the overall accuracy is highest (above 95.8% for NDSI and 95.5% for NDSII). Generally, images generated based on OLI data shows better overall accuracy (above 97%). The threshold of 0.3 gives lower user accuracy and higher producer accuracy of the mapped glacier while for 0.5 this proportion is reversed. The glacier is overestimated when applying threshold 0.3 and underestimated with 0.5. The mean accuracy is best for threshold 0.4 for both classes. The kappa coefficient also indicates that the mid threshold value gives best effects – for all three dates the maps are more than 90% better than a chance. All in all, the most suitable proved to be the value of 0.4. Pixels equal or above this threshold represent the glacier body. The slightly debris-soiled termini were also included (Fig. 21). All accuracy measurements are presented in the App. 4.

NDSII gave very similar results as NDSI – the resulting images were virtually no different from each other. The accuracy measurements differ very slightly indicating a small advantage of NDSI over NDSII. NDSII gives better overall accuracy only for 1986 image (96.9% vs 96.8%). The number of points falling on invalid pixels was less than 2% for TM images and less than 1% for OLI imagery. Generally, the number of invalid pixels outweighs in NDSII. Taking the above into consideration only the NDSI images with 0.4 thresholding applied were retained and used for further analysis.

The differences in sensors are visible on indices derived from imageries. Some differences in the ‘contrast’ of images were noticed – on images derived from OLI data (for 2014) the ‘contrast’ is higher than TM. The NDSI-derived classified image from OLI is much ‘clearer’ than scenes from TM. There are fewer artifacts and outliers. The image seems to be more coherent (Fig. 20, 21).

The sensor differences also influence the distribution of invalid pixels. The invalid pixels of TM images are mostly concentrated on southern slopes of the glacier. OLI imageries invalid pixels seemed to be correlated with shadows cast by slopes. Generally, the number of invalid pixels is higher for NDSII than for NDSI (Fig. 20). It implies that the red band is more ‘problematic’. The amount and location of excluded pixels should not significantly disturb the glaciers border.

The NDSI algorithm shows some inaccuracies when dealing with shadows. Some of them were incorrectly classified as glacier ice. It is noticeable, especially on TM images. The most affected are northern slopes of Eyjafjallajökull.

After reclassification, rasters were converted into vector polygons. The outliers were manually removed. The parts that suffer from invalid pixels, but have clearly represented glacier, were appended. Other smaller gaps (e.g. nunataks), below 0.5 km^2 were neglected. Finally, polygons representing glaciers were smoothed (Fig. 21).

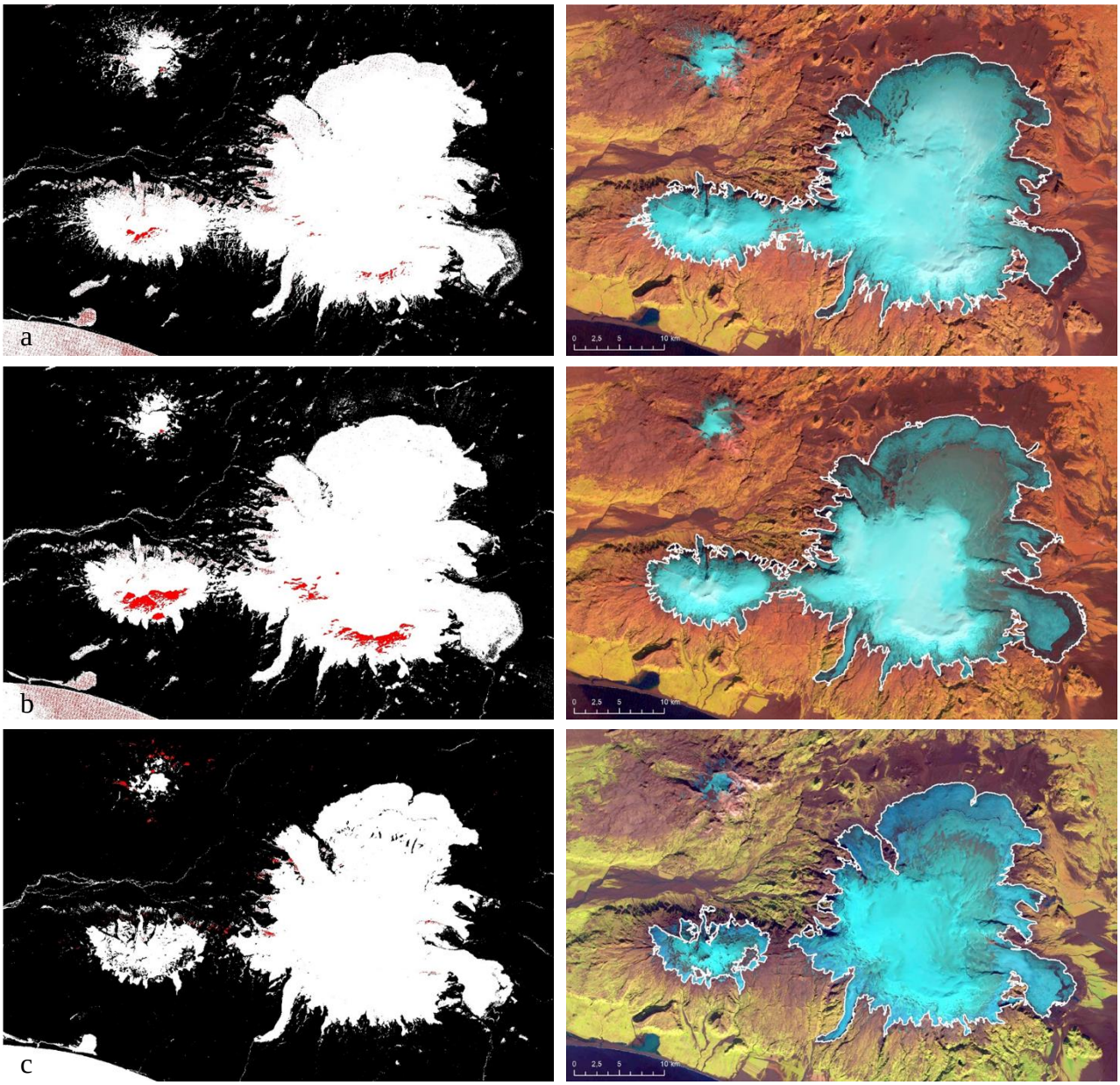

Fig. 21. Normalized Difference Snow Index (NDSI; left) with threshold of 0.4 (white – snow/ice cover, black – no snow/ice; invalid excluded pixels denoted in red) and LandsatLook natural color images with glaciers outlines (right); imageries from a – 16th Sept. 1986, b – 12th Sept. 1988 and c – 20th Sept. 2014. (derived from Landsat Level-2 Science products courtesy of the U.S. Geological Survey Earth Resources Observation and Science Center)

It can be seen that on the image from 1986 the NDSI algorithm could not properly delineate the Kötlujökull outlet glacier (SE part of the Mýrdalsjökull). The front of the glacier is heavily contaminated with debris/tephra overlying cover (Fig. 21, 22). Due to the lack of field observations, high-resolution DigitalGlobe Images provided by Google Earth were used to understand and confirm the phenomena (Fig. 22). Also, the thermal image indicates that there is an ice beneath the debris/tephra cover (Fig. 23). The missing part of Kötlujökull was manually delineated and estimate to approximately 10 km^2.

Fig. 22. A bird's eye view over Kötlujökull and Huldujökull outlet glaciers (Mýrdalsjökull). The tephra layers covering the glacial fronts are visible (Google Earth: Landsat / Copernicus)

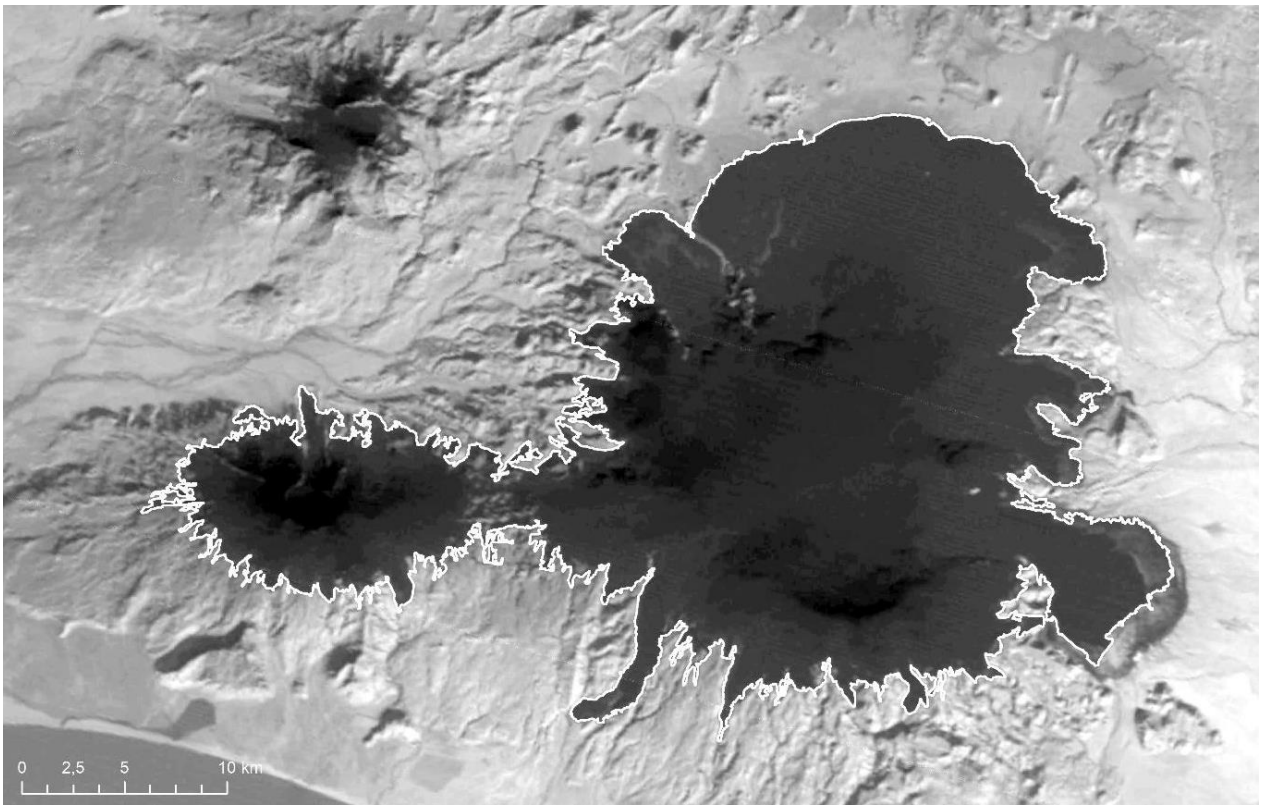

Fig. 23. Glacier outline on the background of Thermal Image, 16th Sept. 1986 (LandsatLook Thermal Image and Landsat Level-2 Science products courtesy of the U.S. Geological Survey Earth Resources Observation and Science Center)

4.9. Delineation of accumulation zone – finding ELA

At the end of the ablation season (late summer), TSL retreats to the maximum altitude and will be likely tie in with the equilibrium line altitude (ELA), where snow accumulation and ablation are equal (Gao and Liu 2001). The TSL delineated in that period should encircle the area of accumulation (cf. ‘2.3. Mass balance and Equilibrium Line Altitude (ELA)). Knowing the spectral characteristics (Fig. 14) of objects of interests, the features can be emphasized through ratio images. To delineate the accumulation area and thus find the ELA, several ratio images combinations were tested.

Ratio images are obtained by performing a mathematical operation on two (or more) spectral extracts. Pixel values from different bands can be divided, subtracted or added to each other, so that information previously invisible can be extracted. Several combinations were tested.

Images created by dividing the spectral extracts received in the NIR and SWIR1 channels are helpful in determining the facies of glaciers (snow, ice, slush zone and moraine). Such a combination was used, among others, by Hall et al. (1987, 1989), Jacobs et al. (1997), Williams et al. (1991). Ice and snow strongly reflect radiation in NIR, while their reflection in SWIR spectrum is rather low. The opposite occurs for vegetation and deglaciated bedrock where the reflectance increases from NIR to SWIR wavelengths spectra (Jacobs et al. 1997). The ratio image created by dividing the extracts from the NIR channel by SWIR gives a great contrast to the areas occupied by snow and ice (Fig. 24). The contrast is best in the accumulation area, where differences between the two spectrums are greatest (Hall et al. 1987; Williams et al. 1991). The reflectance of fresh snow in the NIR region is high, whereas it decreases as snow begin to metamorphose (Hall et al. 1988; O'Brien and Munis 1975).

Visible reflectance is not as dependent on grain size as NIR is. On the other hand, red band is sensitive to contamination and impurities e.g. by dust (Dozier 1984; Dozier and Marks 1987; Hall et al. 1987, 1988)

Another ratio, proposed by Rott (1994) involves red band and SWIR1 (Fig. 24). With further thresholding, it should result in the possibility to differentiate between glacier ice, névé (young, granular snow, which has been melted, refrozen and compacted; might later turn into firn) and snow. Bronge and Bronge (1999) noted that this ratio enhances snow grain-size variations.

Dividing the red band with NIR gives an image on which the size of the ice crystals is well distinguished so that the blue ice and snow types can be classified. Moreover, this combination is insensitive to thin clouds and cloud shadows (Bronge and Bronge 1999; Xiao et al. 2001) – it equalizes influences of shadows as well as tephra and debris covered margins of the glacier (Fig. 24).

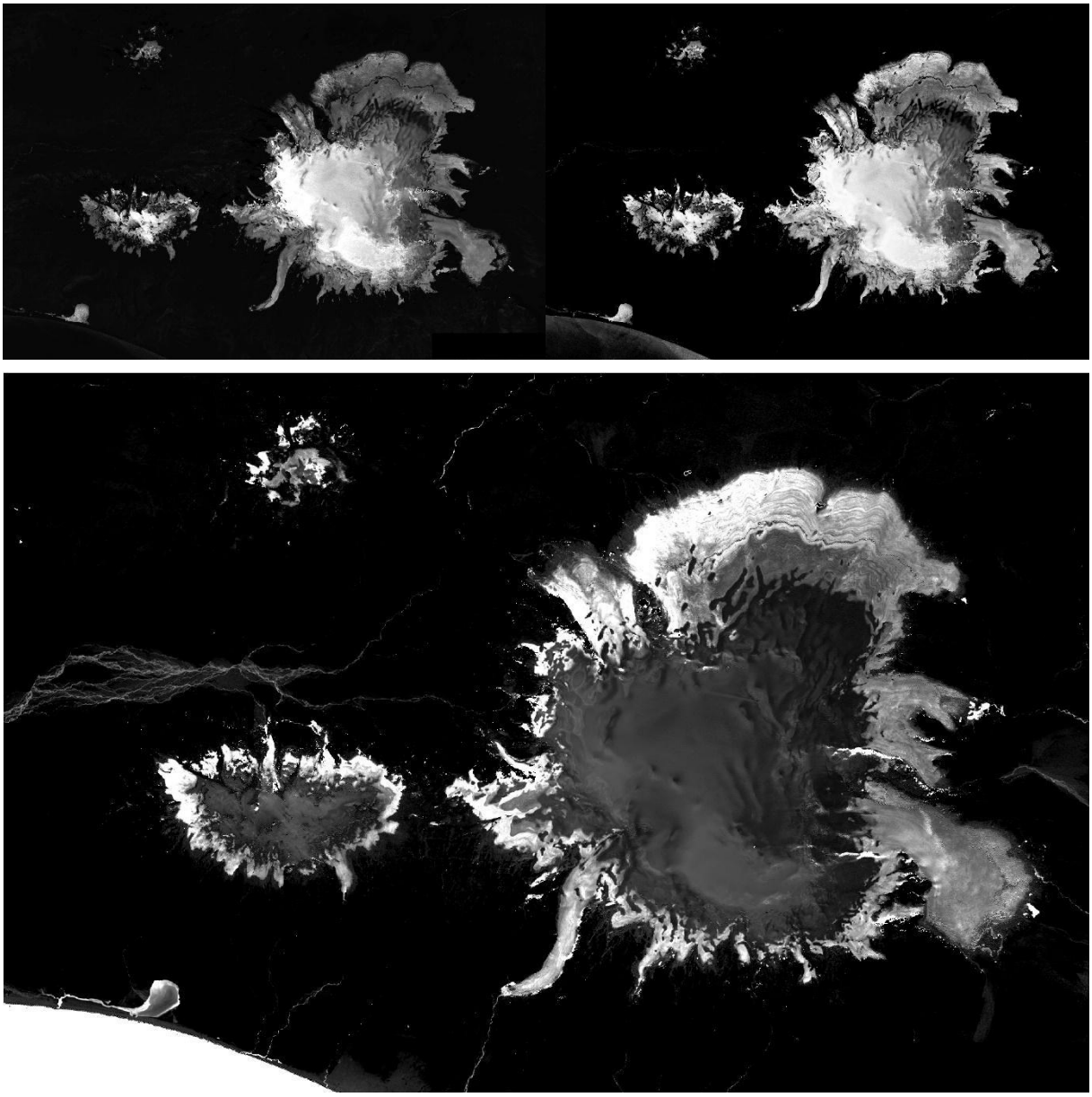

Fig. 24. Ratio Images calculated to define ELA, here an example of the scene from 20th September 2014; top-left – NIR/SWIR1, top-right – R/SWIR1, bottom – R/NIR (derived from Landsat Level-2 Science products courtesy of the U.S. Geological Survey Earth Resources Observation and Science Center)

As previously done for the indices, also the ratio images were calculated with Raster Calculator. Since pixels of values below 0 or above 10 000 are considered invalid, they were filtered out (USGS 2017a, 2017b) and set as null.

In the search for the accurate threshold for differentiation of ice and snow, a number of threshold values were tested. Only for the last combination – the ratio of red band versus NIR (TM3/TM4, OLI4/OLI5; Fig. 24), it was possible to determinate the range of proposed threshold values. The other two images do not show regularity to differentiate the glacier zones – they are not applicative for this case. On Red/NIR image snow and ice differ from each other quite well, especially on OLI image. Ice pixels have higher values than snow and other surfaces.

From the sample points used previously for the quality assurance of glacier boundary delineation, these representing glacier bodies were utilized again. For years 1986, 1988 and 2014 this gives 308, 298 and 244 points accordingly.

For each studied year, for the three segmented Red/NIR ratio images, with threshold values showing the best visual effect in the differentiation of glacier zones, the accuracy was tested. For TM sensor it were 1.10, 1.12 and 1.14 thresholds, while for OLI images it were 1.20, 1.22 and 1.24. Once again, the error matrix (coefficient matrix) was prepared (App. 4). Same accuracy measurements as previously were calculated (cf. ‘4.8. Delineation of glaciers boundaries’).

The mid-values (1.12 for TM and 1.22 for OLI) show best results. The overall accuracy is above 85%. The lover values give maps with underrate snow (accumulation zone) and overestimated ice (ablation zone), while the higher values result in opposite schema. Mean accuracy (higher for the snow class) and Kappa coefficient, confirm these findings. All accuracy assurance measurements are listed in App. 4. Eventually, the threshold value for OLI data was established to be 1.22 while for TM ratio it was set to 1.12.

The differences in sensors are visible. Ratio image generated from OLI data is much more readable and clear (Fig. 25). There is less ‘noise’ and outliers.

On OLI images the invalid pixels are associated with shadowed slopes to the north of Eyjafjallajökull and North-West of Mýrdalsjökull. On TM images the ‘overexposed’ southern slopes generate errors. This is especially problematic in the image from 1988, where invalid pixels cover expansively the southern slope of Eyjafjallajökull. It was noticed that small

lengthwise shadow on the northern slope of Eyjafjallajökull was classified as accumulation zone. Generally, the invalid pixels pose less than 2% of sample points.

The rasters were reclassified according to the threshold, converted to vector polygons. Smaller holes found above ELA were filled in and the outlines smoothed (Fig. 25).

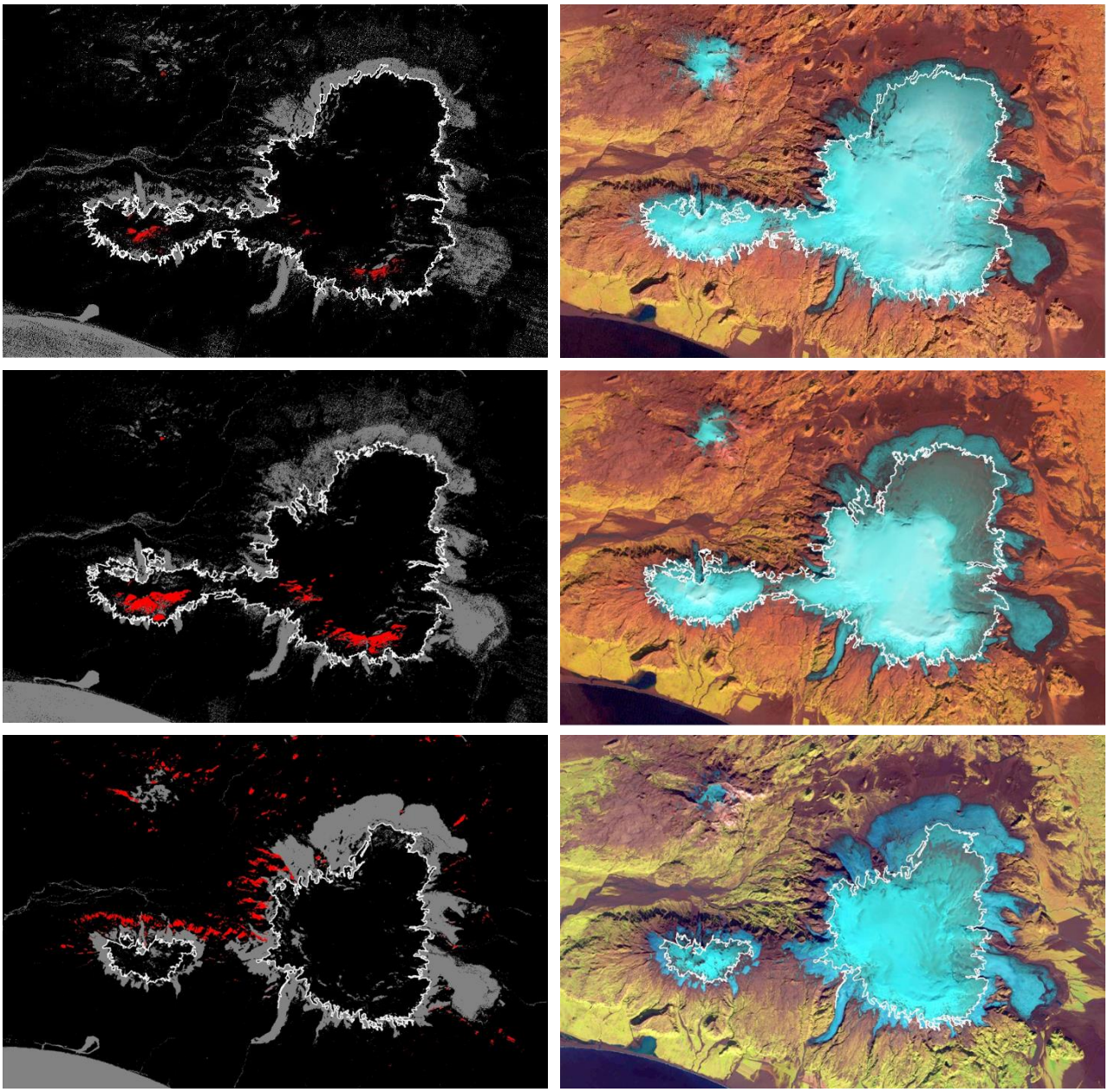

Fig. 25. Classified ratio images with ELA defined (left; invalid pixels highlighted) and LandsatLook Images with ELA; imageries from a – 16th Sept. 1986, b – 12th Sept. 1988 and c – 20th Sept. 2014. (LandsatLook and Landsat Level-2 Science products courtesy of the U.S. Geological Survey Earth Resources Observation and Science Center)

The main problem in defining the proper threshold (and removing vectorized outliers) posed jagged aprons of imposed snow. The high-resolution DigitalGlobe images available via Google Earth were utilized to learn about the nature of the phenomenon (Fig. 26).

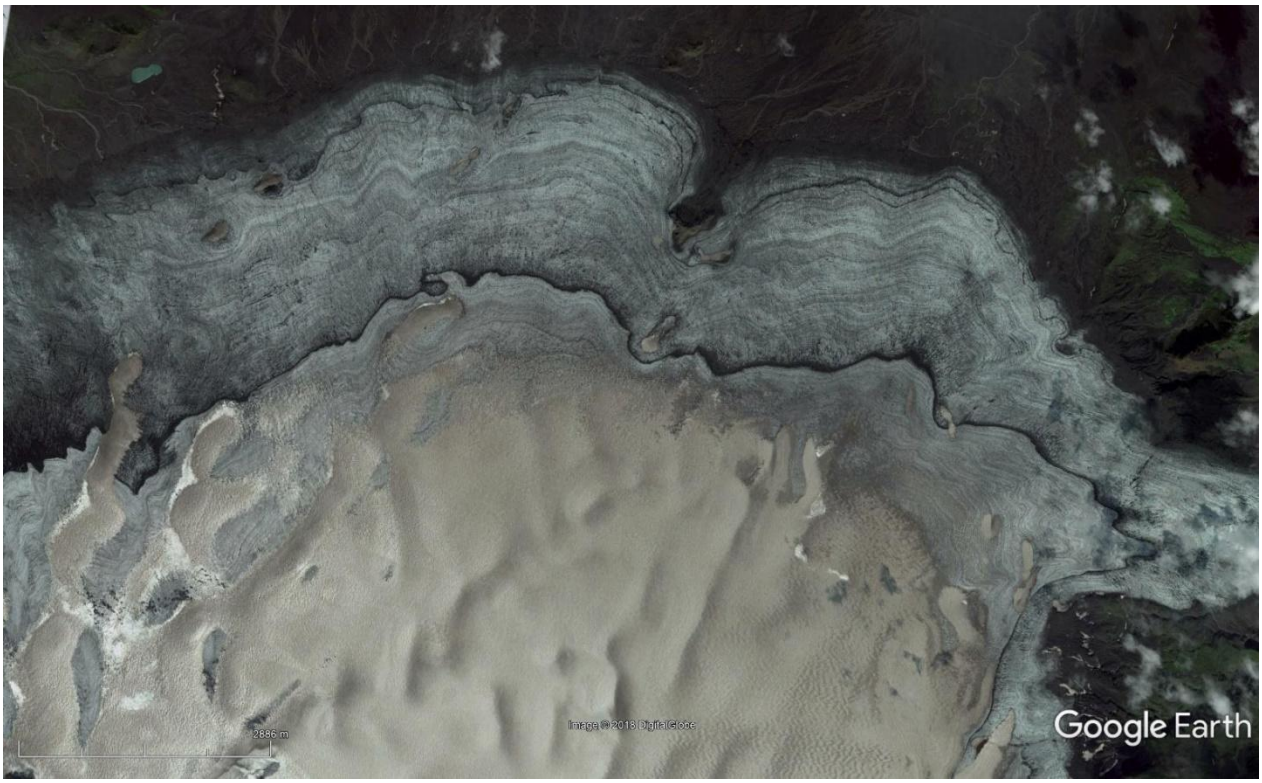

Fig. 26. Jagged aprons of imposed snow on Sléttjökull outlet glacier (Myrdlasjokull) (DigitalGlobe, Google Earth)

5. Results

5.1 Mapping glaciers extent

The ice caps experienced large changes during the study period (Fig. 27; Tab. 5). In the 1980s Mýrdalsjökull and Eyjafjallajökull were linked. In 2014 they were separated into two glaciers. Between 1986 and 1988 both glaciers decreased in size from the south and extended to the north. Both glaciers have shrunk, but the change of Eyjafjallajökull is especially striking. Between 1986 and 2014 its size decreased by more than 40%.

From the north, the ELA runs lower than on the southern slopes (Fig. 27). ELA on the southern slopes of Mýrdalsjökull and Eyjafjallajökull crept up from 900 to 1100 m a.s.l. and from 950 to 1200 m a.s.l. respectively. On Mýrdalsjökull outlet glacier Sléttjökull it raised about 250 m reaching 1000 m a.s.l. in 2014. In less than three decades the accumulation area of Eyjafjallajökull decreased by more than 50% (Tab. 5).

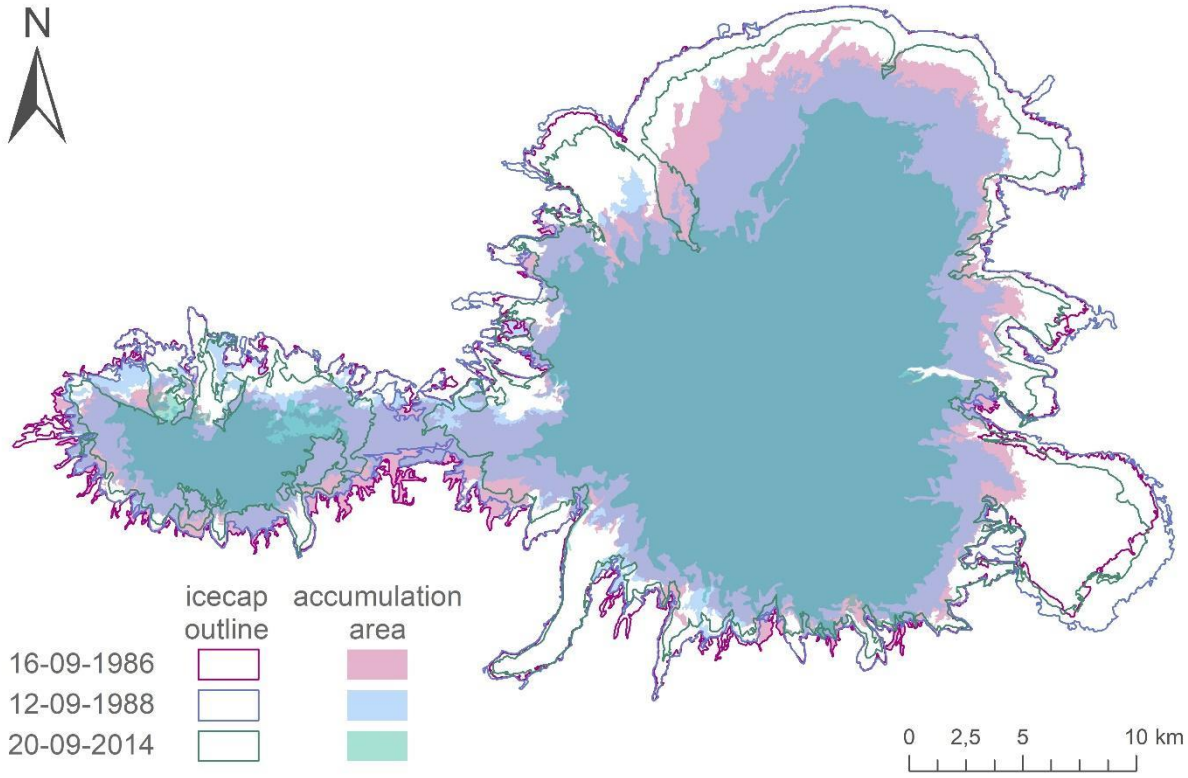

Fig. 27. Change of area of ice caps and accumulation zones (derived based on Landsat Level-2 Science Products courtesy of the U.S. Geological Survey Earth Resources Observation and Science Center)

Based on the study findings (Fig. 27) the AARs in subsequent years for both ice caps were calculated (Tab. 5). AAR is the ratio of the area of accumulation zone to the area of the entire glacier (0 – 100%). The higher the ratio value is, the higher the glacier feed is and thus its lifespan (Jania 1997). The AAR is constant when the glacier is in the steady-state – annual net balance is equal to zero. Glacier geometry does not change, and the margins are stable because it is in equilibrium with the climate (Ignéczi and Nagy 2013).

In the 1980s, the AAR of both glaciers oscillated around 70%. In 2014, it was only just over 50%. Change in the ratio of the accumulation area to the ablation area means decreasing the inflow into the glacier and thus foreruns its contraction in the future.

In the 1980s Mýrdalsjökull and Eyjafjallajökull were linked. In 2014 they are clearly separated (Fig. 27). In order to estimate the two glaciers separately (Tab. 5), the outlines and accumulation areas were splited. The borderline was defined based on comparisons of glacier images from different years as well as on the generated drainage basins and flow accumulation rasters.

Tab. 5. Area of ice caps, Accumulation Zones and Accumulation Area Ratio (AAR)

Year	Ice cap	Area [km2]		
		Entire glacier	Accumulation Area	AAR [%]
1986	Mýrdalsjökull	616*	446	72.40
	Eyjafjallajökull	103	67	65.05
	both ice caps in total	719*	513	71.35
1988	Mýrdalsjökull	620	408	65.81
	Eyjafjallajökull	96	67	69.79
	both ice caps in total	716	475	66.34
2014	Mýrdalsjökull	526	288	54.75
	Eyjafjallajökull	61	32	52.46
	both ice caps in total	587	320	54.51

*The missing part of Kötlujökull estimated to approx. 10 km^2 was added to the Mýrdalsjökull and thus the total area in 1986.

The overall accuracy for glaciers area mapping is above 95% and the kappa coefficient calculations indicate that the maps are at least 90% better than a chance. The accumulation area mapping assures more than 85% overall accuracy and the kappa proves that it is at least nearly 70% better than random agreement (App. 4).

5.2 Drivers of change

It seems that the driving factor for the glacier fluctuations is rising temperature (Fig. 28). The temperature recorded by the meteorological stations in the close proximity of the study area has been steadily rising (Fig. 7.). To prove this, the correlation between the glaciers' area and the temperature was investigated (Tab. 6; Fig. 29).

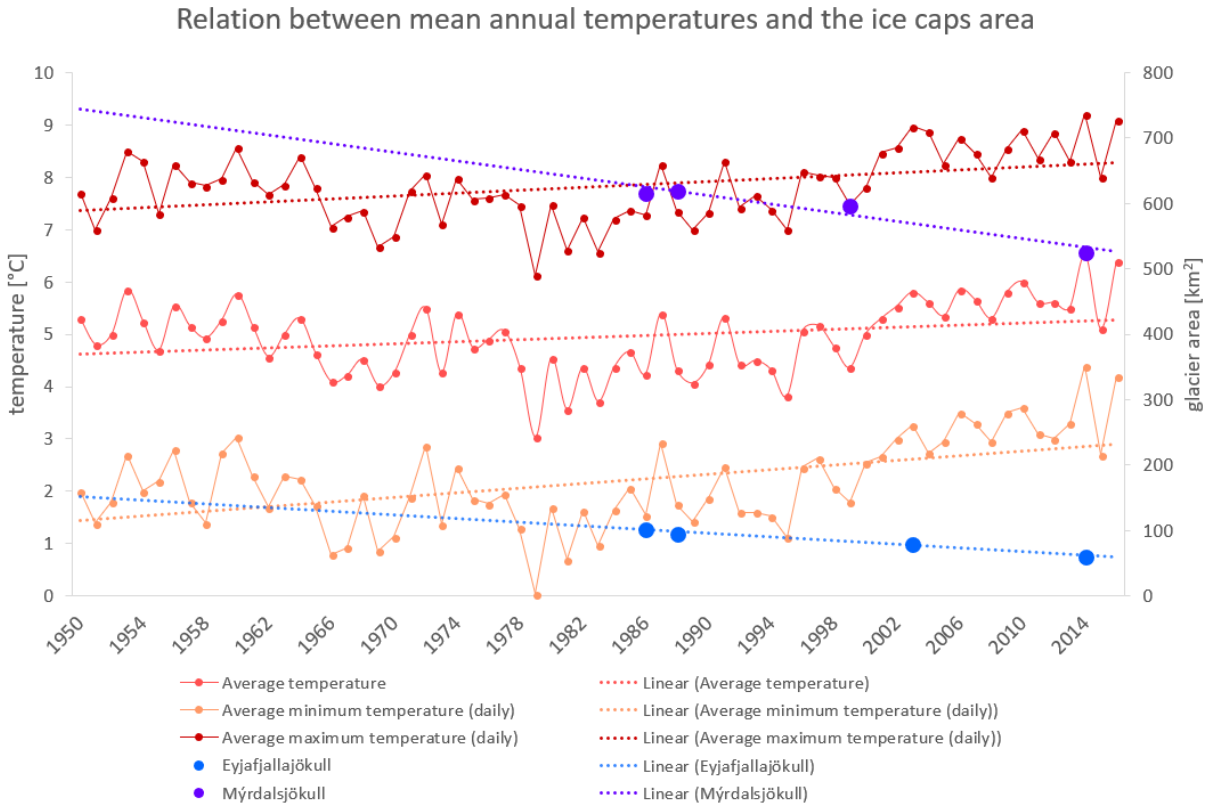

Fig. 28. Relation between the temperature recorded by the meteorological stations in the close proximity of the study area (Icelandic Meteorological Office) and area of Mýrdalsjökull and Eyjafjallajökull ice caps. The area of Mýrdalsjökull in 1999 and Eyjafjallajökull in 2003 were taken from Kargel et al. 2014 (Tab. 2)

The null hypothesis (H_0) assumed that there is no correlation between glacier area and temperature. The alternative hypothesis (H_A) assumed, on the other hand, that glacier area depends on temperature. The target significance level of the test was set to 0.05 ($\alpha = 5\%$). All three temperature measurements (mean, minimum and maximum) were tested.

Tab. 6. Correlation between glaciers' area and temperature (temperature data source: Icelandic Meteorological Office)

	Eyjafjallajökull	Mýrdalsjökull
Annual average temperature		
intercept	170.5465	779.6610
slope	-16.3921	-39.0730
regression model	*y=-16.39x+70.55*	*y=-39.07x+779.66*
r^2	**0.9548**	**0.9584**
F	42.2204	46.0909
F-significance	0.0229	0.0210
hypothesis accepted	H_A	H_A
Average daily maximum temperature		
intercept	224.3990	955.4156
slope	-17.0042	-46.7429
regression model	*y=-17.00x+224.40*	*y=-46.74x+955.42*
r^2	**0.8751**	**0.9728**
F	14.0175	71.5672
F-significance	0.0645	0.0137
hypothesis accepted	H_0	H_A
Average daily minimum temperature		
intercept	122.7647	664.7767
slope	-13.7744	-31.5902
regression model	*y=-13.77x+122.76*	*y=-31.59x+664.78*
r^2	**0.9848**	**0.9599**
F	129.5150	47.8354
F-significance	0.0076	0.0203
hypothesis accepted	H_A	H_A

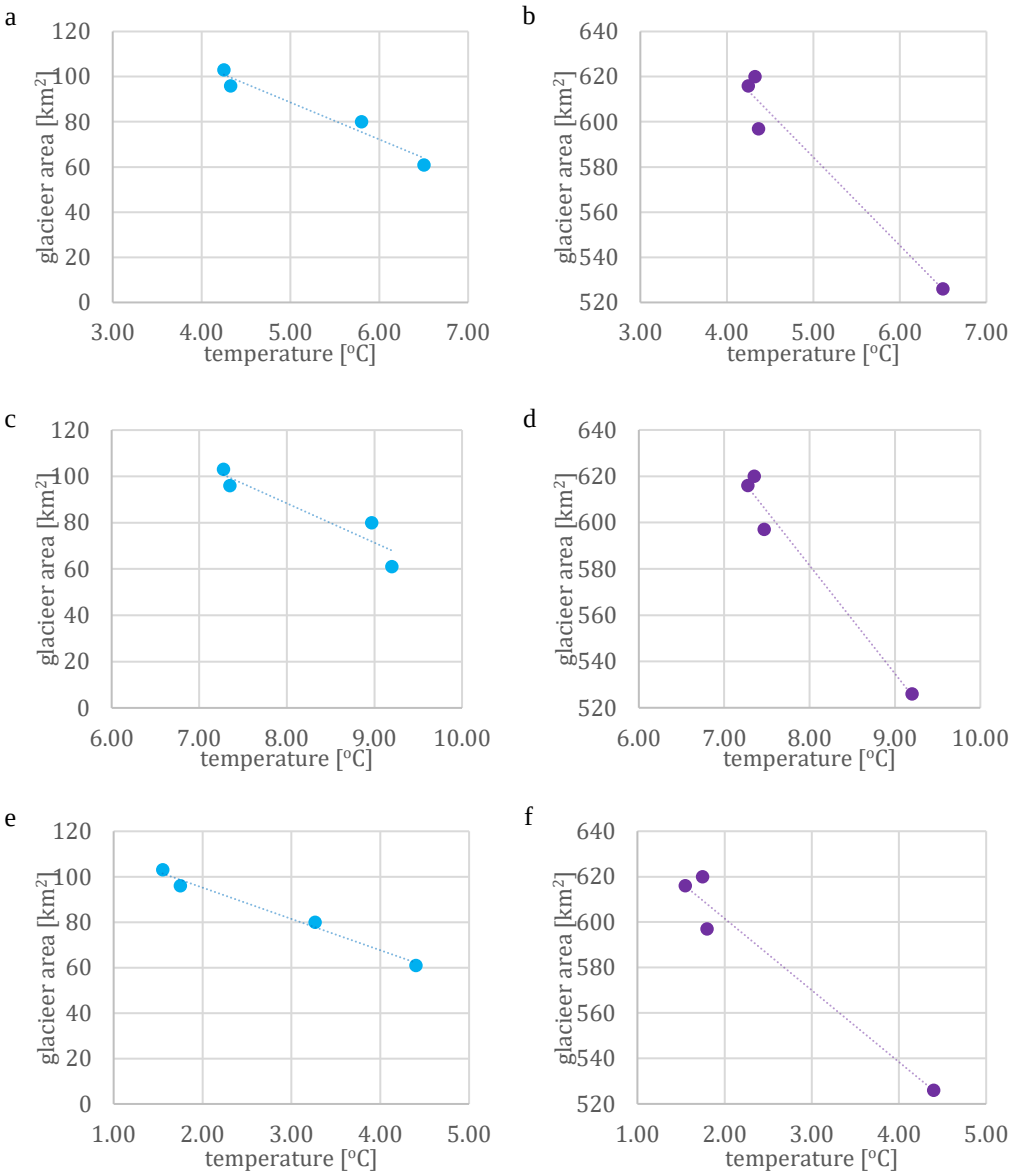

Fig. 29. Scatter plots with regression lines for Eyjafjallajökull (a, c, e) and Mýrdalsjökull (b, d, f) vs mean (a, b), max (c, d) and min (e, f) temperatures (temperature data source: Icelandic Meteorological Office)

The regression analysis was firstly intended to be performed only on glacier measurements from 1986, 1988 and 2014. However, the F-significance test in the majority of cases was failed (F-significance > 0.05). Therefore, the measurements from Kargel et al. (2014) for 1999 for Mýrdalsjökull, and 2003 for Eyjafjallajökull, were incorporated. After adding these observations, all performed tests but one (Eyjafjallajökull area correlated with average from daily maximums), proved to be statistically significant. The analysis proved a strong correlation between glaciers' area and temperature. For all significant tests, the coefficient of determination (r^2) exceeds 0.95 meaning, that more than 95% of the variation in glacier area can be explained by the temperature factor. The results of the analysis are presented in the Tab. 6 and on the Fig. 29.a–f.

Similarly, the precipitation influence on the glaciers was intended to be tested. The precipitation volume in the Mýrdalsjökull glacier group region was rising simultaneously with the temperature (Fig. 7). Since it is the winter part of precipitation levels that contributes to the glacier body growth (Kargel et al. 2014), for the analysis only the records from the winter season preceding the glacier measurements were used. Eventually, regression analysis proved not to be significant for neither of the icecaps.

6. Discussion

6.1 Optimized methodology

The selected methods NDSI and R/NIR ratio images were successfully applied in mapping ice caps and their characteristics. They gave good results although some limitation of the methods and known issues were identified.

The accuracy directly depends on the spatial resolution of the image. While the Landsat pixel size is 30 m x 30 m, thus the accuracy of glacier boundary delineation come to ± 30 m. When it comes to geometric correction accuracy, Root Mean Square Error (RMSE) for the terrain-corrected Level-2 Landsat Scientific Data Products should not be higher than 12 m. This should assure sufficient precision for time-series pixel-level analysis (Young et al. 2017). The accuracy should, however, be double-checked when the mosaicking of adjacent images is involved (as the images taken on the 16th of September 1986 required) (Young et al. 2017). As recommended by Young et al. (2017), the accuracy of the geocoded mosaic was visually double-checked, and no errors were detected. It was done only visually, as no field measurements were available.

Atmospheric effects variate distinctly over the Earth surface and thus can be difficult to be corrected. It is worth to be noted that Landsat Surface Reflectance products uncertainty is greatest at high latitudes. However, since the Eyjafjallajökull summit is located at 63.6 ºN, and USGS (USGS 2017a; USGS 2017b) give the threshold of 65º, it was decided to proceed with this data. Also, according to the approach presented by Selkowitz and Forster (2015), if the manual checking does not rise a flag on significant errors that could violate the ability to discriminate snow and ice, the standardized Landsat surface reflectance products might be successfully used even on higher latitudes. An alternative to using surface reflectance data could be performing relative radiometric correction (applying same radiometric scale to all bands according to the reference) (Young et al. 2017).

Surface reflectance values derived with both LEDAPS and LaSRC algorithms vary between -2000 and 16 000. The valid reflectance ranges from 0 to 10 000 (USGS 2017a, 2017b). Some pixels on particular bands exceed this range. Such pixels were excluded in further analysis. On each stage, their position was assessed towards possible influence on the analysis. All in all, the quality of the three preselected scenes was found sufficient for further analysis.

A number of authors highlight the importance of using corrected surface reflectance instead of raw digital number data (Adamczyk and Będkowski 2005; Burns and Nolin 2014; Hall et al. 1995; Selkowitz and Forster 2015; Young et al. 2017). The study follows the prevailing approach that atmospherically corrected surface reflectance images are better for time series analyses. Nevertheless, it should be noted, that some authors undermine this opinion indicating that digital number values give better results. For example, Paul (2000) claims that raw data gave better results in creating ratio images for studying the glaciers of the Swiss Alps.

The choice of September images was driven by the assumption, that as the summer progressed, the area covered with snow can only be reduced by melting, while there is a low likelihood for a significant snowfall (Górzyńska 2008). This is crucial to accurately define equilibrium line altitude (ELA). Visual inspection does not unveil fresh precipitation, notwithstanding this possibility cannot be completely ruled out.

Although the images were carefully selected against cloud occurrence (Fig. 17, 18), a presence of smaller clouds and their shadows seemed to be inevitable, especially in maritime climate zones and in areas situated close to the sea. Snow and clouds share a similar spectral signature, especially in the visible and IR wavelengths (Gao and Liu 2001). Even small clouds and cloud shadows can cause some minor errors.

It needs to be emphasized that errors due to mountainous topography can significantly influence the results. Since the landscape on satellite imageries is represented as a flat surface, the snow covering steeper slopes is omitted in area calculations. This might lead to serious underestimation of snow-cover area (Hall et al. 1995). Moreover, images of mountain areas are radiometrically varied due to the high differences in the terrain exposure, which arise from the relation of the solar radiation angle, the slope, and aspect. As a result, clear differences in reflectance values of individual slopes are observed (Adamczyk and Będkowski 2005; Gao and Liu 2001).

Even though the Landsat images Level-2 are co-registered across the Landsat satellites series, when dealing with data from different sensor groups caution is required (Roy et al. 2016). One needs to keep in mind that differences in OLI sensor versus previous instruments (TM, ETM, ETM+; spectral resolution in particular), as well as changes in preprocessing algorithm (LaSRC vs LEDAPS), might create issues and have an influence on time series analyses (Holden and Woodcock 2016). There are visible differences between pictures taken in 2014 and in the 1980s

(Fig. 17). The natural color composites show different tins – more greenish for OLI images. Images acquired by Landsat 5 TM show some saturation, especially in the red band, however, affected pixels are located on the top of the glaciers (not on more 'sensitive' boundary zone), so it should not influence the delineation of the glacier body.

NDSI and NDSII, calculated to map the spatial extent of the ice caps, were virtually no different from each other (Fig. 20; App. 4). Generally, the number of invalid pixels is higher for NDSII than for NDSI. Due to these facts, the NDSI was retained and used for further analysis. Similar conclusions have been drawn by Górzyńska (2008) and Xiao et al. (2001).

The most suitable NDSI threshold for delineating glacier boundaries turned out to be the value of approximately 0.4 (Fig. 21, App. 4). Pixels equal or above this threshold represents the glacier body. This choice is in line with Hall et al. (1995) findings from studies on snow cover across the United States and Iceland.

One of the main problems in separating glaciers from the surrounding ground was caused by the similarity of the surface of the debris-covered front of the glacier to the surrounding rocks. When the glacier stagnates or recedes, the deposited material carried by the glacier melts with the ice. So-called supraglacial debris forms on the termini surface. The surface of the glacier, covered in debris, gives a very similar spectral signature, as the surrounding soil, which causes considerable difficulties in their discrimination (Williams et al. 1997). In case of Icelandic glaciers, additionally, possible tephra deposition pose similar difficulties. Some help in the interpretation might give auxiliary features, such as melt lakes at the glacier front – it is easy to distinguish ice, even covered with rubble, from a water reservoir. Another possible solution would be using stereoscopic images to distinguish the moraine (Górzyńska 2008). This issue emerged in the delineation of Kötlujökull outlet glacier (the south-east part of the Mýrdalsjökull; Fig. 12.a). Based on information from TIRS sensor (Fig. 23) and DigitalGlobe high-resolution image (Fig. 22), the missing part of Kötlujökull was manually digitized and its area estimated to approximately 10 km^2.

In comparison with LandsatLook quality images (Fig. 17), the glaciers are much better delineated. It is, however, worth noticing that shadows on TM images seemed to be slightly better extracted on USGS products. On the other hand, LandsatLook quality images cannot cope with debris covered fronts – in this case, NDSI shows a much better performance.

According to Hall et al. (1995), the NDSI method performance is better than a supervised classification. Nevertheless, the analysis could also be further extended by various classification methods – supervised and unsupervised. Notwithstanding, one should consider using for this purpose different software. Although ArcGIS ArcMap ESRI provides some basic classification tools, it is still more GIS-oriented, while such extensive and advanced remote sensing analysis, might require special remote sensing dedicated software (e.g. Envi or Erdas). In the presented study another roadblock in applying classification was the fact, that there were no available field measurements, based on which it would be possible to check the reliability of the classification. Therefore, classes could have been aggregated only visually, based on comparisons with color composites.

In the search for a suitable method for delineating equilibrium line altitude (ELA), several ratio images combinations were tested (Fig. 24). NIR/SWIR1 was recommended by among others Hall et al. (1987, 1989), Jacobs et al. (1997), Williams et al. (1991). Red/SWIR1 was used by Rott (1994) and Bronge L. and Bronge C. (1999). R/ NIR proposed also by Bronge and Bronge 1999, Xiao et al. 2001, turned out to work best on analyzed data and was used in further operations.

In general, the delineation of glacier zones was more difficult to perform than mapping the spatial extent of the glaciers. The main problem in defining the proper threshold posed jagged aprons of imposed snow (Fig. 26). This issue was also raised by Williams et al. (1991).

Despite using level-2 Landsat data products, the differences between TM and OLI sensors are visible virtually on each stage of the analysis (Fig. 17). Both the index ‘contrast’ as well as in the distribution of invalid pixels (Fig. 20) are affected. This fact had an influence on the analysis and might have had affected the results.

The invalid pixels of TM images are mostly concentrated on ‘overexposed’ southern slopes of the glacier (Fig. 20, 25). This is especially problematic in the image from 1988, where invalid pixels cover expansively the southern slope of Eyjafjallajökull. OLI imageries invalid pixels seemed to be correlated with shadows cast by slopes (Fig. 20, 25).

Slopes to the north of Eyjafjallajökull and North-West of Mýrdalsjökull are enshadowed and the NDSI algorithm shows some inaccuracies when dealing with these areas. Some of them were incorrectly classified as glacier ice. It is noticeable, especially on TM images. The most affected are northern slopes of Eyjafjallajökull.

It can be noticed that both the NDSI classified image as well as the ratio image generated from OLI data, are much more readable and clear than scenes from TM (Fig. 20, 21, 25). There are fewer artifacts and outliers. The images seem to be more coherent with less ‘noise’.

Images acquired by the two sensors demanded different threshold value when it comes to segmentation of ratio images. For OLI data it was established to be 1.22 while for TM ratio it was set to 1.12 (Fig. 25). This variation, as well as the difference in ratio image legibility, eventuate from different spectral resolutions of the two Landsat sensors.

In 1980s Mýrdalsjökull and Eyjafjallajökull formed one ice body. On the image from 2014, they were separated into two glaciers (Fig. 27). In order to calculate the area and accumulation zones of the two ice caps, the outlines were split based on a comparison of glacier images from different years as well as on the generated drainage basins and flow accumulation rasters. This operation might have introduced some inaccuracies.

6.2 Evolution of Mýrdalsjökull and Eyjafjallajökull glaciers

Both glaciers have shrunk (Fig. 21, 27; Tab. 5), but the change of Eyjafjallajökull is especially striking. Between 1986 and 2014 its spatial extent depleted for almost a half.

From the north, the ELA runs lower than on the southern slopes. It might be due to ocean proximity. Also, the southern slopes are steeper (Fig. 8). It does not seem to be caused by precipitation pattern. Actually, the precipitations are even higher in the south (Fig. 9).

The general downward trend in glaciers spatial extent is in accordance with the information harvested within Global Land Ice Measurements from Space (GLIMS) program framework (Kargel et al. 2014). Although it seems that from the beginning of the 21st century (when the GLIMS measurements were conducted for Mýrdalsjökull (1999) and Eyjafjallajökull (2003)) this process has speeded up. This conclusion is in line with records of termini positions by WGMS and Iceland Glaciological Society (Fig. 13; App. 2). The termini monitoring records for the Mýrdalsjökull outlet Sólheimajökull and Gígjökull – the Eyjafjallajökull outlet glacier, cover similar time period as discussed in this study. These measurements generally consent with the project findings. During the years 1986 – 2014 Sólheimajökull terminus has retreated by approximately 850 m, while Gígjökull (latest records available for 2012) by almost 1100 m. In addition, WGMS measurements of Mýrdalsjökull thickness shows that between 2010 and 2015, the glacier thinned for about 1.9 m (App. 3) (WGMS 2017). There is a general decile in mass and volume of glaciers and ice caps (Olsen et al. 2011). The majority of the loss is attributable to anthropogenic causes (Box and Sharp 2017).

The correlation analysis (Tab. 6; Fig. 29) reaffirm that the rising temperature recorded by the meteorological stations around the study area (Fig. 7), is a driving factor for the glaciers' fluctuations. It is difficult though to decide which temperature measurements (mean, minimum or maximum) have the strongest influence on the glaciers. Larger sample size could shed some more light on this aspect. It might also help prospect the glaciers' response time.

The fact that precipitation volume in the study area was rising simultaneously with the temperature (Fig. 7), coincides with the theory that the increase in evaporation from the oceans conduces the formation of clouds, and that the generally increased intensity of the hydrologic cycle accompanying the global warming, might lead to increase in precipitation levels (Prowse 2009; Mård et al. 2017; Jania 2008). However, despite the increased snow deposition, the glaciers were shrinking. This suggests that the rise in temperature that the ice caps are exposed

to, overshadow the effect of heightened precipitation. To similar conclusions come Björnsson and Pálsson (2008), Jaenicke et al. (2006), Jóhannesson and Sigurdsson (1998) and Sigurðsson et al. (2007), highlighting that the rising temperature is more important for the observed glaciers change than the precipitation.

The behavior of the glaciers is very complex and is a subject to many influences. The important influence on such dramatic change in glacier size, aside from climatic variations, most likely had also the recent Eyjafjallajökull eruption in spring 2010. The eruption resulted not only in a direct snow and ice melting, but also led to jökulhlaups and thus the further glacier mass loss. Additionally, associated tephra deposit decreased the albedo and speeded up further melting.

The mass loss rate for Icelandic glaciers for years 2003 – 2009 was estimated to be 10 ± 2 Gt y-1. Owing to its sub-Arctic latitudes and maritime climate, Icelandic glaciers are temperate and experience relatively high rates of accumulation. Therefore, they tend to be more sensitive to climate warming (Box and Sharp 2017). Recent researches show that the Arctic climate has entered the warmest period since the instrumental record (Overland et al. 2017a) and some paleo-reconstructions indicate that current Arctic summer temperatures are highest in the past 2000 years (Callaghan et al. 2011b; Olsen et al. 2011).

The changes of glaciers are of crucial importance both globally as well as for local scale. The main rivers of Iceland are of glacial origin. Many of them have been harnessed to generate hydropower and have great economic value for the country. The glacial recession will have a significant impact on Iceland's energy planning and management. When glaciers melt away, river discharge will come solely from precipitation. Some of the rivers without a glacial supply are expected to dry up entirely (Björnsson and Pálsson 2008).

7. Conclusions

This study aimed to assess how the Icelandic glaciers from Mýrdalsjökull group have evolved over the last decades (from the 1980s to 2014). It involves both mapping the spatial extent of the glacier as well as defining the equilibrium line altitude (ELA) and thus the accumulation zone vs ablation zone. The best results were obtained by using the Normalized Difference Snow Index (NDSI) to determine the boundaries of glaciers, and Red / Near-Infrared ratio images for determining accumulation and ablation zones and thus finding equilibrium line altitude (ELA). The accuracy was examinated and suitable thresholding was applied on calculated images. During the last decades (from the 1980s to 2014), the ice caps of the Mýrdalsjökull group in the Suðurland region have dramatically reduced their surface area. Eyjafjallajökull has decreased by more than 40%. Once joined, currently, the ice caps form two separate ice bodies. These results are consistent with the Global Land Ice Measurements from Space (GLIMS) program findings and the World Glacier Monitoring Service (WGMS) and Iceland Glaciological Society observations of termini positions. Moreover, the decrease in the ratio of accumulation zone to entire glacier extent (AAR) gives an outlook of an even greater reduction of the glacial spatial extent in the future. The dominant driving factor for such a dramatic change seems to be an increase in temperature associated with observed global climate warming.

Known issues include, in particular, debris covered termini, and, specific for volcanically active regions, tephra layers; which spectral signatures are similar to the spectral response of surrounding basalt rocks. Moreover, jaded aprons of imposed snow make it difficult to unambiguously identify ELA. In addition, since the study area is mountainous, there are shadows cast by ridges and protruding rocks. An issue posed also the differences between the two generations of Landsat sensors – OLI and TM.

The cryosphere is an integral part of the global climate system. Its occurrence is dependant on climatic conditions but also significantly affects the climate. Changing climate is having widespread impacts, and these will be presumably even more intensified in the future. Climate change will have severe consequences both globally (first and foremost increasing ocean level) as well as on the local scale. Observations of glaciers, as Earth's components extremely sensitive to these factors, allows to better estimate current and future changes. In addition, ice masses melting triggers a number of feedbacks that further accelerate climate change. The disappearance of glaciers intrinsically has also direct consequences. It will affect both glacial-

dependent unique ecosystems as well as local communities, for which glaciers constitute a reservoir of drinking water and feed glacial rivers producing hydropower.

8. References

Adamczyk J., Będkowski K., 2005: Metody cyfrowe w teledetekcji (Digital methods in remote sensing). Wydawnictwo SGGW, Warszawa.

AMAP, 2017. Snow, Water, Ice and Permafrost in the Arctic (SWIPA) 2017. Arctic Monitoring and Assessment Programme (AMAP), Oslo, Norway.

Aniya, m., Sato, h., Naruse, R., Skvarca, P. & Casassa, G. 1996. The use of satellite and airborne imagery to inventory outlet glaciers of the Southern Patagonian Icefield, South America. Photogrammetric Engineering and Remote Sensing 62: 1361-1369

Arrhenius, S., 1896. On the influence of carbonic acid in the air upon the temperature of the ground. The London, Edinburgh, and Dublin Philosophical Magazine and Journal of Science, 41(251), pp.237-276.

Bamber, J.L. and Payne, A.J. eds., 2004. Mass balance of the cryosphere: observations and modelling of contemporary and future changes. Cambridge University Press.

Barber, D. G., Meier, W. N., Gerland, S., Mundy, C.J., Holland, m., Kern, S., Li, Z., Michel, C., Perovich, D. K., Tamura T., 2017, Arctic sea ice', in Snow, Water, Ice and Permafrost' in the Arctic (SWIPA) 2017, Arctic Monitoring and Assessment Programme (AMAP), Oslo, Norway.

Benson, C. S., 1960. Stratigraphic studies in the in the snow and firn of the Greenland ice sheet (Ph.D. Dissertation). California Institute of Technology.

Björnsson, h. and Pálsson, F., 2008. Icelandic glaciers. Jökull, 58, pp.365-386.

Björnsson, h., Pálsson, F. and Guðmundsson, m.T., 2000. Surface and bedrock topography of the Mýrdalsjökull ice cap: The Katla caldera, eruption sites and routes of jökulhlaups. Jökull, 49, pp.29-46.

Björnsson, h., Pálsson, F., Gudmundsson, S., Magnússon, E., Adalgeirsdóttir, G., Jóhannesson, T., Berthier, E., Sigurdsson, O. and Thorsteinsson, T., 2013. Contribution of Icelandic ice caps to sea level rise: Trends and variability since the Little Ice Age. Geophysical Research Letters, 40(8), pp.1546-1550.

Bonecki h. eds., 1974. Encyklopedia Powszechna PWN. T. 2. G-M. Warszawa, Państwowe Wydawnictwo Naukowe, s. 303

Box, J. E. and Colgan W. T., 2017, Sea level rise contribution from Arctic land ice: 1850-2100. In: Snow, Water, Ice and Permafrost' in the Arctic (SWIPA) 2017, Arctic Monitoring and Assessment Programme (AMAP), Oslo, Norway.

Box, J. E., and Sharp m., 2017, Changes to Arctic land ice. In: Snow, Water, Ice and Permafrost' in the Arctic (SWIPA) 2017, Arctic Monitoring and Assessment Programme (AMAP), Oslo, Norway.

Bronge, L. B. and Bronge, C., 1999. Ice and snow-type classification in the Vestfold Hills, East Antarctica, using Landsat-TM data and ground radiometer measurements. International Journal of Remote Sensing, 20(2), pp.225-240.

Brown, I. A., Kirkbride, m.P. and Vaughan, R.A., 1999. Find the firn line! The suitability of ERS-1 and ERS-2 SAR data for the analysis of glacier facies on Icelandic ice caps. International Journal of Remote Sensing, 20(15-16), pp.3217-3230.

Brown, R., Vikhamar Schuler, D., Bulygina, O., Derksen, C., Luojus, K., Mudryk, L., Wang, L., Yang, D. 2017, 'Arctic terrestrial snow cover'. In the Arctic (SWIPA) 2017, Arctic Monitoring and Assessment Programme (AMAP), Oslo, Norway.

Burns, P. and Nolin, A., 2014. Using atmospherically-corrected Landsat imagery to measure glacier area change in the Cordillera Blanca, Peru from 1987 to 2010. Remote Sensing of Environment, 140, pp.165-178.

Callaghan, T.V., Johansson, m., Brown, R.D., Groisman, P.Y., Labba, N., Radionov, V., Barry, R.G., Bulygina, O.N., Essery, R.L., Frolov, D.M. and Golubev, V.N., 2011a. The changing face of Arctic snow cover: A synthesis of observed and projected changes. AMBIO: A Journal of the Human Environment, 40(sup 1), pp.17-31.

Callaghan, T.V., Johansson, m., Brown, R.D., Groisman, P.Y., Labba, N., Radionov, V., Bradley, R.S., Blangy, S., Bulygina, O.N., Christensen, T.R. and Colman, J.E., 2011b. Multiple effects of changes in Arctic snow cover. AMBIO: A Journal of the Human Environment, 40(sup 1), pp.32-45.

Callaghan, T.V., Johansson, m., Key, J., Prowse, T., Ananicheva, m. and Klepikov, A., 2011c. Feedbacks and interactions: From the Arctic cryosphere to the climate system. AMBIO: A Journal of the Human Environment, 40(sp1), pp.75-86.

Callaghan, T.V., Johansson, m., Prowse, T.D., Olsen, m.S. and Reiersen, L.O., 2011d. Arctic cryosphere: changes and impacts. AMBIO: A Journal of the Human Environment, 40(sup1), pp.3-5.

Christensen, T., R., Rysgaard, S., Bendtsen, I., Else, B., Glud, R., N., Huissteden, K., Parmentier, F-J., W., Sachs, T., Vonk J. E., 2017, Arctic carbon cycling. In: Snow, Water, Ice and Permafrost' in the Arctic (SWIPA) 2017, Arctic Monitoring and Assessment Programme (AMAP), Oslo, Norway.

Dozier, J. and Marks, D., 1987. Snow mapping and classification from Landsat Thematic Mapper data. Annals of Glaciology, 9, pp.97-103.

Dozier, J., 1984. Snow reflectance from Landsat-4 thematic mapper. IEEE Transactions on Geoscience and Remote Sensing, (3), pp.323-328.

Fick, S.E. and Hijmans, R.J., 2017. WorldClim 2: new 1-km spatial resolution climate surfaces for global land areas. International Journal of Climatology, 37(12), pp.4302-4315; http://worldclim.org/

Flowers, G.E., Björnsson, h., Geirsdóttir, Á., Miller, G.H., Black, J.L. and Clarke, G.K., 2008. Holocene climate conditions and glacier variation in central Iceland from physical modelling and empirical evidence. Quaternary Science Reviews, 27(7-8), pp.797-813.

Gao, J. and Liu, Y., 2001. Applications of remote sensing, GIS and GPS in glaciology: a review. Progress in Physical Geography, 25(4), pp.520-540.

Geirsdóttir, Á., Miller, G.H., Axford, Y. and Ólafsdóttir, S., 2009. Holocene and latest Pleistocene climate and glacier fluctuations in Iceland. Quaternary Science Reviews, 28(21-22), pp.2107-2118.

Górzyńska m., 2008. Zmiana zasięgu lodowca Vatnajökull na Islandii w latach 1991–1999 na podstawie obrazów satelitarnych wykonanych przez satelitę Landsat (Changes in range of Vatnajökull ice cap (Iceland), based on Landsat imagery, 1991–1999). Teledetekcja Środowiska, Vol. 40, pp. 85-99.

Guðjónsdóttir, S., 2015. Landshagir 2015 (Statistical Yearbook of Iceland 2015). Statistics Iceland, vol. 25.

Hall, D.K., Chang, A.T. and Siddalingaiah, h., 1988. Reflectances of glaciers as calculated using Landsat-5 Thematic Mapper data. Remote Sensing of Environment, 25(3), pp.311-321.

Hall, D.K., Chang, A.T.C., Foster, J.L., Benson, C.S. and Kovalick, W.M., 1989. Comparison of in situ and Landsat derived reflectance of Alaskan glaciers. Remote Sensing of Environment, 28, pp.23-31.

Hall, D.K., Ormsby, J.P., Bindschadler, R.A. and Siddalingaiah, h., 1987. Characterization of snow and ice reflectance zones on glaciers using Landsat Thematic Mapper data. Annals of Glaciology, 9, pp.104-108.

Hall, D.K., Riggs, G.A. and Salomonson, V.V., 1995. Development of methods for mapping global snow cover using moderate resolution imaging spectroradiometer data. Remote sensing of Environment, 54(2), pp.127-140.

Holden, C.E. and Woodcock, C.E., 2016. An analysis of Landsat 7 and Landsat 8 underflight data and the implications for time series investigations. Remote Sensing of Environment, 185, pp.16-36.

Ignéczi, Á. and Nagy, B., 2013. Determining steady-state accumulation-area ratios of outlet glaciers for application of outlets in climate reconstructions. Quaternary international, 293, pp.268-274.

Jacobs, J.D., Simms, É.L. and Simms, A., 1997. Recession of the southern part of Barnes Ice Cap, Baffin Island, Canada, between 1961 and 1993, determined from digital mapping of Landsat TM. Journal of Glaciology, 43(143), pp.98-102.

Jaenicke, J., Mayer, C., Scharrer, K., Münzer, U. and Gudmundsson, Á., 2006. The use of remote-sensing data for mass-balance studies at Mýrdalsjökull ice cap, Iceland. Journal of Glaciology, 52(179), pp.565-573.

Jania J., 1997.Glacjologia (Glaciology). PWN Warszawa.

Jania J., 2008. Konsekwencje globalnego ocieplenia dla kriosfery (eng. Consequences of the Global Warming on the Kriosphere). Nauka 3: pp. 35-58

Jonsell, U., Hock, R. and Holmgren, B., 2003. Spatial and temporal variations in albedo on Storglaciären, Sweden. Journal of Glaciology, 49(164), pp.59-68.

Jóhannesson, T. and Sigurðsson, O., 1998. Interpretation of glacier variations in Iceland 1930-1995. Jökull, 45, 27-34.

Jóhannesson, T., Aðalgeirsdóttir, G., Björnsson, h., Crochet, P., Elíasson, E.B., Guðmundsson, S., Jónsdóttir, J.F., Ólafsson, h., Pálsson, F., Rögnvaldsson, Ó. and Sigurðsson, O., 2007. Effect of climate change on hydrology and hydro-resources in Iceland. Orkustofnun.

Jóhannesson, T., Björnsson, h., Magnússon, E., Guðmundsson, S., Pálsson, F., Sigurðsson, O., Thorsteinsson, T. and Berthier, E., 2013. Ice-volume changes, bias estimation of mass-balance measurements and changes in subglacial lakes derived by lidar mapping of the surface of Icelandic glaciers. Annals of Glaciology, 54(63), pp.63-74.

Kargel, J.S., Leonard, G.J., Bishop, m.P., Kääb, A. and Raup, B.H. eds., 2014. Global land ice measurements from space. Springer. Kohut M, Kwasniak m. Islandia-unikatowa kraina trzech żywiołów (Iceland – unique land of three elements). Wszechświat. 2012;113(01-03), pp. 62–67.

Khorram, S., Koch, F.H., van der Wiele, C.F. and Nelson, S.A., 2012. Remote sensing. Springer

Kokelaar, B.P. and Durant, G.P., 1983. The submarine eruption and erosion of Surtla (Surtsey), Iceland. Journal of Volcanology and Geothermal Research, 19(3-4), pp.239-246.

Mård, J., Box, J., E., Brown, R., Mack, m., Mernild, S., h., Walker, D., Walsh J., 2017, Cross-cutting scientific issues. In: Snow, Water, Ice and Permafrost' in the Arctic (SWIPA) 2017, Arctic Monitoring and Assessment Programme (AMAP), Oslo, Norway.

Molewski P. eds., 2005. Rekonstrukcja procesów glacjalnych w wybranych strefach marginalnych lodowców Islandii – formy i osady: terenowe warsztaty geomorfologiczne, Islandia, 14-28 sierpnia 2005: przewodnik wycieczki terenowej (Reconstruction of glacial processes in the chosen marginal zones of the Icelandic glaciers – forms and deposits). Instytut Geografii UMK, Stowarzyszenie Geomorfologów Polskich

O'Brien, h. W., and Munis, R. h., 1975Red and near-infrared spectral reflectance of snow. NASA. Goddard Space Flight Center Operational Appl. of Satellite Snowcover Observations; p 345-360

Olsen, m.S., Callaghan, T.V., Reist, J.D., Reiersen, L.O., Dahl-Jensen, D., Granskog, m.A., Goodison, B., Hovelsrud, G.K., Johansson, m., Kallenborn, R. and Key, J., 2011. The changing Arctic cryosphere and likely consequences: An overview. AMBIO: A Journal of the Human Environment, pp.111-118.

Overland, J., Walsh, J., Kattsov V., 2017a, Trends and feedbacks. In: Snow, Water, Ice and Permafrost' in the Arctic (SWIPA) 2017, Arctic Monitoring and Assessment Programme (AMAP), Oslo, Norway.

Overland, J., Walsh, J., Kattsov, V., Barber, D., Box, J. E., Brown, R., Mård, J., Olsen, m. S., Romanovsky V., 2017b, Synthesis: summary and implications of findings. In: Snow, Water, Ice and Permafrost' in the Arctic (SWIPA) 2017, Arctic Monitoring and Assessment Programme (AMAP), Oslo, Norway.

Orheim, O., 2013. Satellite image atlas of glaciers of the world. State of the Earth's cryosphere at the beginning of the 21st century: glaciers, global snow cover, floating ice, and permafrost and periglacial environments. Journal of Glaciology, 59, pp.795-796.

Paul, F., 2000. Evaluation of different methods for glacier mapping using Landsat TM. EARSeL eProceedings, 1, pp.239-245.

Pellikka, P. and Rees, W.G. eds., 2009. Remote sensing of glaciers: techniques for topographic, spatial and thematic mapping of glaciers. CRC Press.

Prowse, T., Alfredsen, K., Beltaos, S., Bonsal, B., Duguay, C., Korhola, A., McNamara, J., Pienitz, R., Vincent, W.F., Vuglinsky, V. and Weyhenmeyer, G.A., 2011a. Past and future changes in Arctic lake and river ice. AMBIO: A Journal of the Human Environment, 40(sup 1), pp.53-62.

Prowse, T. D., Alfredsen, K., Beltaos, S., Bonsal, B., Duguay, C., Korhola, A., McNamara, J., Vincent, W.F., Vuglinsky, V. and Weyhenmeyer, G.A., 2011b. Arctic freshwater ice and its climatic role. AMBIO: A Journal of the Human Environment, 40(sup 1), pp.46-52.

Prowse, T. D., Bring, A., Carmack, E., C., Holland, m., m., Instanes, A., Mård, J., Vihma, T., Wrona, F., J., 2017. Freshwater. In: Snow, Water, Ice and Permafrost' in the Arctic (SWIPA) 2017, Arctic Monitoring and Assessment Programme (AMAP), Oslo, Norway.

Prowse, T.D., 2009. Introduction: hydrologic effects of a shrinking cryosphere. Hydrological Processes, 23(1), pp.1-6.

Romanovsky, V., Isaksen, K., Drozdov, D., Anisimov, O., Instanes, A., Leibman, m., McGuire, A. D., Shiklomanov, N., Smith, S., and Walker, D. 2017, 'Changing permafrost and its

impacts'. In: Snow, Water, Ice and Permafrost' in the Arctic (SWIPA) 2017, Arctic Monitoring and Assessment Programme (AMAP), Oslo, Norway.

Rott, h., 1994. Thematic studies in alpine areas by means of polarimetric SAR and optical imagery. Advances in Space Research, 14(3), pp.217-226.

Roy, D.P., Kovalskyy, V., Zhang, h.K., Vermote, E.F., Yan, L., Kumar, S.S. and Egorov, A., 2016. Characterization of Landsat-7 to Landsat-8 reflective wavelength and normalized difference vegetation index continuity. Remote Sensing of Environment, 185, pp.57-70.

Schuur, E.A.G., McGuire, A.D., Schädel, C., Grosse, G., Harden, J.W., Hayes, D.J., Hugelius, G., Koven, C.D., Kuhry, P., Lawrence, D.M. and Natali, S.M., 2015. Climate change and the permafrost carbon feedback. Nature, 520(7546), pp.171-179.

Selkowitz, D.J. and Forster, R.R., 2015. An automated approach for mapping persistent ice and snow cover over high latitude regions. Remote Sensing, 8(1), p.16.

Sigurðsson, O., 2005. Variations of termini of glaciers in Iceland in recent centuries and their connection with climate. Developments in Quaternary Sciences, Vol. 5, Iceland Modern Processes & Past Environments, pp. 241-255.

Sigurđsson, O., Jónsson, T. and Jóhannesson, T., 2007. Relation between glacier-termini variations and summer temperature in Iceland since 1930. Annals of Glaciology, 46, pp.170-176.

Sigurðsson, O., Williams, R.S., 2008. Geographic names of Iceland's glaciers: historic and modern. US Geological Survey.

Sigurjsson, O., 1998. Glacier variations in Iceland 1930–1995. Jökull, 45, pp.3-26.

Sudnik-Wójcikowska, B., 2011. Aktywność wulkanów w Islandii a naturalna i antropogeniczna roślinność w strefie tundry (Volcanic activity in Iceland and the natural and anthropogenic vegetation in the tundra zone). Kosmos, 3(60), pp.305-312.

Tedesco, m., 2014. Remote sensing of the cryosphere. John Wiley & Sons.

U.S. Geological Survey, 2012. Landsat Ecosystem Disturbance Adaptive Processing System (Ledaps) Algorithm Description Document. Department of Interior U.S. Geological Survey https://landsat.usgs.gov/sites/default/files/documents/ledaps_add.pdf

U.S. Geological Survey, 2015. Landsat surface reflectance data (ver. 1.1, June 16, 2015): U.S. Geological Survey Fact Sheet 2015–3034, 1 p.

U.S. Geological Survey, 2017a. Product Guide: Landsat 4-7 Surface Reflectance Product. Department of Interior U.S. Geological Survey https://landsat.usgs.gov/sites/default/files/documents/ledaps_product_guide.pdf

U.S. Geological Survey, 2017b. Product Guide: Landsat 8 Surface Reflectance Product. Department of Interior U.S. Geological Survey https://landsat.usgs.gov/sites/default/files/documents/lasrc_product_guide.pdf

U.S. Geological Survey, 2017c. Landsat Quality Assurance ArcGIS Toolbox. U.S. Geological Survey software release.

Vincent, W.F., Callaghan, T.V., Dahl-Jensen, D., Johansson, m., Kovacs, K.M., Michel, C., Prowse, T., Reist, J.D. and Sharp, m., 2011. Ecological implications of changes in the Arctic cryosphere. AMBIO: A Journal of the Human Environment, pp.87-99.

Williams, R.S., 1987. Satellite remote sensing of Vatnajökull, Iceland. Annals of Glaciology, 9, pp.127-135.

Williams, R.S., Hall, D.K. and Benson, C.S., 1991. Analysis of glacier facies using satellite techniques. Journal of Glaciology, 37(125), pp.120-128.

Williams, R.S., Hall, D.K., Sigurðsson, O. and Chien, J.Y., 1997. Comparison of satellite-derived with ground-based measurements of the fluctuations of the margins of Vatnajökull, Iceland, 1973–92. Annals of Glaciology, 24, pp.72-80.

Williams, R.S., Jr., and Ferrigno, J.G., eds., 2012, State of the Earth's cryosphere at the beginning of the 21st century – Glaciers, global snow cover, floating ice, and permafrost and periglacial environments: U.S. Geological Survey Professional Paper 1386–A, 546 p.

Xiao, X., Shen, Z. and Qin, X., 2001. Assessing the potential of VEGETATION sensor data for mapping snow and ice cover: a Normalized Difference Snow and Ice Index. International Journal of Remote Sensing, 22(13), pp.2479-2487.

Young, N.E., Anderson, R.S., Chignell, S.M., Vorster, A.G., Lawrence, R. and Evangelista, P.H., 2017. A survival guide to Landsat preprocessing. Ecology, 98(4), pp.920-932.

European Environment Agency (EEA) – Corine Land Cover (CLC) program data, release v.18.5. dated 02/2016; http://www.eea.eu.

European Space Agency ESA – EduSpace; https://www.esa.int/SPECIALS/Eduspace_Global_EN/

GLIMS and NSIDC (2005, updated 2017): Global Land Ice Measurements from Space glacier database. Compiled and made available by the international GLIMS community and the National Snow and Ice Data Center, Boulder CO, U.S.A.; https://nsidc.org/glims

Google Earth: Landsat, Copernicus, DigitalGlobe; https://www.google.com/earth/

Iceland Glaciological Society; http://spordakost.jorfi.is

Icelandic Meteorological Office; http://en.vedur.is

NASA – Earth Observatory; https://earthobservatory.nasa.gov/Features/RemoteSensing/printall.php

NASA – Landsat Science; https://landsat.gsfc.nasa.gov/

NASA – Science; https://science.nasa.gov/

National Land Survey of Iceland; http://http://www.lmi.is//

Statistics Island; https://statice.is/

U.S. Geological Survey – EarthExplorer; https://earthexplorer.usgs.gov/

U.S. Geological Survey – Earth Resources Observation and Science Center; https://eros.usgs.gov/

U.S. Geological Survey – Earthquake Hazards program; https://earthquake.usgs.gov/

U.S. Geological Survey – Landsat Missions; https://landsat.usgs.gov/

U.S. Geological Survey – ScienceBase; https://www.sciencebase.gov/

U.S. Geological Survey; https://www.usgs.gov/

Website of Ólafur Ingólfsson – Professor of glacial and Quaternary Geology – University of Iceland – Department of Geology and Geography and Institute of Earth Sciences; https://notendur.hi.is/oi/

World Glacier Monitoring Service (WGMS 2017); http://wgms.ch/

9. Appendices

Appendix 1. Mýrdalsjökull and Eyjafjallajökull ice caps, outlet glaciers and other associated glacier-places (based on Sigurðsson and Williams 2008)

Modern name	Alternative names / spelling variations	Historic names	Surging	Coordinates*
Mýrdalsjökull ice cap and associated outlet glaciers				
Mýrdalsjökull	Miðdalsjökull, Mirdalsjökull, Mýdalsjökull	Austurjökull, Eyjafjallajökull, Höfðabrekkujökull, Höfðajökull, Höfðárjökull, Kötlugjárjökull, Kötlujökull, Sólheimajökull, Austurjöklar, Þykkvabæjarjökull	No	63°48′N, 19°26′W 63°31′N, 18°47′W
Entujökull			No	63°45′N, 19°18′W
Hafursárjökull			No	63°32′N, 19°05′W
		Hrunakvíslarjökull	No	63°40′N, 19°23′W
Hrunárjöklar			No	63°39′N, 19°24′W
Huldujökull	Hvítijökull		No	63°34′N, 18°55′W
Jökulsárgilsjökull			No	63°35′N, 19°20′W
Klifurárjökull	Klifandajökull, Klifandijökull		No	63°32′N, 19°13′W
Krossárjökull			No	63°41′N, 19°22′W
Kötlujökull	Höfðabrekkujökull	Kötlufalljökull	No	63°35′N, 18°49′W
Sandfellsjökull			No	63°40′N, 18°50′W
Sléttjökull	Mælifellsjökull		Yes	63°46′N, 19°01′W
Sólheimajökull			No	63°32′N, 19°21′W
Thoroddsengletscher			No	63°32′N, 19°02′W
Tungnakvíslarjökull			No	63°40′N, 19°23′W
Öldufellsjökull			Yes	63°44′N, 18°51′W
Internal ice domes (Mýrdalsjökull ice cap)				
Goðabunga			No	63°39′N, 19°16′W
Hábunga	Háabunga		No	63°35′N, 19°07′W
Merkurjökull	Þórsmerkurjökull		No	63°39′N, 19°16′W
Ice-margins (Mýrdalsjökull ice cap)				
Botnjökull		Emstrujökull, Botnjökull	No	63°47′N, 18°56′W
Goðalandsjökull			No	63°45′N, 19°13′W
Hrunajökull			No	63°39′N, 19°16′W
		Sólheimajökull	No	63°39′N, 19°24′W
Eyjafjallajökull ice cap and associated outlet glaciers				
Eyjafjallajökull		Austurjökull, Hájökull	No	63°40′N, 19°45′W 63°35′N, 19°27′W
Akstaðajökull	Kaplaskarðsjökull		No	63°39′N, 19°45′W
Gígjökull	Falljökull	Skriðjökull	No	63°40′N, 19°38′W
Hvannárjökull			No	63°39′N, 19°28′W
Kaldaklifsjökull			No	63°35′N, 19°32′W
Seljavallajökull		Tungugilsjökull	No	63°36′N, 19°37′W
Steinsholtsjökull			No	63°40′N, 19°33′W

** latitude and longitude of the approx. glacier center (for ice caps, two sets of bounding coordinates are given)*

Appendix 2. Glaciers termini variation, based on data from Iceland Glaciological Society (top) and World Glacier Monitoring Service (bottom; WGMS 2017)

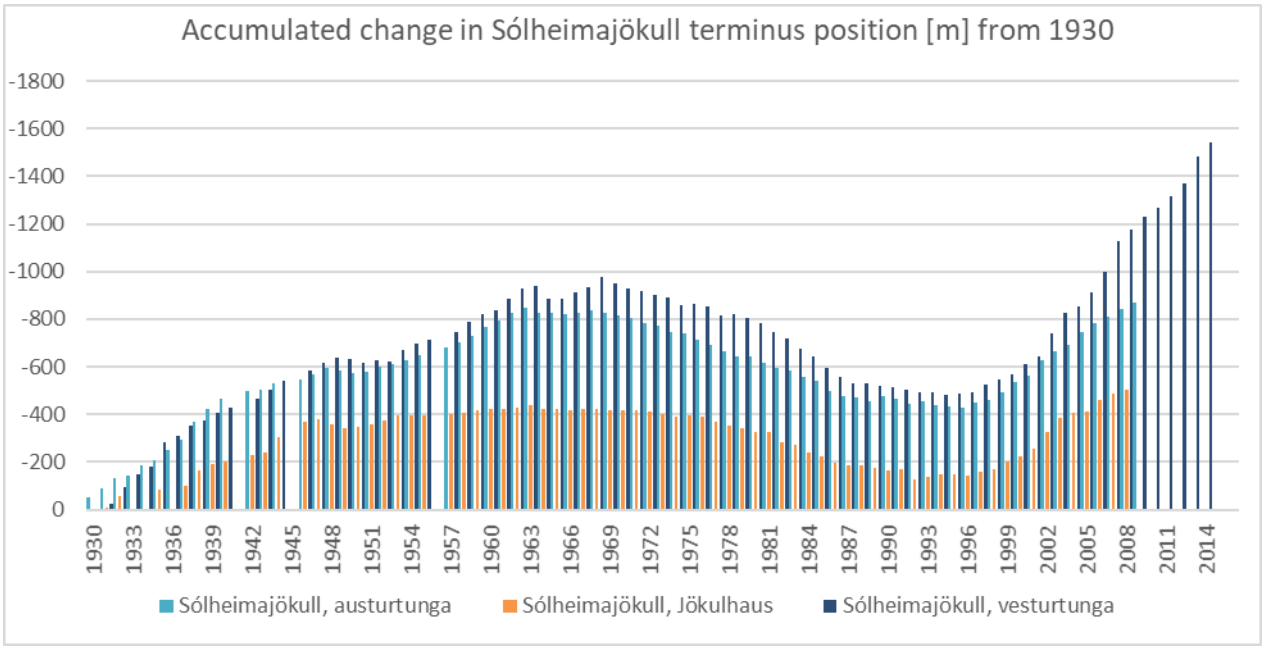

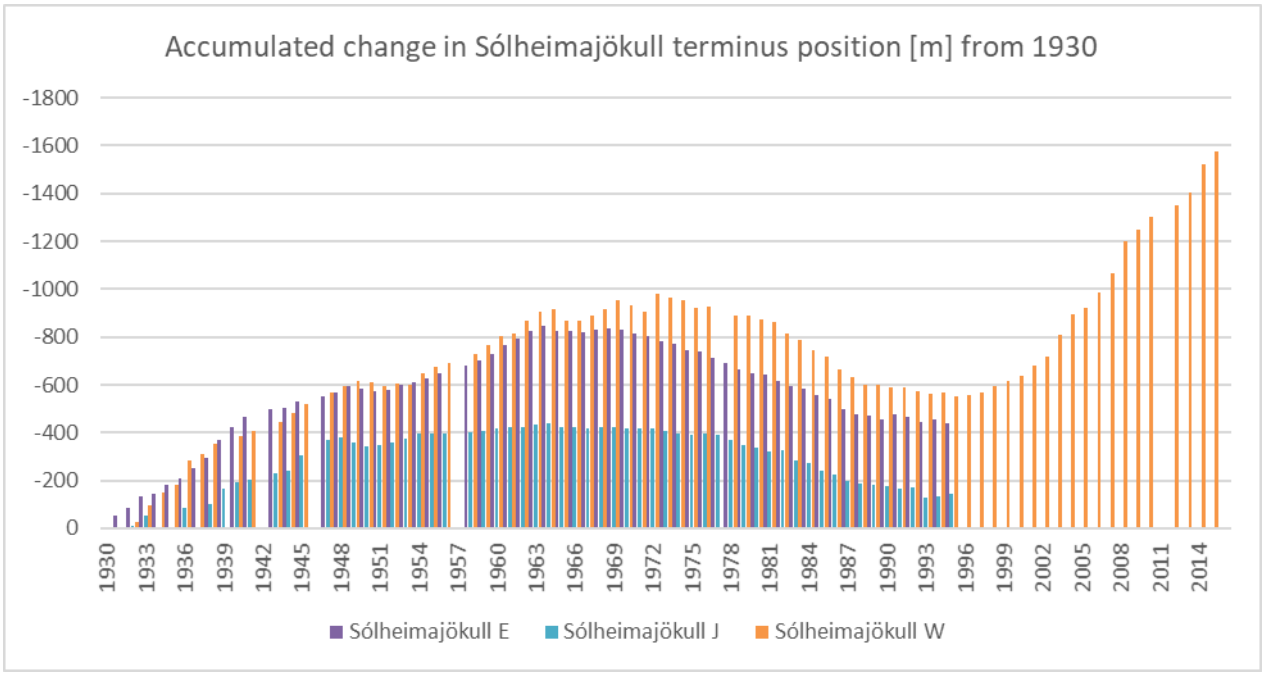

Glaciers termini variation – Sólheimajökull (Mýrdalsjökull outlet), based on data from Iceland Glaciological Society (top) and World Glacier Monitoring Service (bottom; WGMS 2017)

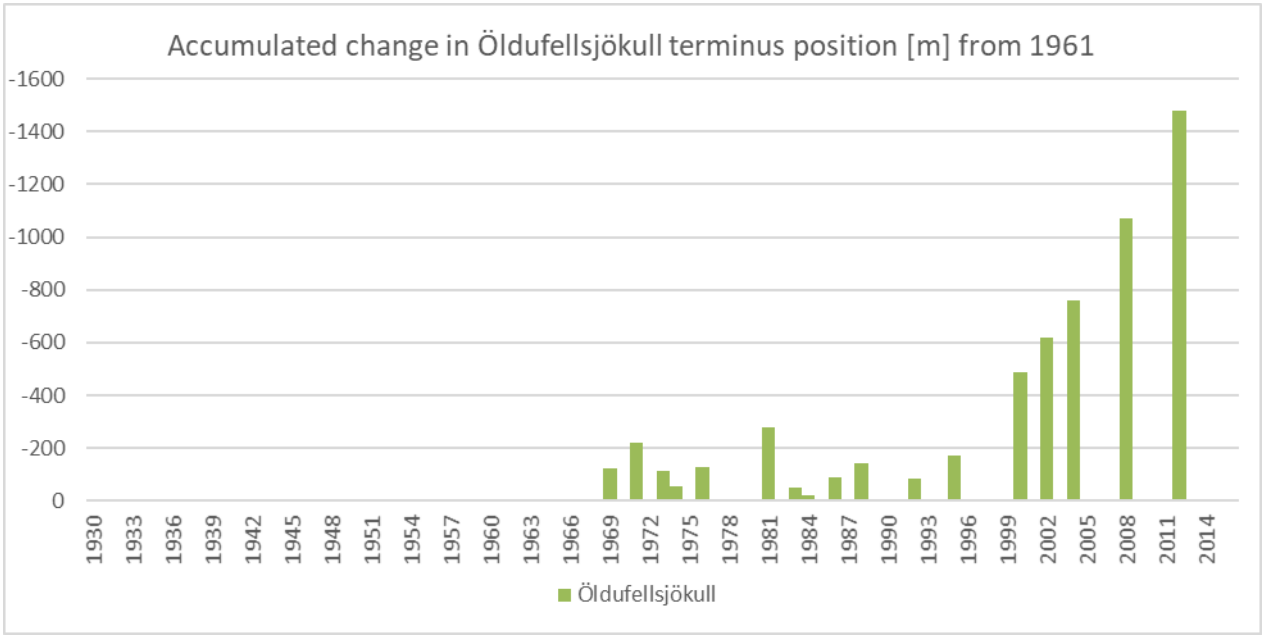

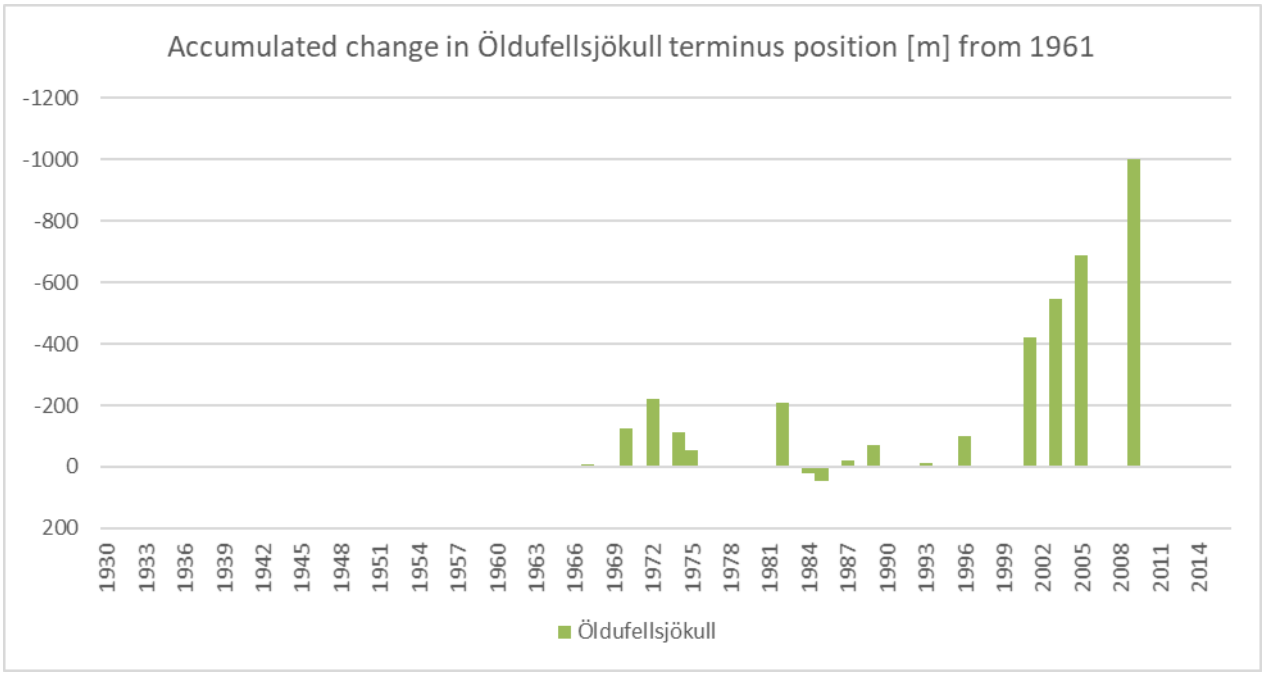

Glaciers termini variation – Öldufellsjökull (Mýrdalsjökull outlet), based on data from Iceland Glaciological Society (top) and World Glacier Monitoring Service (bottom; WGMS 2017)

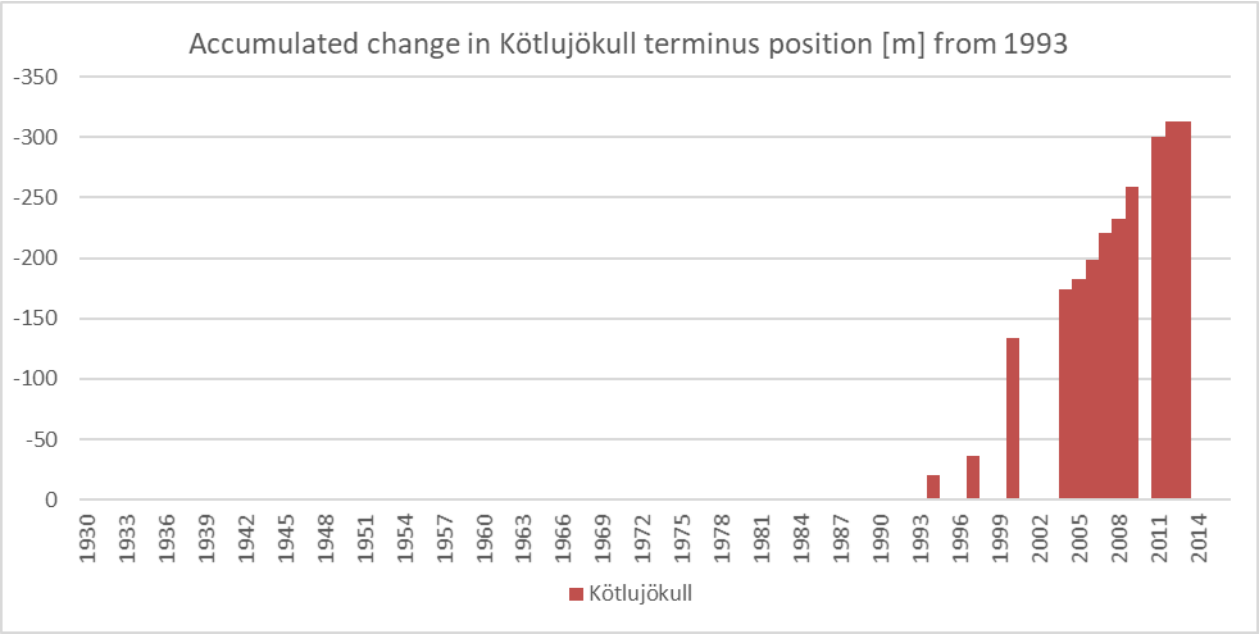

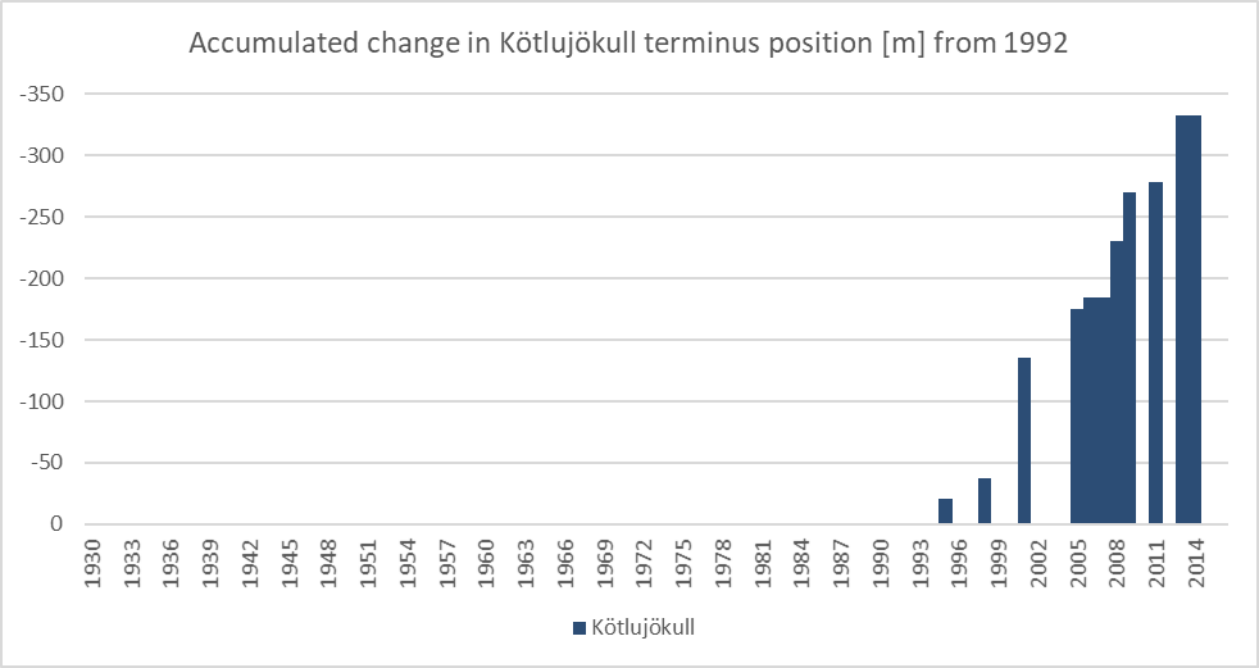

Glaciers termini variation – Kötlujökull (Mýrdalsjökull outlet), based on data from Iceland Glaciological Society (top) and World Glacier Monitoring Service (bottom; WGMS 2017)

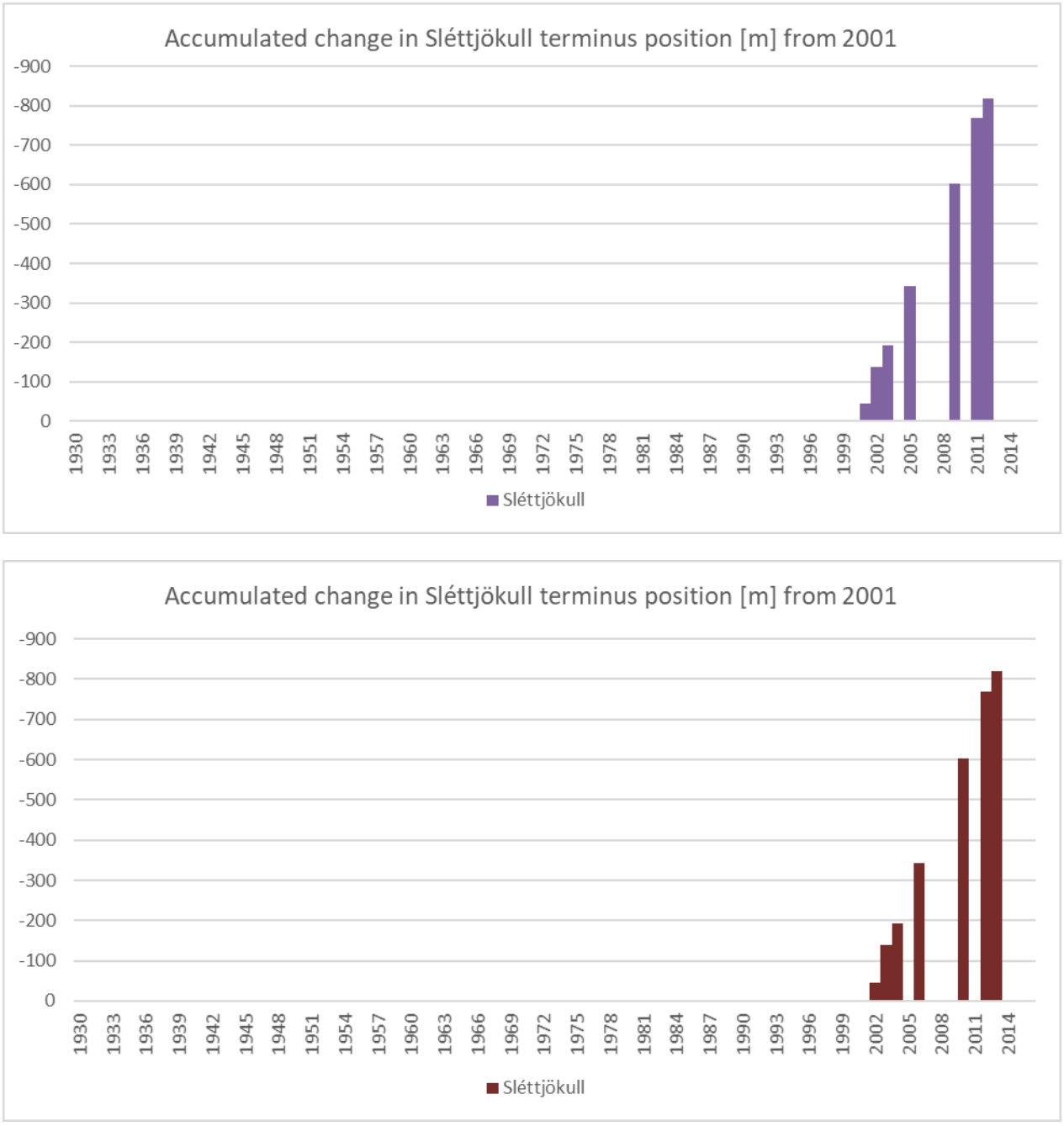

Glaciers termini variation – Sléttjökull (Mýrdalsjökull outlet), based on data from Iceland Glaciological Society (top) and World Glacier Monitoring Service (bottom; WGMS 2017)

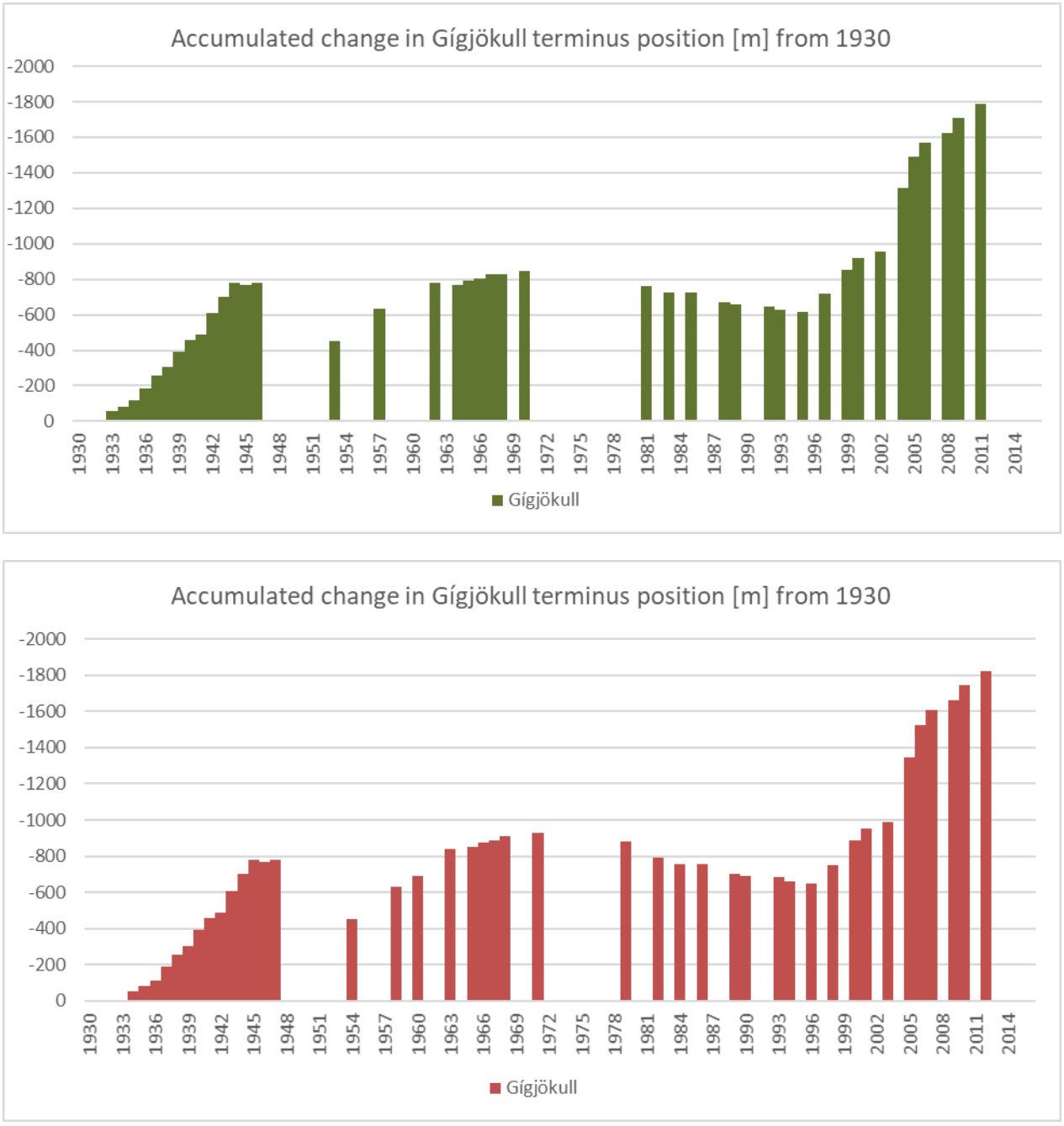

Glaciers termini variation – Gígjökull (Eyjafjallajökull outlet), based on data from Iceland Glaciological Society (top) and World Glacier Monitoring Service (bottom; WGMS 2017)

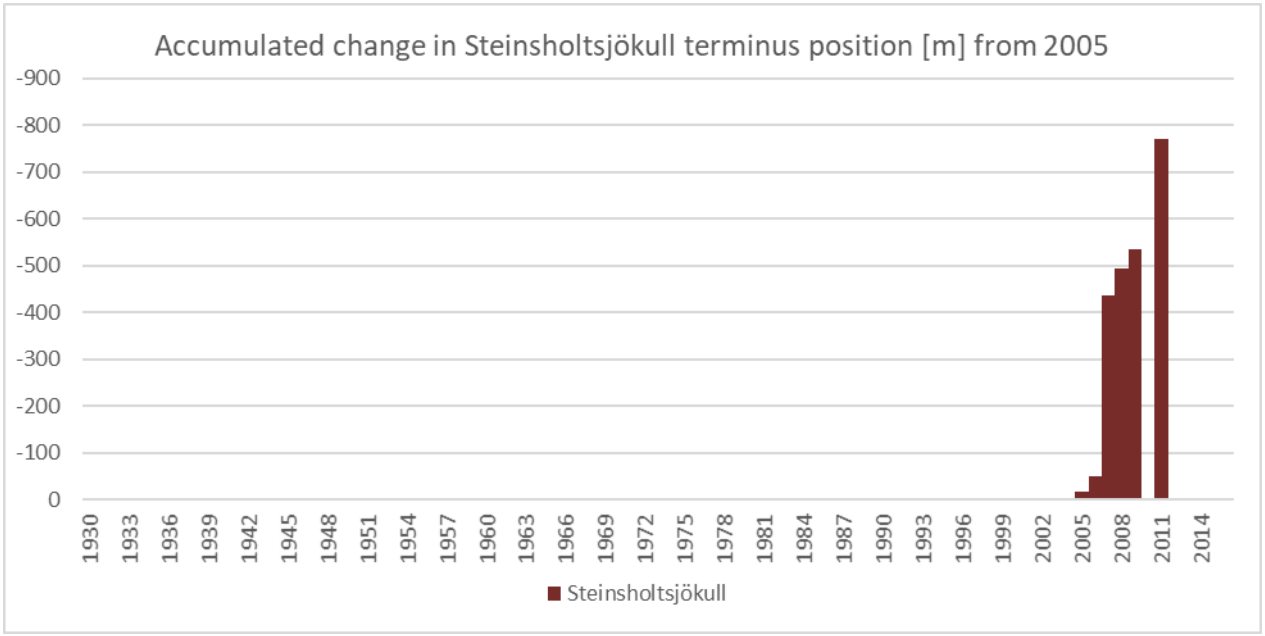

Glaciers termini variation – Steinsholtsjökull (Eyjafjallajökull outlet) (Iceland Glaciological Society)

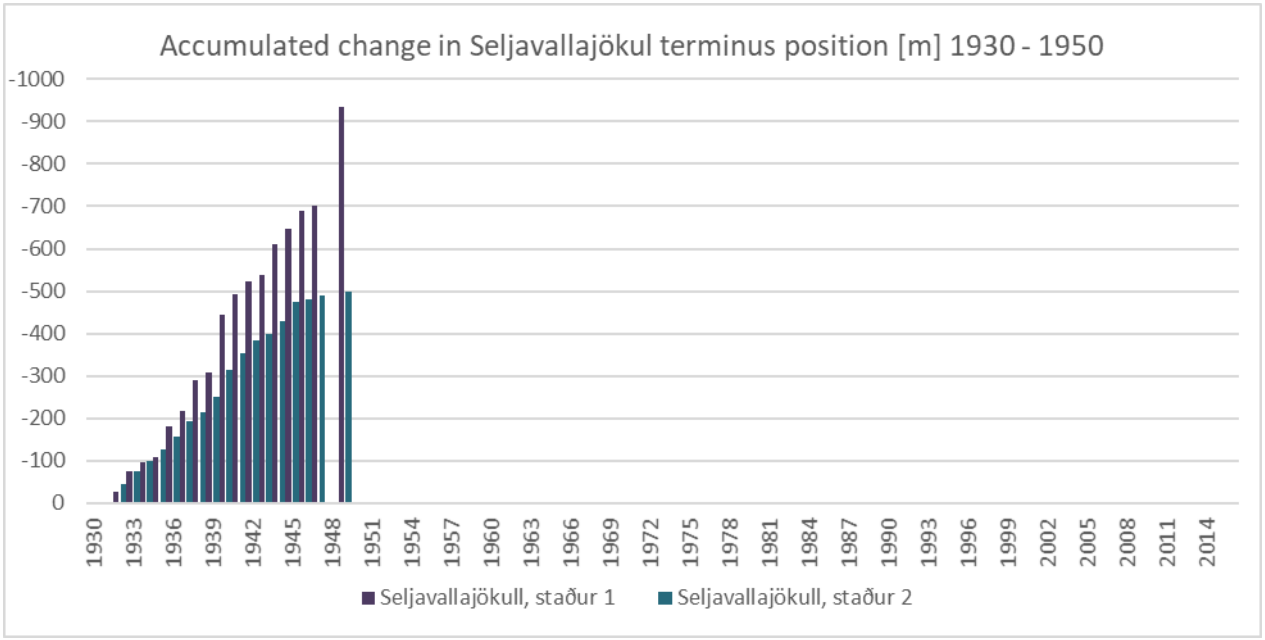

Glaciers termini variation – Seljavallajökul (Eyjafjallajökull outlet) (Iceland Glaciological Society)

Appendix 3. Approximate locations of termini measurements of Iceland Glaciological Society (top) and World Glacier Monitoring Service (WGMS) – Global Land Ice Measurements from Space (GLIMS; bottom)

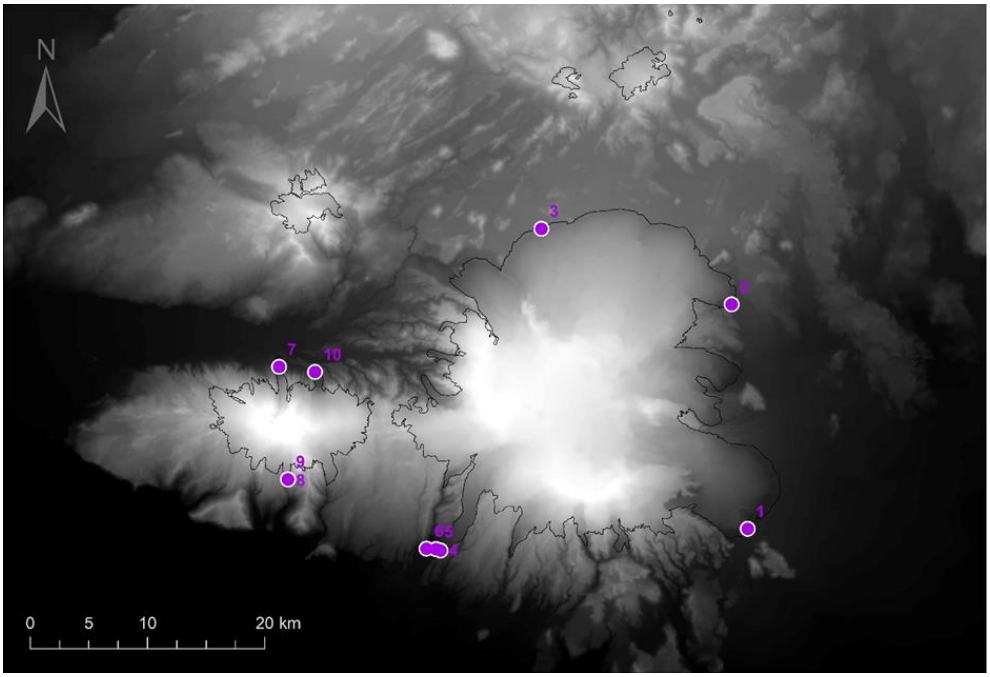

1. Kötlujökull
2. Öldufellsjökull
3. Sléttjökull
4. Sólheimajökull, austurtunga;
5. Sólheimajökull, Jökulhaus;
6. Sólheimajökull, vesturtunga
7. Gígjökull
8. Seljavallajökull, staður 1
9. Seljavallajökull, staður 2
10. Steinsholtsjökull

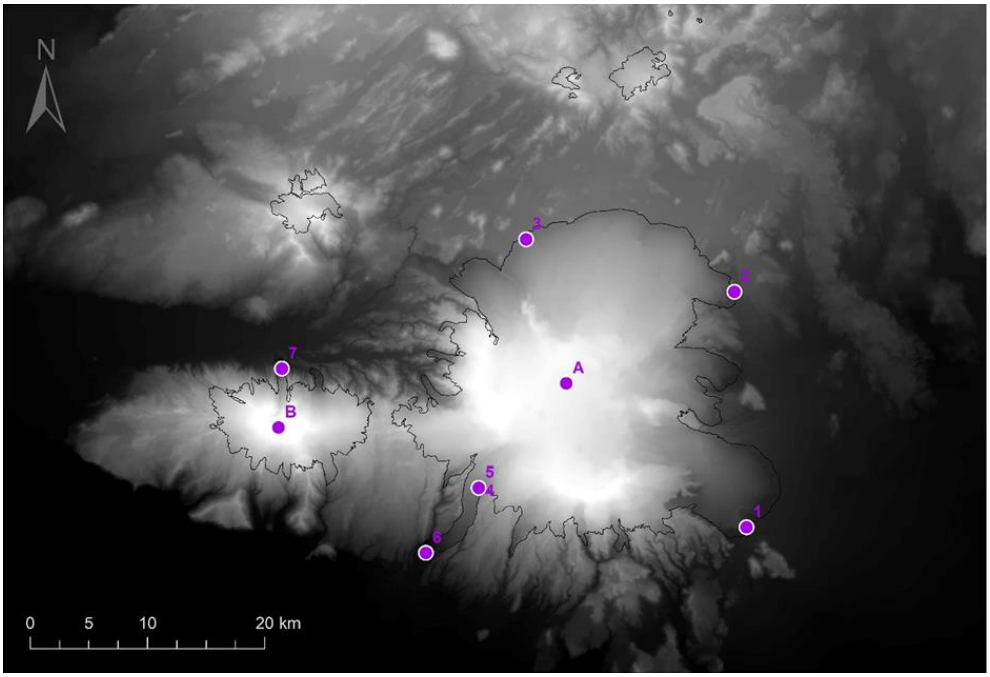

A.- Mýrdalsjökull
B. Eyjafjallajökull
1. Kötlujökull
2. Öldufellsjökull
3. Sléttjökull
4. Sólheimajökull-E
5. Sólheimajökull-J
6. Sólheimajökull-W
7. Gígjökull

Appendix 4. Accuracy – Coefficient (error) Matrix

NDSI

Threshold	Year	Coefficient matrix		Ground truth: Glacier	Ground truth: Other	Ground truth: Invalid	Map data points	Correctly mapped points	Overall accuracy	User (object) accuracy	Producer (classification) accuracy	Mean accuracy	Areal difference	Kappa	
0,3	1986	Map Data	Glacier	305	26	0	331	305	96,20	92,15	99,03	95,46	7,47	0,99	0,91
			Other	0	657	0	657	657		100,00	94,94	97,41	-5,06	0,85	
			Invalid	3	9	0	12	NA		NA					
		ground-truth points		308	692	0	1000	962							
	1988	Map Data	Glacier	283	43	0	326	283	93,90	86,81	94,97	90,71	9,40	0,93	0,86
			Other	2	656	0	658	656		99,70	93,45	96,47	-6,27	0,81	
			Invalid	13	3	0	16	NA		NA					
		ground-truth points		298	702	0	1000	939							
	2014	Map Data	Glacier	244	29	0	273	244	97,10	89,38	100,00	94,39	11,89	1,00	0,92
			Other	0	727	0	727	727		100,00	96,16	98,04	-3,84	0,86	
			Invalid	0	0	0	0	NA		NA					
		ground-truth points		244	756	0	1000	971							
0,4	1986	Map Data	Glacier	303	18	0	321	303	96,80	94,39	98,38	96,34	4,22	0,98	0,93
			Other	2	665	0	667	665		99,70	96,10	97,87	-3,61	0,88	
			Invalid	3	9	0	12	NA		NA					
		ground-truth points		308	692	0	1000	968							
	1988	Map Data	Glacier	282	23	0	305	282	95,80	92,46	94,63	93,53	2,35	0,92	0,90
			Other	3	676	0	679	676		99,56	96,30	97,90	-3,28	0,88	
			Invalid	13	3	0	16	NA		NA					
		ground-truth points		298	702	0	1000	958							
	2014	Map Data	Glacier	244	21	0	265	244	97,90	92,08	100,00	95,87	8,61	1,00	0,94
			Other	0	735	0	735	735		100,00	97,22	98,59	-2,78	0,90	
			Invalid	0	0	0	0	NA		NA					
		ground-truth points		244	756	0	1000	979							
0,5	1986	Map Data	Glacier	293	14	0	307	293	96,20	95,44	95,13	95,28	-0,32	0,93	0,91
			Other	12	669	0	681	669		98,24	96,68	97,45	-1,59	0,90	
			Invalid	3	9	0	12	NA		NA					
		ground-truth points		308	692	0	1000	962							
	1988	Map Data	Glacier	275	22	0	297	275	95,20	92,59	92,28	92,44	-0,34	0,89	0,89
			Other	10	677	0	687	677		98,54	96,44	97,48	-2,14	0,89	
			Invalid	13	3	0	16	NA		NA					
		ground-truth points		298	702	0	1000	952							
	2014	Map Data	Glacier	240	21	0	261	240	97,50	91,95	98,36	95,05	6,97	0,98	0,93
			Other	4	735	0	739	735		99,46	97,22	98,33	-2,25	0,89	
			Invalid	0	0	0	0	NA		NA					
		ground-truth points		244	756	0	1000	975							

NDSII

Threshold	Year	Coefficient matrix		Ground truth: Glacier	Ground truth: Other	Ground truth: Invalid	Map data points	Correctly mapped points	Overall accuracy	User (object) accuracy	Producer (classification) accuracy	Mean accuracy	Areal differene	Kappa	
0,3	1986	Map Data	Glacier	303	21	0	324	303	96,50	93,52	98,38	95,89	5,19	0,98	0,92
			Other	2	662	0	664	662		99,70	95,66	97,64	-4,05	0,87	
			Invalid	3	9	0	12	NA		NA					
		ground-truth points		308	692	0	1000	965							
	1988	Map Data	Glacier	282	28	0	310	282	95,30	90,97	94,63	92,76	4,03	0,92	0,89
			Other	2	671	0	673	671		99,70	95,58	97,60	-4,13	0,86	
			Invalid	14	3	0	17	NA		NA					
		ground-truth points		298	702	0	1000	953							
	2014	Map Data	Glacier	243	24	0	267	243	97,00	91,01	99,59	95,11	9,43	0,99	0,92
			Other	0	727	0	727	727		100,00	96,16	98,04	-3,84	0,86	
			Invalid	1	5	0	6	NA		NA					
		ground-truth points		244	756	0	1000	970							
0,4	1986	Map Data	Glacier	299	13	0	312	299	96,90	95,83	97,08	96,45	1,30	0,96	0,93
			Other	6	670	0	676	670		99,11	96,82	97,95	-2,31	0,90	
			Invalid	3	9	0	12	NA		NA					
		ground-truth points		308	692	0	1000	969							
	1988	Map Data	Glacier	277	21	0	298	277	95,50	92,95	92,95	92,95	0,00	0,90	0,90
			Other	7	678	0	685	678		98,98	96,58	97,76	-2,42	0,89	
			Invalid	14	3	0	17	NA		NA					
		ground-truth points		298	702	0	1000	955							
	2014	Map Data	Glacier	243	20	0	263	243	97,40	92,40	99,59	95,86	7,79	0,99	0,93
			Other	0	731	0	731	731		100,00	96,69	98,32	-3,31	0,88	
			Invalid	1	5	0	6	NA		NA					
		ground-truth points		244	756	0	1000	974							
0,5	1986	Map Data	Glacier	291	10	0	301	291	96,40	96,68	94,48	95,57	-2,27	0,92	0,92
			Other	14	673	0	687	673		97,96	97,25	97,61	-0,72	0,91	
			Invalid	3	9	0	12	NA		NA					
		ground-truth points		308	692	0	1000	964							
	1988	Map Data	Glacier	272	18	0	290	272	95,30	93,79	91,28	92,52	-2,68	0,88	0,89
			Other	12	681	0	693	681		98,27	97,01	97,63	-1,28	0,90	
			Invalid	14	3	0	17	NA		NA					
		ground-truth points		298	702	0	1000	953							
	2014	Map Data	Glacier	240	19	0	259	240	97,20	92,66	98,36	95,43	6,15	0,98	0,93
			Other	3	732	0	735	732		99,59	96,83	98,19	-2,78	0,88	
			Invalid	1	5	0	6	NA		NA					
		ground-truth points		244	756	0	1000	972							

Ratio Images (Red/NIR)

Threshold	Year	Coefficient matrix		Ground truth: Ice	Ground truth: Snow	Ground truth: Invalid	Map data points	Correctly mapped points	Overall accuracy	User (object) accuracy	Producer (classification) accuracy	Mean accuracy	Areal differene	Kappa	
1,10	1986	Map Data	Ice	89	23	0	112	89	85,39	79,46	80,91	80,18	1,82	0,70	0,68
			Snow	21	174	0	195	174		89,23	87,88	88,55	-1,52	0,67	
			Invalid	0	1	0	1	NA		NA					
		ground-truth points		110	198	0	308	263							
	1988	Map Data	Ice	97	20	0	117	97	83,22	82,91	85,09	83,98	2,63	0,76	0,67
			Snow	17	151	0	168	151		89,88	82,07	85,80	-8,70	0,61	
			Invalid	0	13	0	13	NA		NA					
		ground-truth points		114	184	0	298	248							
1,20	2014	Map Data	Ice	105	13	0	118	105	93,03	88,98	96,33	92,51	8,26	0,94	0,86
			Snow	3	122	0	125	122		97,60	90,37	93,85	-7,41	0,84	
			Invalid	1	0	0	1	NA		NA					
		ground-truth points		109	135	0	244	227							
1,12	1986	Map Data	Ice	81	3	0	84	81	89,29	96,43	73,64	83,51	-23,64	0,64	0,75
			Snow	29	194	0	223	194		87,00	97,98	92,16	12,63	0,93	
			Invalid	0	1	0	1	NA		NA					
		ground-truth points		110	198	0	308	275							
	1988	Map Data	Ice	83	0	0	83	83	85,23	100,00	72,81	84,26	-27,19	0,63	0,69
			Snow	31	171	0	202	171		84,65	92,93	88,60	9,78	0,79	
			Invalid	0	13	0	13	NA		NA					
		ground-truth points		114	184	0	298	254							
1,22	2014	Map Data	Ice	105	4	0	109	105	96,72	96,33	96,33	96,33	0,00	0,94	0,93
			Snow	3	131	0	134	131		97,76	97,04	97,40	-0,74	0,95	
			Invalid	1	0	0	1	NA		NA					
		ground-truth points		109	135	0	244	236							
1,14	1986	Map Data	Ice	65	0	0	65	65	85,06	100,00	59,09	74,29	-40,91	0,48	0,64
			Snow	45	197	0	242	197		81,40	99,49	89,55	22,22	0,98	
			Invalid	0	1	0	1	NA		NA					
		ground-truth points		110	198	0	308	262							
	1988	Map Data	Ice	68	0	0	68	68	80,20	100,00	59,65	74,73	-40,35	0,48	0,57
			Snow	46	171	0	217	171		78,80	92,93	85,29	17,93	0,76	
			Invalid	0	13	0	13	NA		NA					
		ground-truth points		114	184	0	298	239							
1,24	2014	Map Data	Ice	100	4	0	104	100	94,67	96,15	91,74	93,90	-4,59	0,88	0,89
			Snow	8	131	0	139	131		94,24	97,04	95,62	2,96	0,95	
			Invalid	1	0	0	1	NA		NA					
		ground-truth points		109	135	0	244	231							

Series from Lund University

Department of Physical Geography and Ecosystem Science

Master Thesis in Geographical Information Science

1. *Anthony Lawther:* The application of GIS-based binary logistic regression for slope failure susceptibility mapping in the Western Grampian Mountains, Scotland (2008).
2. *Rickard Hansen:* Daily mobility in Grenoble Metropolitan Region, France. Applied GIS methods in time geographical research (2008).
3. *Emil Bayramov:* Environmental monitoring of bio-restoration activities using GIS and Remote Sensing (2009).
4. *Rafael Villarreal Pacheco:* Applications of Geographic Information Systems as an analytical and visualization tool for mass real estate valuation: a case study of Fontibon District, Bogota, Columbia (2009).
5. *Siri Oestreich Waage:* a case study of route solving for oversized transport: The use of GIS functionalities in transport of transformers, as part of maintaining a reliable power infrastructure (2010).
6. *Edgar Pimiento:* Shallow landslide susceptibility – Modelling and validation (2010).
7. *Martina Schäfer:* Near real-time mapping of floodwater mosquito breeding sites using aerial photographs (2010).
8. *August Pieter van Waarden-Nagel:* Land use evaluation to assess the outcome of the programme of rehabilitation measures for the river Rhine in the Netherlands (2010).
9. *Samira Muhammad:* Development and implementation of air quality data mart for Ontario, Canada: A case study of air quality in Ontario using OLAP tool. (2010).
10. *Fredros Oketch Okumu*: Using remotely sensed data to explore spatial and temporal relationships between photosynthetic productivity of vegetation and malaria transmission intensities in selected parts of Africa (2011).
11. *Svajunas Plunge:* Advanced decision support methods for solving diffuse water pollution problems (2011).
12. *Jonathan Higgins:* Monitoring urban growth in greater Lagos: A case study using GIS to monitor the urban growth of Lagos 1990 - 2008 and produce future growth prospects for the city (2011).
13. *Mårten Karlberg:* Mobile Map Client API: Design and Implementation for Android (2011).
14. *Jeanette McBride:* Mapping Chicago area urban tree canopy using color infrared imagery (2011).
15. *Andrew Farina:* Exploring the relationship between land surface temperature and vegetation abundance for urban heat island mitigation in Seville, Spain (2011).
16. *David Kanyari*: Nairobi City Journey Planner: An online and a Mobile Application (2011).

17. *Laura V. Drews:* Multi-criteria GIS analysis for siting of small wind power plants - A case study from Berlin (2012).
18. *Qaisar Nadeem:* Best living neighborhood in the city - A GIS based multi criteria evaluation of ArRiyadh City (2012).
19. *Ahmed Mohamed El Saeid Mustafa:* Development of a photo voltaic building rooftop integration analysis tool for GIS for Dokki District, Cairo, Egypt (2012).
20. *Daniel Patrick Taylor*: Eastern Oyster Aquaculture: Estuarine Remediation via Site Suitability and Spatially Explicit Carrying Capacity Modeling in Virginia's Chesapeake Bay (2013).
21. *Angeleta Oveta Wilson:* A Participatory GIS approach to *unearthing* Manchester's Cultural Heritage '*gold mine'* (2013).
22. *Ola Svensson:* Visibility and Tholos Tombs in the Messenian Landscape: A Comparative Case Study of the Pylian Hinterlands and the Soulima Valley (2013).
23. *Monika Ogden:* Land use impact on water quality in two river systems in South Africa (2013).
24. *Stefan Rova:* A GIS based approach assessing phosphorus load impact on Lake Flaten in Salem, Sweden (2013).
25. *Yann Buhot:* Analysis of the history of landscape changes over a period of 200 years. How can we predict past landscape pattern scenario and the impact on habitat diversity? (2013).
26. *Christina Fotiou:* Evaluating habitat suitability and spectral heterogeneity models to predict weed species presence (2014).
27. *Inese Linuza:* Accuracy Assessment in Glacier Change Analysis (2014).
28. *Agnieszka Griffin:* Domestic energy consumption and social living standards: a GIS analysis within the Greater London Authority area (2014).
29. *Brynja Guðmundsdóttir:* Detection of potential arable land with remote sensing and GIS - A Case Study for Kjósarhreppur (2014).
30. *Oleksandr Nekrasov:* Processing of MODIS Vegetation Indices for analysis of agricultural droughts in the southern Ukraine between the years 2000-2012 (2014).
31. *Sarah Tressel:* Recommendations for a polar Earth science portal in the context of Arctic Spatial Data Infrastructure (2014).
32. *Caroline Gevaert:* Combining Hyperspectral UAV and Multispectral Formosat-2 Imagery for Precision Agriculture Applications (2014).
33. *Salem Jamal-Uddeen:* Using GeoTools to implement the multi-criteria evaluation analysis - weighted linear combination model (2014).
34. *Samanah Seyedi-Shandiz:* Schematic representation of geographical railway network at the Swedish Transport Administration (2014).
35. *Kazi Masel Ullah:* Urban Land-use planning using Geographical Information System and analytical hierarchy process: case study Dhaka City (2014).
36. *Alexia Chang-Wailing Spitteler:* Development of a web application based on MCDA and GIS for the decision support of river and floodplain rehabilitation projects (2014).
37. *Alessandro De Martino:* Geographic accessibility analysis and evaluation of potential changes to the public transportation system in the City of Milan (2014).
38. *Alireza Mollasalehi:* GIS Based Modelling for Fuel Reduction Using Controlled Burn in Australia. Case Study: Logan City, QLD (2015).

39. *Negin A. Sanati:* Chronic Kidney Disease Mortality in Costa Rica; Geographical Distribution, Spatial Analysis and Non-traditional Risk Factors (2015).
40. *Karen McIntyre:* Benthic mapping of the Bluefields Bay fish sanctuary, Jamaica (2015).
41. *Kees van Duijvendijk:* Feasibility of a low-cost weather sensor network for agricultural purposes: A preliminary assessment (2015).
42. *Sebastian Andersson Hylander:* Evaluation of cultural ecosystem services using GIS (2015).
43. *Deborah Bowyer:* Measuring Urban Growth, Urban Form and Accessibility as Indicators of Urban Sprawl in Hamilton, New Zealand (2015).
44. *Stefan Arvidsson:* Relationship between tree species composition and phenology extracted from satellite data in Swedish forests (2015).
45. *Damián Giménez Cruz*: GIS-based optimal localisation of beekeeping in rural Kenya (2016).
46. *Alejandra Narváez Vallejo:* Can the introduction of the topographic indices in LPJ-GUESS improve the spatial representation of environmental variables? (2016).
47. *Anna Lundgren:* Development of a method for mapping the highest coastline in Sweden using breaklines extracted from high resolution digital elevation models (2016).
48. *Oluwatomi Esther Adejoro:* Does location also matter? A spatial analysis of social achievements of young South Australians (2016).
49. *Hristo Dobrev Tomov:* Automated temporal NDVI analysis over the Middle East for the period 1982 - 2010 (2016).
50. *Vincent Muller:* Impact of Security Context on Mobile Clinic Activities A GIS Multi Criteria Evaluation based on an MSF Humanitarian Mission in Cameroon (2016).
51. *Gezahagn Negash Seboka:* Spatial Assessment of NDVI as an Indicator of Desertification in Ethiopia using Remote Sensing and GIS (2016).
52. *Holly Buhler:* Evaluation of Interfacility Medical Transport Journey Times in Southeastern British Columbia. (2016).
53. *Lars Ole Grottenberg*: Assessing the ability to share spatial data between emergency management organisations in the High North (2016).
54. *Sean Grant:* The Right Tree in the Right Place: Using GIS to Maximize the Net Benefits from Urban Forests (2016).
55. *Irshad Jamal:* Multi-Criteria GIS Analysis for School Site Selection in Gorno-Badakhshan Autonomous Oblast, Tajikistan (2016).
56. *Fulgencio Sanmartín:* Wisdom-volkano: A novel tool based on open GIS and time-series visualization to analyse and share volcanic data (2016).
57. *Nezha Acil:* Remote sensing-based monitoring of snow cover dynamics and its influence on vegetation growth in the Middle Atlas Mountains (2016).
58. *Julia Hjalmarsson:* A Weighty Issue: Estimation of Fire Size with Geographically Weighted Logistic Regression (2016).
59. *Mathewos Tamiru Amato:* Using multi-criteria evaluation and GIS for chronic food and nutrition insecurity indicators analysis in Ethiopia (2016).
60. *Karim Alaa El Din Mohamed Soliman El Attar:* Bicycling Suitability in Downtown, Cairo, Egypt (2016).

61. *Gilbert Akol Echelai:* Asset Management: Integrating GIS as a Decision Support Tool in Meter Management in National Water and Sewerage Corporation (2016).
62. *Terje Slinning:* Analytic comparison of multibeam echo soundings (2016).
63. *Gréta Hlín Sveinsdóttir:* GIS-based MCDA for decision support: A framework for wind farm siting in Iceland (2017).
64. *Jonas Sjögren:* Consequences of a flood in Kristianstad, Sweden: A GIS-based analysis of impacts on important societal functions (2017).
65. *Nadine Raska:* 3D geologic subsurface modelling within the Mackenzie Plain, Northwest Territories, Canada (2017).
66. *Panagiotis Symeonidis*: Study of spatial and temporal variation of atmospheric optical parameters and their relation with PM 2.5 concentration over Europe using GIS technologies (2017).
67. *Michaela Bobeck:* A GIS-based Multi-Criteria Decision Analysis of Wind Farm Site Suitability in New South Wales, Australia, from a Sustainable Development Perspective (2017).
68. *Raghdaa Eissa*: Developing a GIS Model for the Assessment of Outdoor Recreational Facilities in New Cities Case Study: Tenth of Ramadan City, Egypt (2017).
69. *Zahra Khais Shahid*: Biofuel plantations and isoprene emissions in Svea and Götaland (2017).
70. *Mirza Amir Liaquat Baig*: Using geographical information systems in epidemiology: Mapping and analyzing occurrence of diarrhea in urban - residential area of Islamabad, Pakistan (2017).
71. *Joakim Jörwall*: Quantitative model of Present and Future well-being in the EU-28: A spatial Multi-Criteria Evaluation of socioeconomic and climatic comfort factors (2017).
72. *Elin Haettner*: Energy Poverty in the Dublin Region: Modelling Geographies of Risk (2017).
73. *Harry Eriksson*: Geochemistry of stream plants and its statistical relations to soil- and bedrock geology, slope directions and till geochemistry. A GIS-analysis of small catchments in northern Sweden (2017).
74. *Daniel Gardevärn:* PPGIS and Public meetings – An evaluation of public participation methods for urban planning (2017).
75. *Kim Friberg:* Sensitivity Analysis and Calibration of Multi Energy Balance Land Surface Model Parameters (2017).
76. *Viktor Svanerud:* Taking the bus to the park? A study of accessibility to green areas in Gothenburg through different modes of transport (2017).
77. *Lisa-Gaye Greene*: Deadly Designs: The Impact of Road Design on Road Crash Patterns along Jamaica's North Coast Highway (2017).
78. *Katarina Jemec Parker*: Spatial and temporal analysis of fecal indicator bacteria concentrations in beach water in San Diego, California (2017).
79. *Angela Kabiru*: An Exploratory Study of Middle Stone Age and Later Stone Age Site Locations in Kenya's Central Rift Valley Using Landscape Analysis: A GIS Approach (2017).
80. *Kristean Björkmann*: Subjective Well-Being and Environment: A GIS-Based Analysis (2018).
81. *Williams Erhunmonmen Ojo*: Measuring spatial accessibility to healthcare for people living with HIV-AIDS in southern Nigeria (2018).

82. *Daniel Assefa*: Developing Data Extraction and Dynamic Data Visualization (Styling) Modules for Web GIS Risk Assessment System (WGRAS). (2018).
83. *Adela Nistora*: Inundation scenarios in a changing climate: assessing potential impacts of sea-level rise on the coast of South-East England (2018).
84. *Marc Seliger*: Thirsty landscapes - Investigating growing irrigation water consumption and potential conservation measures within Utah's largest master-planned community: Daybreak (2018).
85. *Luka Jovičić*: Spatial Data Harmonisation in Regional Context in Accordance with INSPIRE Implementing Rules (2018).
86. *Christina Kourdounouli*: Analysis of Urban Ecosystem Condition Indicators for the Large Urban Zones and City Cores in EU (2018).
87. *Jeremy Azzopardi*: Effect of distance measures and feature representations on distance-based accessibility measures (2018).
88. *Patrick Kabatha*: An open source web GIS tool for analysis and visualization of elephant GPS telemetry data, alongside environmental and anthropogenic variables (2018).
89. *Richard Alphonce Giliba*: Effects of Climate Change on Potential Geographical Distribution of Prunus africana (African cherry) in the Eastern Arc Mountain Forests of Tanzania (2018).
90. *Eiður Kristinn Eiðsson*: Transformation and linking of authoritative multi-scale geodata for the Semantic Web: A case study of Swedish national building data sets (2018).
91. *Niamh Harty*: HOP!: a PGIS and citizen science approach to monitoring the condition of upland paths (2018).
92. *José Estuardo Jara Alvear*: Solar photovoltaic potential to complement hydropower in Ecuador: A GIS-based framework of analysis (2018).
93. *Brendan O'Neill*: Multicriteria Site Suitability for Algal Biofuel Production Facilities (2018).
94. *Roman Spataru*: Spatial-temporal GIS analysis in public health – a case study of polio disease (2018).
95. *Alicja Miodońska*: Assessing evolution of ice caps in Suðurland, Iceland, in years 1986 - 2014, using multispectral satellite imagery (2019).